FLECS_WT3.2_5.1_5.2_5.3_TN
https://doi.org/10.48441/4427.2053

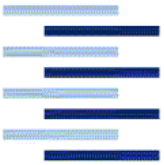

Hochschule für Angewandte Wissenschaften Hamburg
Hamburg University of Applied Sciences

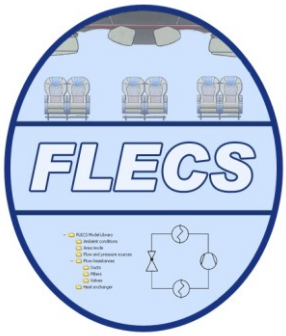

Functional Model Library of the Environmental Control System (FLECS) – Application

Parameter and Characteristic Maps
Definition of Test Cases
Validation of Subsystems
Validation of Basis Concepts

Christian Müller
Dieter Scholz

2008-03-15

Technical Note

Aircraft Design and Systems Group (AERO)
Department of Automotive and Aeronautical Engineering
Hamburg University of Applied Sciences (HAW Hamburg)
Berliner Tor 9
D - 20099 Hamburg

Dokumentationsblatt

<table>
<tr><td>1. Berichts-Nr.
FLECS_WT3.2_5.1_5.2_5.3_TN</td><td>2. Auftragstitel
FLECS - Funktionale Modellbibliothek des Environmental Control Systems</td><td>3. ISSN / ISBN
---</td></tr>
<tr><td colspan="2" rowspan="2">4. Sachtitel und Untertitel (Work Tasks)
WT3.2: Parameter und Kennfelder
WT5.1: Definition von Testfällen
WT5.2: Validation von Subsystemen
WT5.3: Validation von Grundsystemen</td><td>5. Abschlussdatum
15.03.2008</td></tr>
<tr><td>6. Ber. Nr. Auftragnehmer
---</td></tr>
<tr><td colspan="2" rowspan="2">7. Autor(en) (Vorname, Name)
Christian Müller
Dieter Scholz (info@ProfScholz.de)</td><td>8. Vertragskennzeichen
HH59</td></tr>
<tr><td>9. Projektnr.
FLAND05-006</td></tr>
<tr><td colspan="2" rowspan="3">10. Durchführende Institution (Name, Anschrift)
Studiendepartment Fahrzeugtechnik und Flugzeugbau
Hochschule für Angewandte Wissenschaften Hamburg (HAW)
Berliner Tor 9
D - 20099 Hamburg</td><td>11. Berichtsart
Technische Niederschrift</td></tr>
<tr><td>12. Berichtszeitraum
05.09.2005 - 15.03.2008</td></tr>
<tr><td>13. Seitenzahl
108</td></tr>
<tr><td colspan="2" rowspan="3">14. Fördernde Institution / Projektträger (Name, Anschrift)
Behörde für Wirtschaft und Arbeit (BWA)
Alter Steinweg 4, D - 20459 Hamburg

Deutsches Zentrum für Luft- und Raumfahrt e.V. (DLR), PT-LF
Königswinterer Straße 522-524, D - 53227 Bonn</td><td>15. Literaturangaben
23</td></tr>
<tr><td>16. Tabellen
15</td></tr>
<tr><td>17. Bilder
53</td></tr>
<tr><td colspan="3">18. Zusätzliche Angaben
Sprache: Englisch, URL: http://FLECS.ProfScholz.de</td></tr>
<tr><td colspan="3">19. Kurzfassung

Die Grundlagen für diese Technische Niederschrift (TN) sind die physikalischen Beschreibungen der auf MATLAB/Simulink basierenden Funktionalen Modellbibliothek des Environmental Control Systems – FLECS (siehe FLECS_WT3.1_3.3_3.4_TN, https://doi.org/10.48441/4427.2052). In dieser TN werden aus den elementaren Komponenten größere Einheiten des Environmental Control Systems (ECS) aufgebaut (Pack, Kabine, Regler, Kaltdampfklimasystem) und schließlich das komplette ECS eines Passagierflugzeugs. Die verschiedenen Air Conditioning Grundsysteme, die mit FLECS modelliert wurden, werden auf Stabilität und Echtzeitfähigkeit getestet. Zusätzlich werden verschiedene Systemkonfigurationen mit Hilfe von Messdaten von Flugzeugen oder Beispielen aus der Literatur validiert.</td></tr>
<tr><td colspan="3">20. Deskriptoren / Schlagwörter
Flugzeug, System, Klimaanlage, Kabine, Simulation, Modellbibliothek, MATLAB, Simulink</td></tr>
<tr><td colspan="3">21. Bezugsquelle
Studiendepartment F+F, HAW Hamburg, Berliner Tor 9, D - 20099 Hamburg</td></tr>
<tr><td>22. Sicherheitsvermerk
öffentlich</td><td>23.</td><td>24. Preis</td></tr>
</table>

Report Documentation Page

1. Report-Number FLECS_WT3.2_5.1_5.2_5.3_TN	**2. Project Title** FLECS - Functional Model Library of the Environmental Control System	**3. ISSN / ISBN** N/A
4. Title and Subtitle (Work Tasks) WT3.2: Parameter and Characteristic Maps WT5.1: Definition of Test Cases WT5.2: Validation of Subsystems WT5.3: Validation of Basis Concepts		**5. Report Date** 2008-03-15 **6. Performing Org. Rep. No** N/A
7. Author(s) (First Name, Last Name) Christian Müller Dieter Scholz (info@ProfScholz.de)		**8. Contract Code** HH59 **9. Project Number** FLAND05-006
10. Performing Agency (Name, Address) Department of Automotive and Aeronautical Engineering Hamburg University of Applied Sciences (HAW) Berliner Tor 9 D - 20099 Hamburg		**11. Report Type** Technical Note **12. Time Period** 2005-09-05 to 2008-03-15 **13. Number of Pages** 108
14. Sponsoring / Monitoring Agency (Name, Address) Behörde für Wirtschaft und Arbeit (BWA) Alter Steinweg 4, D - 20459 Hamburg Deutsches Zentrum für Luft- und Raumfahrt e.V. (DLR), PT-LF Königswinterer Straße 522-524, D - 53227 Bonn		**15. Number of References** 23 **16. Number of Tables** 15 **17. Number of Figures** 53
18. Supplementary Notes Language: English, URL: http://FLECS.ProfScholz.de		
19. Abstract The basis for this Technical Note (TN) are the physical descriptions of the MATLAB/Simulink Functional Model Library of the Environmental Control System – FLECS (see FLECS_WT3.1_3.3_3.4_TN, https://doi.org/10.48441/4427.2052). In this TN, larger units (pack, cabin, controller, vapor compression cycle system) of the Environmental Control System (ECS) are constructed from the elementary components. Finally, the complete ECS of a passenger aircraft is modeled. The various basic air conditioning systems that were built with FLECS are tested for stability and real-time capability. In addition, various system configurations are validated using measurement data from aircraft or examples from the literature.		
20. Subject Terms aircraft, system, air conditioning, ECS, cabin, simulation, model library, MATLAB, Simulink		
21. Distribution Department F+F, HAW Hamburg, Berliner Tor 9, D - 20099 Hamburg		
22. Classification / Availability public / unlimited	**23.**	**24. Price**

Table of Contents

Page

List of Figures 5
List of Tables 7
List of Symbols 8
List of Abbreviations 11

1 Introduction 12

2 Basic Considerations 14

3 Network Configuration and Stability Tests 16
3.1 Test of Compressible Flow Conditions 20
3.2 Simulation of Aircraft Cabin Temperature Control 25
3.3 Dynamical Simulations of Heat Exchangers 36

4 Validation of the FLECS Database 41
4.1 Supply Duct System 41
4.2 Cabin Model 48
4.3 Air Conditioning Pack 52
4.3.1 Simulation Model of an Air Conditioning Pack 55
4.3.2 Simulation of an Aircraft Cabin Temperature Control in Combination with a Dynamic Pack Model 89
4.4 Vapor Compression Cycle 90
4.4.1 Inner Structure of a Vapor Compression Cycle (VCM) 91
4.4.2 Validation of the Vapor Compression Cycle (VCM) 95
4.4.3 Control Aspects of the Vapor Compression Cycle 97
4.4.4 Dynamic Simulation of a VCM Air Conditioning System 98
4.4.5 Comparison of an Air Conditioning System Consisting of an ACM with a VCM Pack Model 104

Bibliography 107

List of Figures

Figure 1 Schematic drawing of the environmental control system 13
Figure 2 The principal configuration of a model block 14
Figure 3 The parameter input mask of a volume block and flow resistance block 15
Figure 4 Stable and instable configuration airflow simulation 16
Figure 5 Different configuration of a basic element of an air distribution network 18
Figure 6 Incompressible conditions: the temperature profiles inside the volume V_{right} 19
Figure 7 Compressible conditions: The temperature profiles inside the volume V_{right} 19
Figure 8 Different configuration compressible flow simulation 21
Figure 9 The temperature profiles inside the test volume V_{test} 21
Figure 10 A highly dynamic simulation of a T-joint. The Simulink result is compared with a Flowmaster data set 24
Figure 11 The control aspects of a cabin simulation 25
Figure 12 Simulink Configuration of an environmental control system of a cabin model consisting of 2 zones (see Figure 1 and Figure 11) 31
Figure 13 Profiles of the aircraft altitude, cabin pressure and rotational speed 32
Figure 14 a) Simulated temperature profiles in zone and zone 2 and the used skin temperature profile
b) Opening angle of trim air valves of zone 1 and zone 2 32
Figure 15 a) … c) Input parameter mask of a cabin model.
The shown parameters correspond to A320 aircraft 33
Figure 16 Different heat exchanger types (Allied-Signal 1990) 36
Figure 17 Different heat exchanger configurations 37
Figure 18 a) Simulated outlet temperature profiles of different heat exchanger types
b) Simulated temperature profiles of the heat transfer walls 40
Figure 19 Supply duct system of an A340-600 in combination with a cabin model 42
Figure 20 Measured datasets of supply duct inlet temperature, the cabin inlet temperature, the cabin temperature and the skin temperature 43
Figure 21 Measured datasets of supply duct inlet temperature, the cabin inlet temperature and the simulated cabin inlet temperature. The time range 4000 s … 14000 s is focussed out 45
Figure 22 Measured datasets of supply duct inlet temperature,
the cabin temperature and the simulated cabin inlet temperature.
The time range 4000 s … 14000 s is enlarged 50
Figure 23 Schematic diagram of an aircraft pack (**Allied-Signal 1990**) 52
Figure 24 Schematic diagram of an air cycle machine (**Allied-Signal 1990**) 53
Figure 25 Schematic diagram of an aircraft environmental control system 53
Figure 26 Schematic diagram of an engine core 54
Figure 27 Simulink simulation model of a pack 55
Figure 28 Schematic diagram of a condenser 57
Figure 29 Characteristic maps of the different heat exchanger inside the pack model 60

Figure 30 Inner structure of a hot bar element 61
Figure 31 Schematic diagram of a ram air channel and of NACA respectively Scoop configuration of a ram air inlet 62
Figure 32 Characteristic maps of the ram air fan 66
Figure 33 Schematic diagram of a combination of a ram air fan, a compressor and a turbine affixed to a single shaft 67
Figure 34 Characteristic maps of a compressor 68
Figure 35 Characteristic maps of the compressor 69
Figure 36 Bearing configuration inside a pack (A320) 70
Figure 37 Comparison of a pack simulation with static and dynamic heat exchangers and different test volume sizes (A00C2) 71
Figure 38 Test case G00H2, a) Compressor outlet temperature, b) Pack outlet temperature, c) Mass flow compressor, d) Out flowing mass flow pack, e) Rotational Speed.. 76
Figure 39 Test case M10H2, a) Compressor outlet temperature, b) Pack outlet temperature, c) Mass flow compressor, d) Out flowing mass flow pack, e) Rotational Speed.. 79
Figure 40 Test case M20H2, a) Compressor outlet temperature, b) Pack outlet temperature, c) Mass flow compressor, d) Out flowing mass flow pack, e) Rotational Speed.. 82
Figure 41 Test case M30H2, a) Compressor outlet temperature, b) Pack outlet temperature, c) Mass flow compressor, d) Out flowing mass flow pack, e) Rotational Speed.. 85
Figure 42 Test case C35H2, a) Compressor outlet temperature, b) Pack outlet temperature, c) Mass flow compressor, d) Out flowing mass flow pack, e) Rotational Speed.. 88
Figure 43 Results of a simulation of an aircraft cabin temperature control 89
Figure 44 Characteristic maps of vapor compression cycle model 92
Figure 45 p-h, T-s respectively T-h diagrams of R134a refrigerant 94
Figure 46 Validation of the VCM algorithm with help of an example given in [Baehr 2006] 96
Figure 47 Arrangement for the vapor compression system inside air conditioning system.. 98
Figure 48 Characteristic maps of the air compressor 99
Figure 49 The target temperature of the bleed air 99
Figure 50 The dynamic behavior of the VCM air conditioning system under different ambient conditions ..... …101
Figure 51 The relative derivation Δhh under different ambient conditions 103
Figure 52 A cascade refrigeration cycle 103
Figure 53 Time dependent ambient conditions 106

List of Tables

Table 1 List of parameters (see Figure 5) 17
Table 2 List of parameters (see Figure 8) 20
Table 3 List of parameters (see Figure 10) 22
Table 4 List of parameters (see Figure 12) 28
Table 5 List of parameters (see Figure 17) 38
Table 6 List of parameters supply duct system (see Figure 19) 45
Table 7 List of parameters cabin model (see Figure 19) 51
Table 8 List of parameters of the heat exchangers inside the pack 58
Table 9 List of parameters of the bypass valves inside the pack 70
Table 10 List of global parameters of the validation of the A320 pack 72
Table 11 Test cases pack validation 73
Table 12 List of global parameters test case A00C2 73
Table 13 Validation Example [Baehr 2006] 95
Table 14 Set of efficiencies 95
Table 15 Set of efficiencies 98

List of Symbols

a	Sonic Speed	m/s
A	Surface	m^2
b	Thickness	m
c	Specific Heat Capacity	J/kg K
C	Heat Capacity	J/K
D	Diameter	m
E	Total Energy	J
h	Altitude	ft
	Specific Enthalpy	J/kg
H	Enthalpy	J
L	Length	m
m	Mass	kg
M	Mole Mass	g/mol
Ma	Mach Number	–
Nu	Nusselt Number	–
p	Pressure	Pa
P	Power	W
	Probability	–
Pr	Prandtl Number	–
r	Radius	m
	Ratio	–
R	Specific Gas Constant	J/kg K
Re	Reynolds Number	–
q	Heat Flux	J/m^2
Q	Heat	J
s	Specific Entropy	J/kg
S	Entropy	J
t	Time	s
T	Thermodynamically Temperature	K
u	Specific Intrinsic Energy	J/kg
U	Intrinsic Energy	J
v	Velocity	m/s
V	Volume	m^3
W	Work	J

x	Mass Fraction (Normalized to Mass Dry Air)	–
	Ratio	–
α	Convection Heat Transfer Coefficient	$W/m^2 K$
β	Angle	°
ε	Emissivity	–
γ	Ratio Specific Heat Capacity	–
η	Dynamic Viscosity	Pa s
	Efficiency	–
φ	Humidity	–
κ	Compressibility	1/K
λ	Drag Coefficient	–
	Thermal Conductivity	W/m K
ν	Kinematic Viscosity	m^2/s
ρ	Density	kg/m^3
σ	Stefan Boltzmann constant	$5.67 \cdot 10^8$ J/s m^2 K
τ	Response Time	s
υ	Empirical Temperature	°C
ω	Angular Speed	°/s
ξ	Minor Loss Coefficient	–

Indices

0	Standard Condition
	Initial Condition
air	Dry air
CO2	CO_2
comp	Compressor
cond	Condensation
	Heat Conduction
conv	Heat Convection
corr	Corrected value
db	Dry Bulb
dar	Dry Air Rated
evap	Evaporation
H2O,gas	Water Vapor
H2O,liq	Free Water
hot	Hot Condition
in	Input Value
init	Initialization Value
inlet	Inlet of a Component
lim	Limit value
max	Maximum Value
min	Minimum Value
mix	Value of a mixed air flow
outlet	Outlet of a Component
p	Constant Pressure
v	Constant Volume
out	Output Value
s	Surface
sat	Saturation
trb	Turbine

List of Abbreviations

1D	One Dimension
	One Aperture
2D	Two Apertures
3D	Three Dimension
	Three Apertures
4D	Four Apertures
ACM	Air Cycle Machine
CFD	Computational Fluid Mechanics
CPU	Central Processing Unit
ECS	Environmental Control System
FLECS	Functional Model Library of the Environmental Control System Flow
FR	Resistance
HIL	Hardware in the Loop
ISA	International Standard Atmosphere
LCD	Light Crystal Display
NTU	Number of Transfer Units
PC	Personal Computer
SAT-COM	Satellite Communication
TN	Technical Note
TN_APP	Technical Note Applications (FLECS_WT3.2_5.1_5.2_5.3_TN)
TN_PD	Technical Note Physical Description (FLECS_WT3.1_3.3_3.4_TN)
VCC	Video Control Compartment
VCM	Vapor Cycle Machine

1 Introduction

Within the scope of the FLECS-project (FLECS: *Functional Model Library of the Environmental Control System*) a model-database should be developed, which enables the end-users to simulate the dynamic behavior of an Environmental Control System (ECS: *Environmental Control System*). The definition of test systems and the adequate parameter sets describing aircraft specifications will be given in this Technical Note (TN). Additionally, the requirements for stable and real time capable code are defined. This TN is based on the technical note, which covers the physical description of the FLECS database. In the following this TN is mentioned as TN_PD (FLECS_WT3.1_3.3_3.4_TN).

FLECS follows a strictly modular approach. Sub-components representing generic physical mechanisms or software functions are assembled to components, representing a piece of aircraft equipment or a certain controller function. Components are grouped into component classes covering major aircraft functions to structure the resulting library. Components of the library are available in three different detail levels "Pre-Design", "Simple Dynamic" and "Detailed Dynamic", (see Figure 1) to cope with the different needs during different design phases. Interfaces of the components are standardized to ensure easy replacement of components with different detail levels.

If the design process enters the phase of prototypes, there is a need for product verification. For hardware in the loop (HIL) testing of controllers, simulated equipment is needed to close the loop. HIL testing takes place in a real-time environment, which needs real-time capable simulation models. Such models are integrated on the test rig as C-code, compiled and linked on the target platform. With the chosen simulation tool for FLECS, MATLAB/Simulink, C-Code can automatically be generated. To fulfill real time constraints for the generated C-Code, the user has to use components up to ‘Simple Dynamic’ level. Surprisingly there are fewer performance constraints on HIL test rigs, because the modular structure of the model allows easy distribution of sub-model parts on different processor cards.

A similar principle is applied to the desktop environment: Within the FLECS project, methods are developed to generate C-Code for sub-models, which include the numerical solver for the sub-model. Different step sizes are applied for the different sub-models. This approach results in an optimized use of CPU time, as every sub-model is solved with the most appropriate solver and time step. For future applications it is envisaged to run the sub-models on different CPUs, allowing the creation of comprehensive Software in the Loop test environment.

The principal configuration of an ECS is shown in Figure 2. A cabin is divided into cabin zones. The temperature in each zone is controlled by an independent trim air valve. Conditioned air from the air generation packs and recirculated air from the cabin are mixed inside the mixing unit. From the mixing unit the air flows to the mixing point, where a small amount of hot trim air is added to achieve the selected cabin temperature. The cabin zone with the lowest target

temperature defines the required temperature inside the mixing unit. The trim air valve of this cabin zone is (almost) closed. The opening angles of the trim air valves of the other zones are opened that much to allow enough hot air to pass into the respective duct to the cabin to achieve the demanded cabin zone air temperature. For an ECS two independent controller types are used to ensure all this: The pack controller controls the pack and hence the pack air temperature. The cabin & duct controller controls primarily the opening angle of the trim air valve and hence the cabin zone temperature. Details of control algorithms of existing aircraft are proprietary data of the respective equipment suppliers.

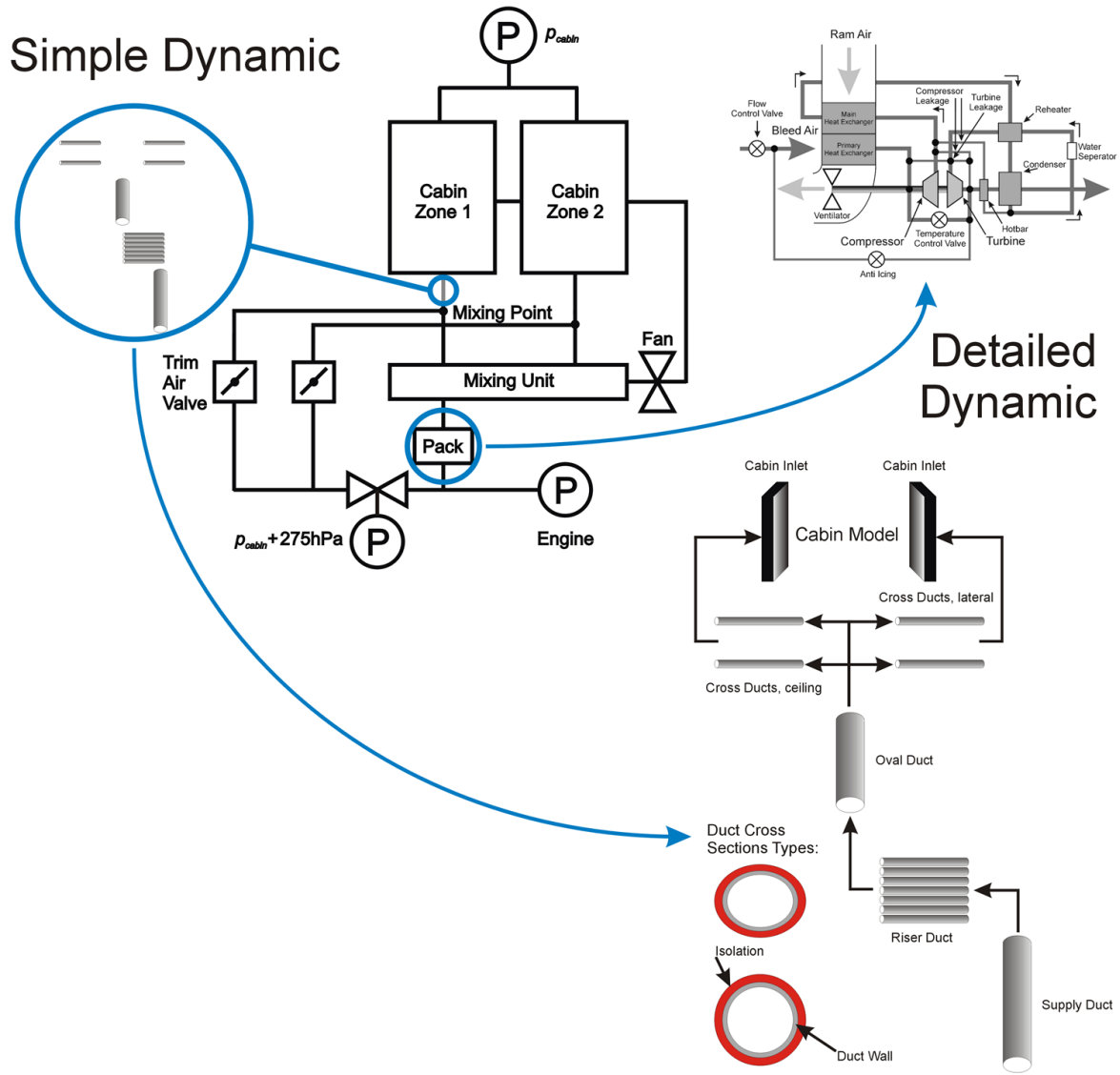

Figure 1: Schematic drawing of the environmental control system

The dynamical behavior of the system is described by state variables, in the following also called dynamical input and output variable. For every dynamical variable a time dependant state equation has to be solved. The thermodynamic and mathematical characterization of these equations should ensure a stable and a real-time capable algorithm. The fundamental configuration respectively the parameterization of this system will be discussed based on a network of volume elements and duct elements.

2 Basic Considerations

With Help of the database elements system simulation can be generated, within these configurations the response to time dependent boundary conditions, and second the system response to certain failure cases can be investigated. MATLAB/Simulink provides the software interface, which enables time resolved simulations.

The inner structure of MATLAB/Simulink is combined with the characterization of time-dependent systems. For each time step *dt* within a given time-range *Δt* the states of the simulated system are calculated (see Figure 2). The state of the system is specified by a set of state variables. The set of state variables is related to a set of state equations. The model blocks can be characterized by two different groups of values. By the constants the medium inside the system is defined. In addition, the parameters characterize the component itself. The state equations are based on thermodynamical and mechanical considerations.

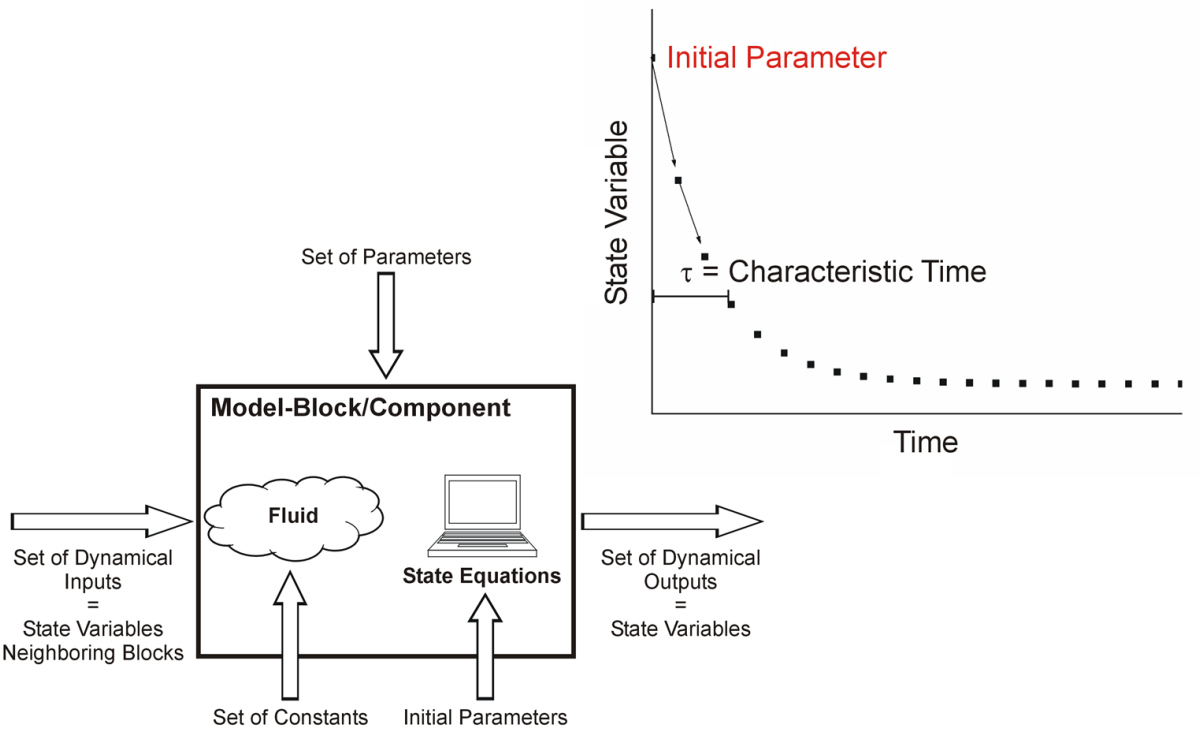

Figure 2: The principal configuration of a model block

Three types of state equations can be distinguished. The rates equations $\dot{y}(t) = f(y(t);t)$, these Equations are related to an integrator and are only solvable, if the initial parameters for each state variable are known. The second type of state equations is a quasi-stationary equation $y(t) = f(t)$, these Equations are solvable without any knowledge of initial parameters. The third type of equations is the steady state type $y(t) = Const$

The integrator is an intrinsic function block of MATLAB/Simulink. The functionality of the integrator is associated with the chosen solver mode. The solver function defines the step size *dt* and the algorithm of integration. MATLAB/Simulink makes available two different solver species. A fixed step solver and a variable step solver. For the developed model-blocks it should be ensured that both solver types are usable, because different processes with different time-velocity constants are looked at. The model tests are carried out with fix step solver types ode4 (Runge-Kutta) and od14x (Newton Solver). In general, a step size of 0.005 s … 0.01 s is chosen. For desktop simulation under variable step solver the stiff solver types ode15s and ode23tb show the best performance. Each Block is parameterized with help of a parameter input mask (see Figure 3).

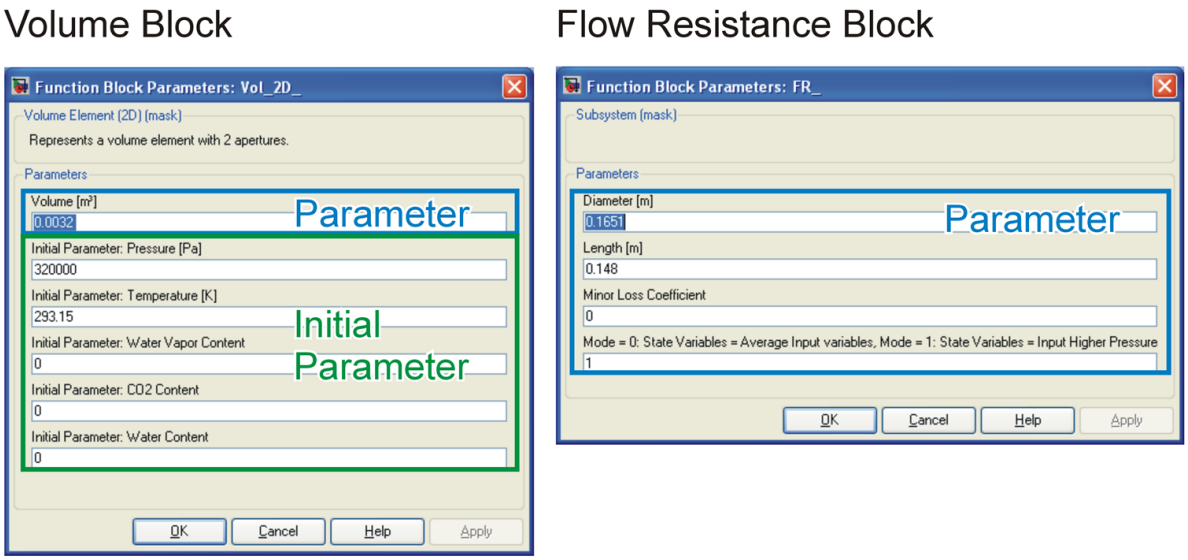

Figure 3: The parameter input mask of a volume block and flow resistance block

In general Simulink blocks, which are related to rate equation (e.g. generalized volume blocks, see Figure 3), need parameters as well as initial parameters as input. Quasi stationary blocks, like a generalized flow resistance, need only parameter as input.

3 Network Configuration and Stability Tests

The stability of a dynamical simulation model is correlated to the configuration of the different model blocks. A simulation consisting of only quasi stationary model blocks (see Figure 4, instable configuration), like flow resistances and nodes is in general dynamical instable. In the case of time dependent boundary limits, high fluctuations can occur. Within quasi stationary blocks the state variables are strongly dependent on the input variables, and therefore strongly dependent of the state variables of the neighboring blocks. Without any integration step a fluctuation inside one block is distributed all over the whole simulation system and can lead to error cases.

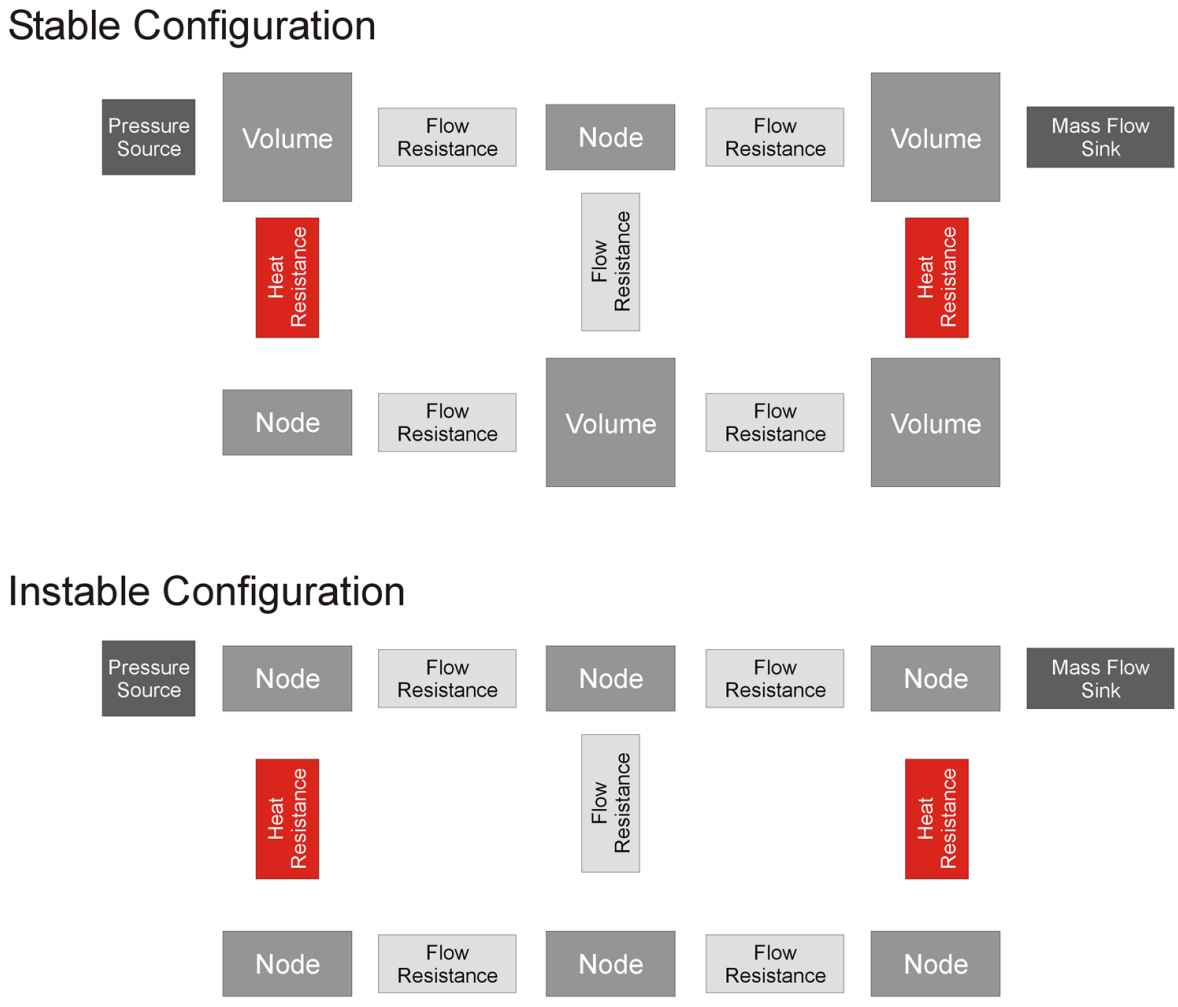

Figure 4: Stable and instable configuration airflow simulation

To overcome this problem, a simulation must be built up with a combination of volume elements and flow resistance (see Figure 4, stable configuration). A volume element is based on rate equations and is related to a thermal capacity. The thermal capacity is described by the mass of the stored air inside the volume. The integration steps stabilize the whole system. With the help of these configurations, also highly dynamic simulation can be run.

The size of the smallest mass respectively the volume inside the system defines the characteristic time τ of the system (see Figure 2) and the value of the usable time step *dt*. The characteristic time of a volume is the described by the ratio of mass m_{air} and the mass flow through the system $\dot{m}_{air}$ ($\tau = m_{air} / \dot{m}_{air}$, τ = 1 s … 50 s)

Therefore, the discretization respectively the number of elements is a critical parameter, which determines the real time capability of the system. For HIL testing the algorithms must run under fix step solver conditions. The developed algorithms are tested with the help of the od4 and od14x solver. To ensure real time capability the time step must be greater than 0.005 s.

The basic element of an air distribution network is a combination of a pair of volumes and a flow resistance (see Figure 5). In Figure 5a a combination of a flow resistance (FR) and two volumes (1D) is shown. The Length of the flow resistance is 10 m (L = 10 m) and the diameter has a value of 0.2 m (D = 0.2m). The volumes on the left hand side (V_{left}) respectively on the right hand side (V_{right}) of the flow resistance have a volume value of 100 m³. The different

Table 1: List of parameters (see Figure 5)

Parameter FR/Duct	
Diameter:	0.2 m
Length:	10.0 m
Minor Loss Coefficient:	0
Mode:	1
Parameter V_{left}	
Volume:	100 m³
Initial Parameter	
Pressure:	120000 Pa
Temperature:	293.15 K
Water Vapor Content:	0
CO_2 Content:	0
Water Content:	0
Parameter V_{right}	
Volume:	100 m³
Initial Parameter	

Pressure:	100000 Pa
Temperature:	293.15 K
Water Vapor Content:	0
CO_2 Content:	0
Water Content:	0

In Figure 5b the flow resistance is split into 2 parts. As pressure defined element in between both flow resistance ($L_1 = L_2 = 5$ m) a node element is used. In Figure 5c the overall flow resistance ($L = 10$ m) is split into three parts ($L_1 = L_2 = L_3 = 3.33$ m). The simulations in Figure 5a … 5c are compared with a simulation consisting of a duct element (see Figure 5d).

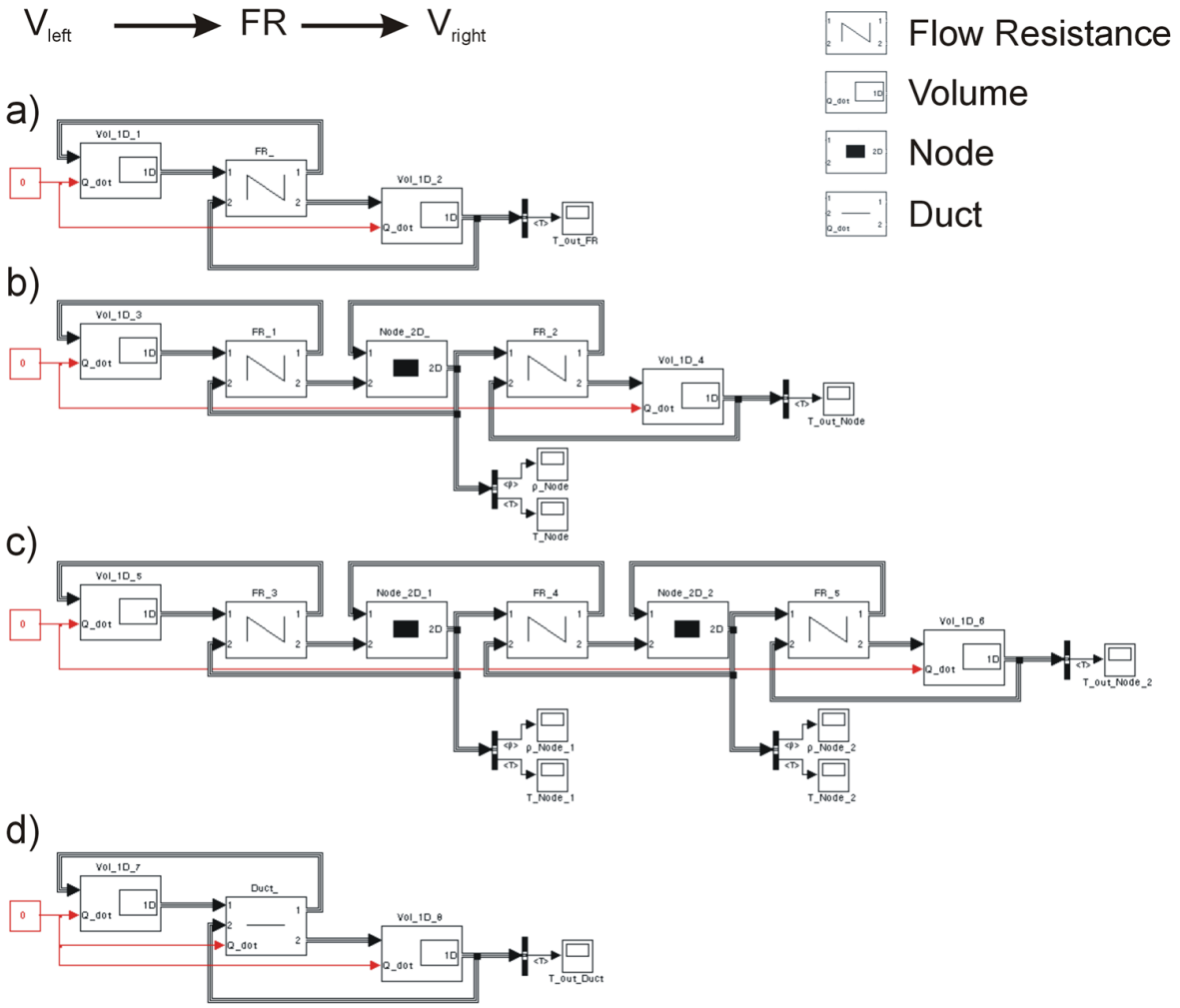

Figure 5: Different configuration of a basic element of an air distribution network

The temperature profiles inside the volume V_{right} is shown in Figure 6. The parameters listed in Table 1 describe the compressible conditions. Under these conditions the four different configurations show an equivalent performance.

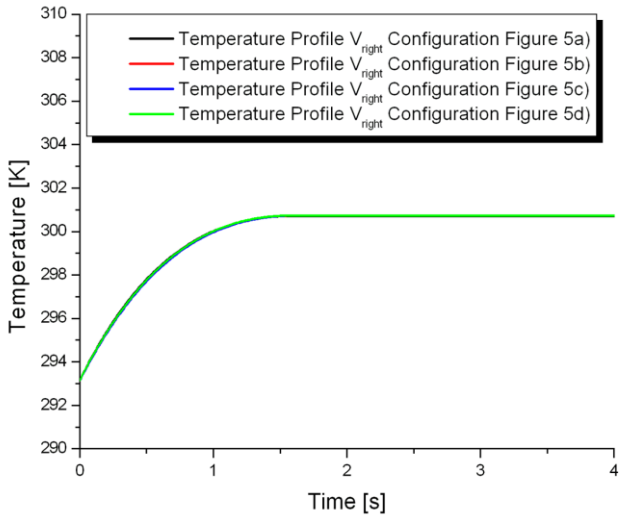

Figure 6: Incompressible conditions: the temperature profiles inside the volume V_{right}

Under compressible conditions the derivations between the four configurations occur (see Figure 7). As higher the discretization of the system as longer the characteristic time τ will become. Assuring compressible condition, the initial pressure inside the volume V_{left} is enhanced to 300000 Pa.

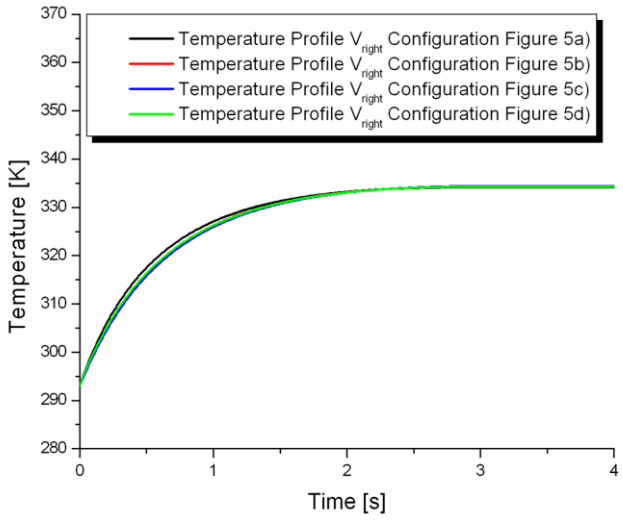

Figure 7: Compressible conditions: The temperature profiles inside the volume V_{right}

3.1 Test of Compressible Flow Conditions

Compressible flow conditions occur when one of the boundary limits of system is time dependent. In Figure 8 a combination of a flow resistance respectively a duct and a so-called test volume is driven by an external pressure source $p_{external}$. $p_{external}$ is heavily time dependent (see Figure 8 and 9). Within a time range of 2.5 s the pressure rises from 320000 Pa up to almost 700000 Pa. In additionally 2.5 s the pressure decrease from 650000 Pa back to value of 280000 Pa. The pressure source pushes the air through the flow resistance into a test volume V_{test}. Test volumes are characterized by a volume respectively a thermal capacity, which has no influence on the characteristic time of the overall system.

Table 2: List of parameters (see Figure 8)

Parameter FR/Duct	
Diameter:	0.2 m
Length:	10.0 m
Minor Loss Coefficient:	0
Mode:	1
Parameter V_{test}	
Volume:	0.05 m³
Initial Parameter	
Pressure:	320000 Pa
Temperature:	293.15 K
Water Vapor Content:	0
CO_2 Content:	0
Water Content:	0
Parameter $p_{external}$	
Temperature:	293.15 K

Three different configurations are compared:

- The air is pushed through a flow resistance into the test volume (see Figure 8a).
- The air is pushed through a duct into the test volume (see Figure 8a).
- The air is pushed through a serial connection of ducts (discretization: 10x) into the test volume (see Figure 8a).

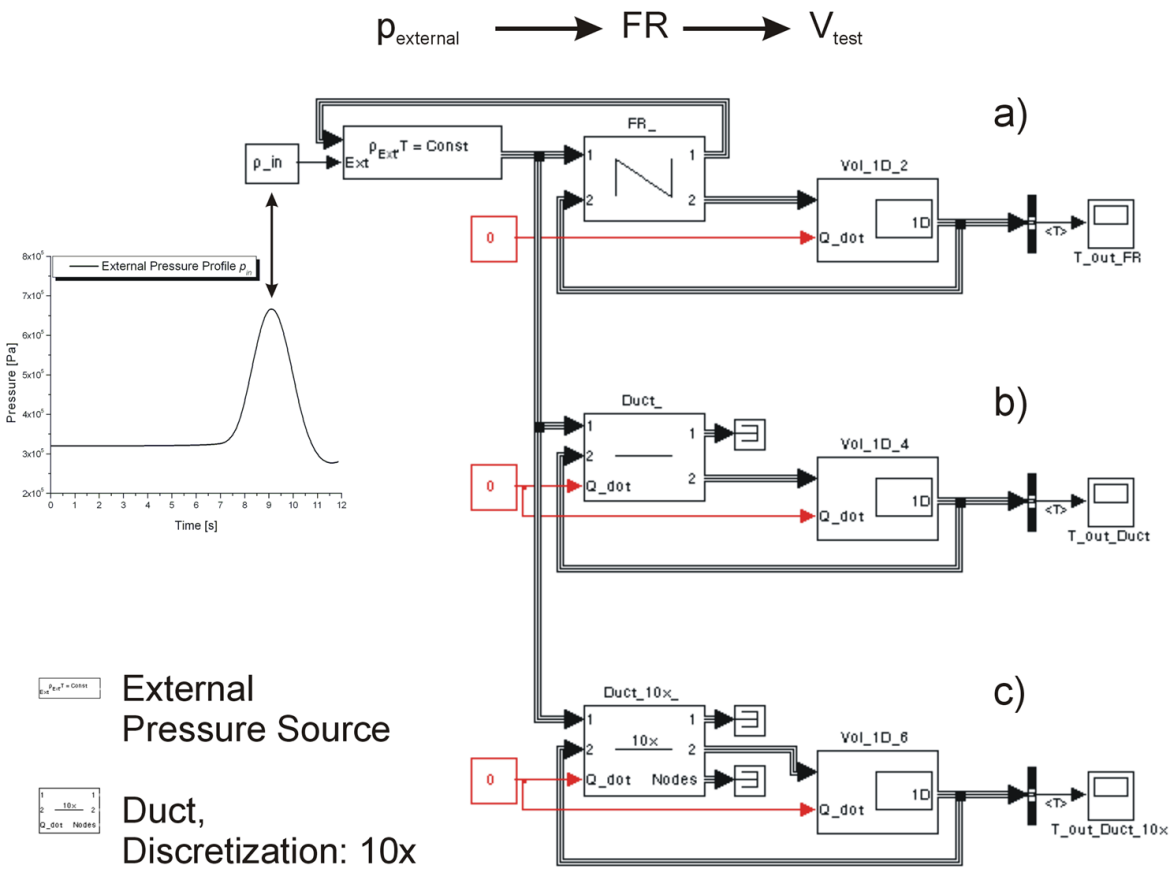

Figure 8: Different configuration compressible flow simulation

The result of the simulations is shown in Figure 9. The configuration based on a flow resistance underestimates obviously the compression inside the flow resistance. The configuration with a duct result in good estimation of the compression. Enhancing the performance the duct has to be discretized. The discretization of a duct is serial connection of several ducts. The best estimation is given by a discretization of 10.

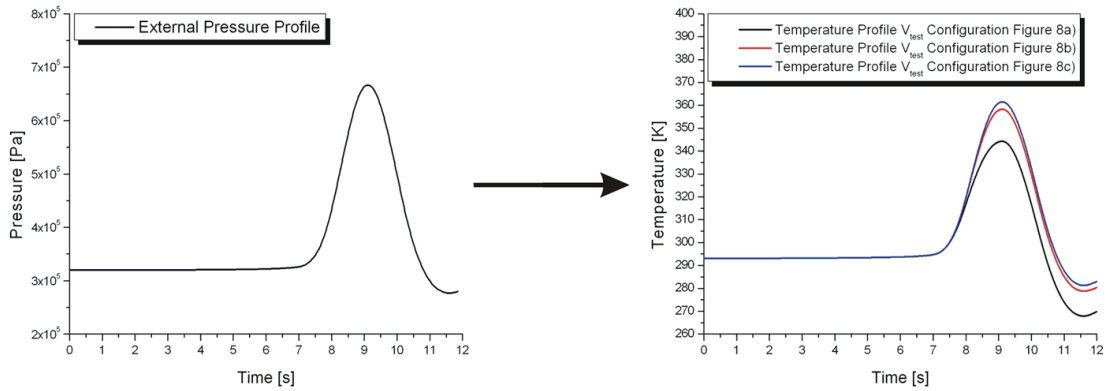

Figure 9: The temperature profiles inside the test volume V_{test}

Based on the consideration above, a highly dynamic flow system can be built up (see Figure 10). During such simulation the stability and the dynamic performance of the developed model blocks can be checked. The shown T-joint is composed of a combination of volume elements and flow resistances respectively a discretized duct (discretization: 10x). Each flow resistance is correlated to a volume. Each volume has size of $(\pi / 4)\, D^2\, L$ (D: Diameter FR, L: Length FR). Via the output a constant mass flow (1 kg/s) leaves the system. The pressure at the input rises up within 2.5 s from 320000 Pa to 650000 Pa (see Figure 9, left graph). As a result, the gas mixture inside the system is compressed by the pressure wave. After the pressure has reached the maximum value, the pressure falls back within 2.5 s to a value of 280000 Pa. As a consequence, the gas is able to expand. One output of the T-joint is closed by an end piece. The T-joint is described with help of a test volume V_{test}. The mass flow inside the end piece is shown in Figure 10, bottom graph. In the time range marked with a blue circle the mass flow changes the sign. The occurrence of small mass flows normally causes instabilities during a simulation. The model blocks used are optimized so that such systems are stable, independently of what kind of solver type is used.

Table 3: List of parameters (see Figure 10)

Parameter Duct Input	
Diameter:	0.165 m
Length:	9.332 m
Minor Loss Coefficient:	0
Mode:	1
Discretization:	10
Parameter FR End Piece	
Diameter:	0.165 m
Length:	0.494 m
Minor Loss Coefficient:	0
Mode:	1
Parameter FR output	
Diameter:	0.165 m
Length:	1.606 m
Minor Loss Coefficient:	0
Mode:	1

Parameter Volume	
Volume:	$(\pi / 4)\, D^2\, L$
Initial Parameter	
Pressure:	320000 Pa
Temperature:	293.15 K
Water Vapor Content:	0
CO_2 Content:	0
Water Content:	0
Parameter V_{test}	
Volume:	0.05 m^3
Initial Parameter	
Pressure:	320000 Pa
Temperature:	293.15 K
Water Vapor Content:	0
CO_2 Content:	0
Water Content:	0
Parameter $p_{external}$	
Temperature:	293.15 K

To check the dynamic behavior of the model blocks, the output temperature is compared with the temperature curve of a Flowmaster Simulation (see Figure 10, top graph). The setup of the simulation within the two programs is comparable. In contrast to the integration of differential equations in the FLECS/Simulink model blocks, Flowmaster uses the hydraulic transient analysis method.

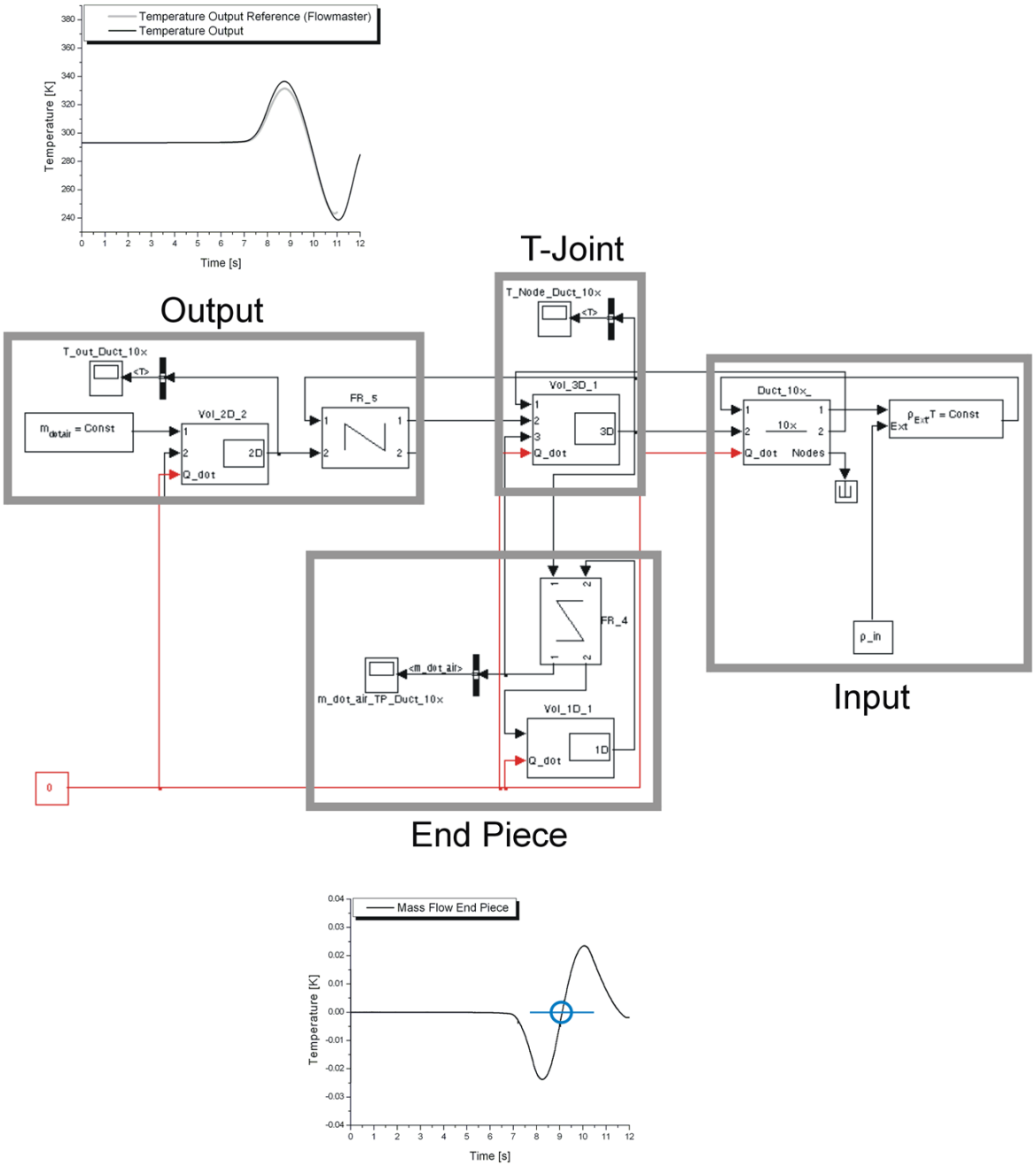

Figure 10: A highly dynamic simulation of a T-joint. The Simulink result is compared with a Flowmaster data set

3.2 Simulation of Aircraft Cabin Temperature Control

A schematic of an environmental control system of an aircraft consisting of 2 zones is shown in Figure 1.

Temperature control details follow from Figure 11: The cabin & duct controller is a serial connection of a PI-type cabin controller, which defines the target temperature for the duct controller. The controlled variable of the cabin & duct controller is the supply temperature in the mixing point. The actuating variable of the duct controller is angular velocity of the opening angle of the trim air valve. The temperature of the pack is controlled by the pack controller. Control algorithms used in the simulation are those proprietary to the equipment manufacturer. Individual simplified control algorithms could be defined based on the control principles explained.

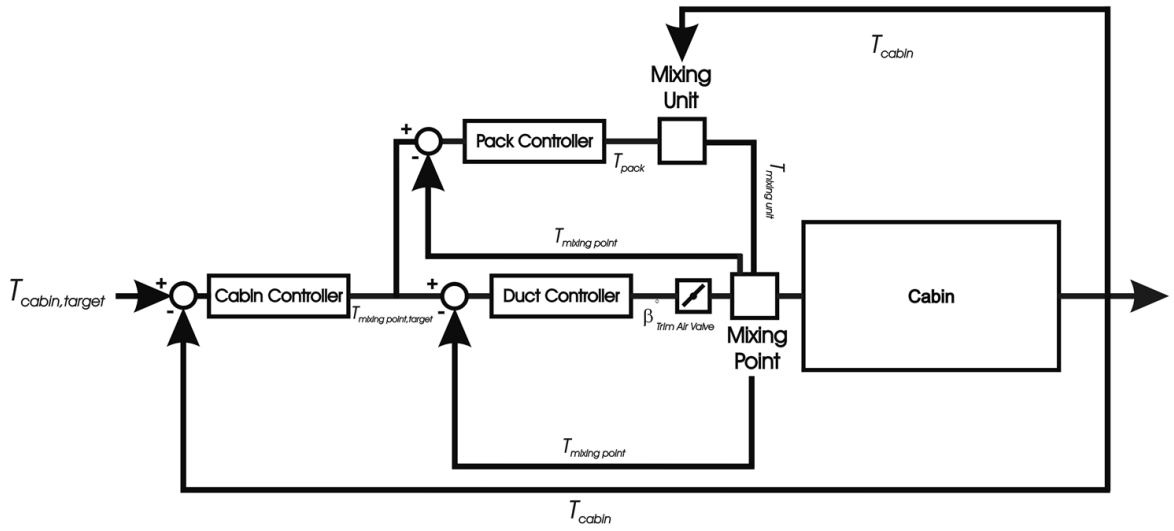

Figure 11: The control aspects of a cabin simulation

Validated FLECS components (see TN_PD) were used to build up a simulation of a generic single aisle air distribution network and aircraft cabin model. The cabin is separated into two zones that are assumed to be identical. Each zone has its own trim air valve (see Figure 1).

The pack is not simulated in detail; instead, a mass flow source is used as simplified pack model. The air of the cabin is recirculated by a fan into the mixing unit. The overall mass flow is fixed to 1.8 kg/s. The fan parameters are chosen in a way that 50 % of this mass flow is contributed by the pack the other 50% is contributed by the recirculation. The parameters describing the different controllers will not be discussed. The parameters and values of the trim air system, the mixing unit, the pack and the recirculation fan as used in the generic simulation (see Figure 12) are given in Table 4. The rotational speed of the fan component (see Figure 13) is adjusted to assure an average mass flow of 0.9 kg/s.

The cabin consists of 2 zones. The simulation model of the cabin is described by the following parameters (see Figure 15a … 15c):

Ambient conditions:

- Flight altitude
- Skin temperature
- Mach number

Cabin zone parameters:

- Air volume
- Mass interior
- Specific heat capacity interior
- Exchange surface cabin/floor
- Exchange surface interior
- Exchange surface cabin/skin
- Number windows
- Area windows
- Number Passengers
- Convection heat transfer coefficient:
    - Skin
    - Floor

The overall heat loads were:
Heat load skin
Heat load floor
Heat load electrical (IFE + lights)
Heat load solar
Heat load galley
Heat load passengers
Heat capacities of a cabin zone were:

- Heat capacity air
- Heat capacity interior

Compared to the air distribution network, the cabin interior can only be described in a simplified way by means of a representative mass, a specific heat capacity and an assumed exchange surface. The thermal capacities of the aircraft skin and the cabin floor are neglected. The electrical load heat can be parameterized in a detailed and simplified form. The detailed description classifies the heat load by personal computer (PC) usage, light crystal display (LCD) usage, video control compartment (VCC) usage and satellite communication (SAT-COM) usage. The simplified form (see Equation 1) distinguishes several passengers (n_{pax}) and flight attendance (n_{att}) dependent part and a constant part ($K_{electrical}$). Each passenger, respectively flight attendant, produces a certain amount of water vapor and CO_2.

Volumic Ratio :

$$x_{cabin} = \frac{V_{cabin,zone}}{V_{cabin}}$$

Heat Load Skin :

$$\dot{Q}_{skin} = x_{cabin}\ \lambda_{skin}\ A_{skin}\ (T_{skin} - T_{cabin})$$

Heat Load Human :

$$\dot{Q}_{human} = (2\ n_{att} + n_{pax})\ (188 - 4.7\ (T_{cabin} - 273.15))$$

$$\left\{\begin{matrix}\dot{Q}_{human} = 0\,, T_{cabin} < 273.15\ \mathrm{K} \\ \dot{Q}_{human} = 0\,, T_{cabin} > 313.15\ \mathrm{K}\end{matrix}\right\}$$

Heat Load Floor :

$$\dot{Q}_{floor} = x_{cabin}\ \lambda_{floor}\ A_{floor}\ (T_{floor} - T_{cabin})$$

Heat Load Interior :

$$\alpha_{interiors} = 4\ v_{air} + 5.6$$

$$\dot{Q}_{interiors} = \alpha_{interiors}\ A_{interiors}\ (T_{interiors} - T_{cabin})$$

$$\dot{T}_{interiors} = -\frac{\dot{Q}_{interiors}}{m_{interiors}\ c_{interiors}}$$

Heat Load Solar :

$$h_{flight} = 0$$

$$h_{flight} = 0 :\ \dot{Q}_{solar} = n_{windows}\ A_{window}\ q_{solar,ground}$$

$$h_{flight} > 0 :\ \dot{Q}_{solar} = n_{windows}\ A_{window}\ q_{solar,flight}$$

$$P_{blind,open} < 0.5 : \qquad \dot{Q}_{solar} = 0$$

$$h_{flight} = 0, T_{skin} < 273.15\ \mathrm{K} : \quad \dot{Q}_{solar} = 0$$

$$P_{cloud} > 0.5 : \qquad \dot{Q}_{solar} = 0$$

$$P_{day,night} < 0.5 : \qquad \dot{Q}_{solar} = 0$$

Heat Load Galley :

$$h_{flight} = 0 :\ \dot{Q}_{galley} = x_{cabin}\ \dot{Q}_{galley,ground}$$

$$h_{flight} > 0 :\ \dot{Q}_{galley} = x_{cabin}\ \dot{Q}_{galley,flight}$$

Electrical Heat Load, Simplified :

$$\dot{Q}_{electrical} = (n_{pax} + n_{att})\ 3.5 + K_{electrical}$$

$$\dot{Q}_{electrical} = (n_{pax}\ 6.4 + n_{att}\ 3.5) + K_{electrical} \qquad (1)$$

Electrical Heat Load, Detailed :

$$h_{flight} = 0:$$

$$Q_{IFE} = (n_{seats} - n_{pax})\,(\dot{Q}_{pc,standby} + \dot{Q}_{lcd,standby}) + n_{pax}\; P_{pc,ground}\; \dot{Q}_{pc,operation}$$
$$+ n_{pax}\; P_{lcd,ground}\; \dot{Q}_{lcd,operation} + n_{pax}\;(1 - P_{pc,ground})\,\dot{Q}_{pc,standby} + n_{pax}\;(1 - P_{lcd,ground})\,Q_{lcd,standby}$$
$$+ n_{pax}\;(\dot{Q}_{vcc} + \dot{Q}_{lcd,projector} + \dot{Q}_{sat,com})$$

$$Q_{light} = \dot{Q}_{cabin,light} + n_{pax}\; P_{reading,ground}\; \dot{Q}_{reading,light}$$

$$h_{flight} > 0:$$

$$Q_{IFE} = (n_{seats} - n_{pax})\,(\dot{Q}_{pc,standby} + \dot{Q}_{lcd,standby}) + n_{pax}\; P_{pc,flight}\; \dot{Q}_{pc,operation}$$
$$+ n_{pax}\; P_{lcd,flight}\; \dot{Q}_{lcd,operation} + n_{pax}\;(1 - P_{pc,flight})\,\dot{Q}_{pc,standby} + n_{pax}\;(1 - P_{lcd,flight})\,Q_{lcd,standby}$$
$$+ n_{pax}\;(\dot{Q}_{vcc} + \dot{Q}_{lcd,projector} + \dot{Q}_{sat,com})$$

$$Q_{light} = \dot{Q}_{cabin,light} + n_{pax}\; P_{reading,flight}\; \dot{Q}_{reading,light}$$

$$\dot{Q}_{electrical} = \dot{Q}_{IFE} + \dot{Q}_{light} \tag{1}$$

Table 4: List of parameters (see Figure 12)

Parameter Trim Air System	
Pressure:	102750 Pa
Temperature:	453.15 K
Diameter:	0.051 m
Length:	5 m
Minor Loss Coefficient:	0.5
Mode:	1
Effective Area:	0.00085 m²
Parameter Supply Duct	
Diameter:	0.2 m
Length:	20 m
Minor Loss Coefficient:	2

Mode:	1
Parameter Mixing Unit	
Volume:	0.7 m²
Initial Parameter	
Pressure:	75250 Pa
Temperature:	293.15 K
Water Vapor Content:	0
CO_2 Content:	0
Water Content:	0
Parameter Pack	
Mass flow:	0.9 kg/s
Parameter Recirculation Fan	
Diameter:	0.2 m
Rotational Speed:	7500 … 10250 1/min
Reference: Rotational Speed:	1 1/min
Lower Limit: Rotational Speed:	3000 1/min
Fan Curve	
a_3:	0
a_2:	-13000 Pa/(kg/s)^2
a_1:	1.6 Pa/(kg/s)
a_0:	-0.0000086 Pa
$\dot{V}_{\text{lim}}$:	2 kg/s

The following test case for a dynamical simulation of the environmental control system of a cabin consisting of 2 zones (see Figure 12 and Figure 13) is defined.

Test Case:
Time: 0 s … 1200 s
The aircraft is on ground. The ambient conditions are described by a temperature of 20 °C = 293.15 K and a pressure of 1013 hPa. The skin temperature is assumed to be 20 °C (cloudy

day). The target temperature of the cabin is also 20 °C. In each cabin zone 3 people of the service personnel and 3 flight attendants are working.

Time: 1200 s … 2400 s
The aircraft is on ground. The service personnel leave the cabin and the boarding starts. The target temperature of the cabin is 20 °C. In 20 minutes, 200 passengers enter the cabin, assuming a constant flow of passengers. The heat load, which flows into the cabin, increases drastically.

Time: 2400 s … 8400 s
2400 s: The boarding is completed. The aircraft starts. In 990 s the aircraft climbs to a flight altitude of 33000 ft (climb rate 2000 ft/min) (see Figure 13). The ambient conditions are described by an ISA condition. Knowing the ambient temperature $T_{ambient}$ the skin temperature T_{skin} can be calculated ($T_{skin} = T_{ambient}$ (1 + 0.18 Ma²), Ma: Mach number) (see Figure 13). The target temperature of the cabin zone 1 is 22 °C = 295.15 K, the target temperature of the cabin zone 2 is 24 °C = 297.15 K. The cabin pressure is fixed to 752 hPa. This value corresponds to a cabin altitude of 7000 ft.

The profiles of the aircraft altitude, cabin pressure and rotational speed of the fan are shown in Figure 13. The simulated temperature profiles in zone 1 and zone 2 are shown in Figure 14a. In the time range 0 s … 1200 s the simulation has to tune itself. At the end the target temperature of 20 °C = 293.15 K is reached. During the boarding the temperatures rise up. The reason for that is the increasing heat load of the passengers. The chosen pack mass flow 0.9 kg/s is too small to control the temperature of the cabin to 20 °C. The ambient temperature at an altitude of 33000 ft is -50.4 °C = 222.75 K. During the climb flight of the aircraft the skin temperature falls from 20 °C to -24.5 °C (293.15 K … 248.65 K). As a result, the cabin loses a huge amount of heat. The temperature in the cabin is controlled to 22 °C = 295.15 K (zone 1) and 24 °C = 297.15 K (zone 2) (see Figure 14a). In the first 150 s the temperatures rise. As a result of the falling skin temperature, the target temperatures cannot be reached. The zone temperatures start to sink. Not until the flight altitude has reached the maximum value can the temperature be controlled to the target values.

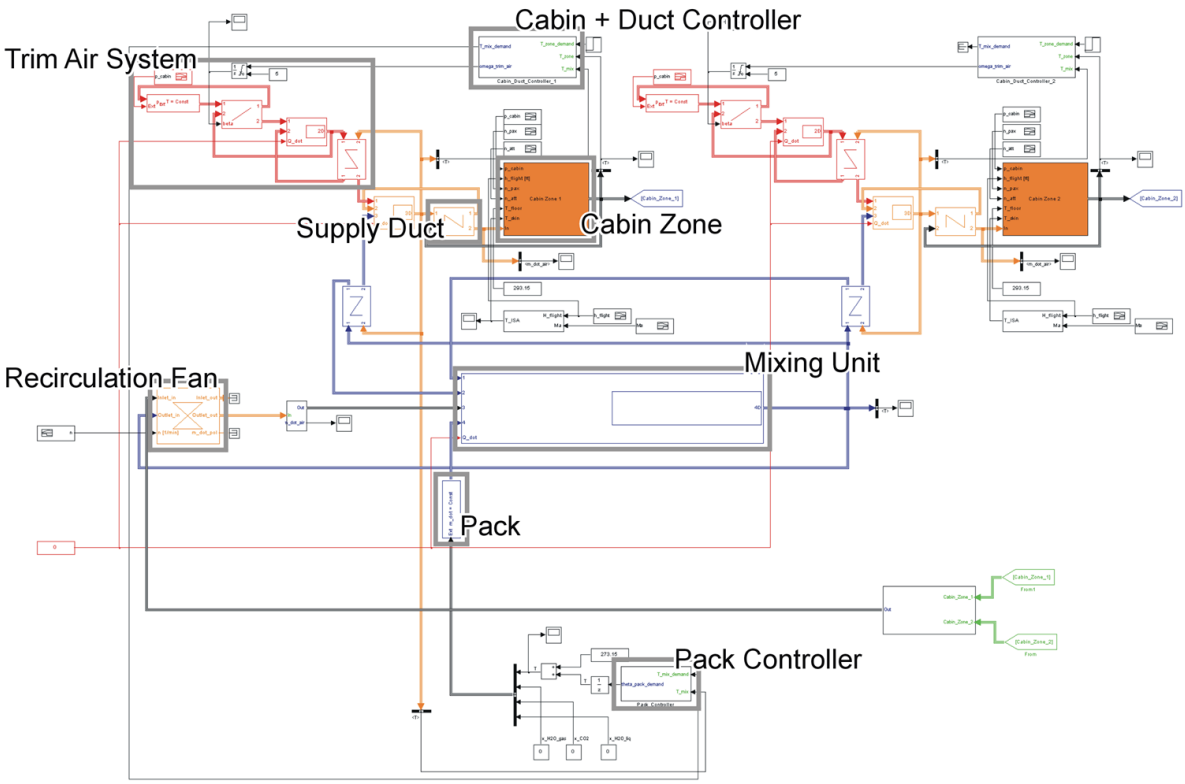

Figure 12: Simulink Configuration of an environmental control system of a cabin model consisting of 2 zones (see Figure 1 and Figure 11)

The control behavior of the cabin & duct controller is shown in Figure 14b. The trim air valve has a minimum opening angle of 5°. In the first 2400 s the trim air valve is fixed to this minimum angle. Only a small amount of hot bleed air flows into the system. Correlated with the start of the flight, the valves open. The valve angles increase. The dynamic of the trim air valve of zone 2 differs clearly compared with the dynamic of the trim air valve of zone 1. At the time when the target temperatures are reached, the opening angle of trim air valve 1 approach 15.3° the limit of the opening angle of trim air valve 2 is 22.2°.

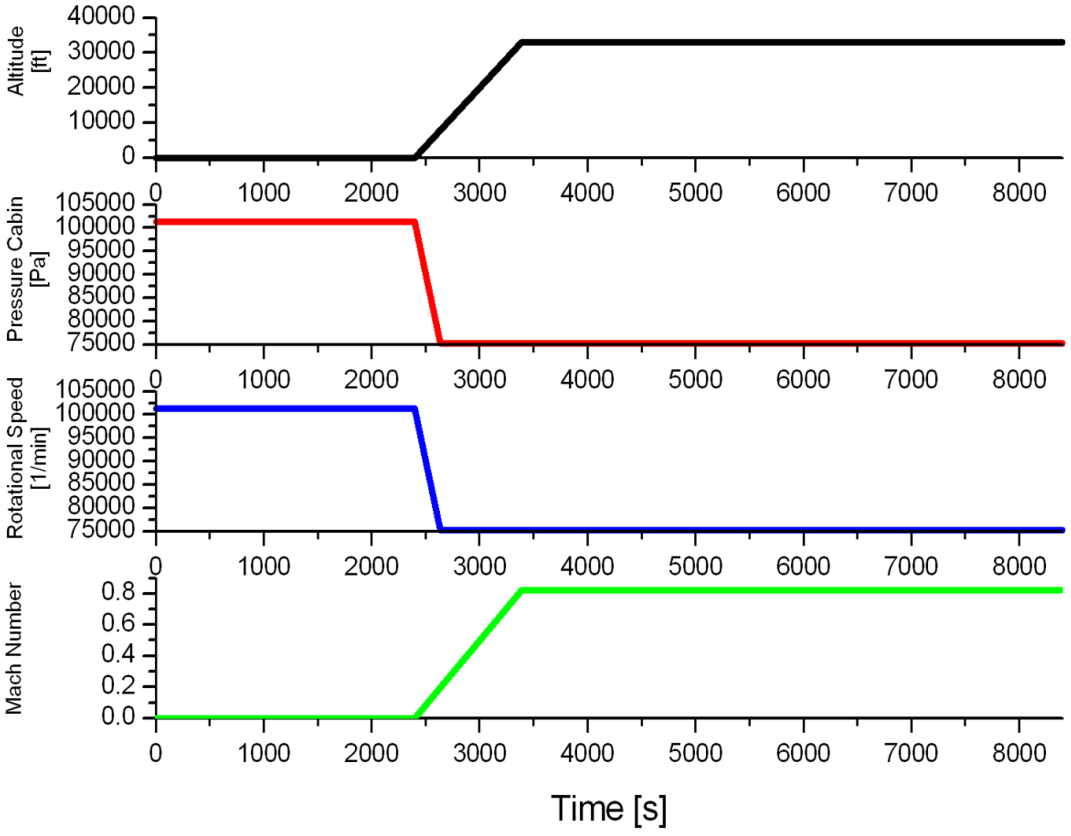

Figure 13: Profiles of the aircraft altitude, cabin pressure and rotational speed

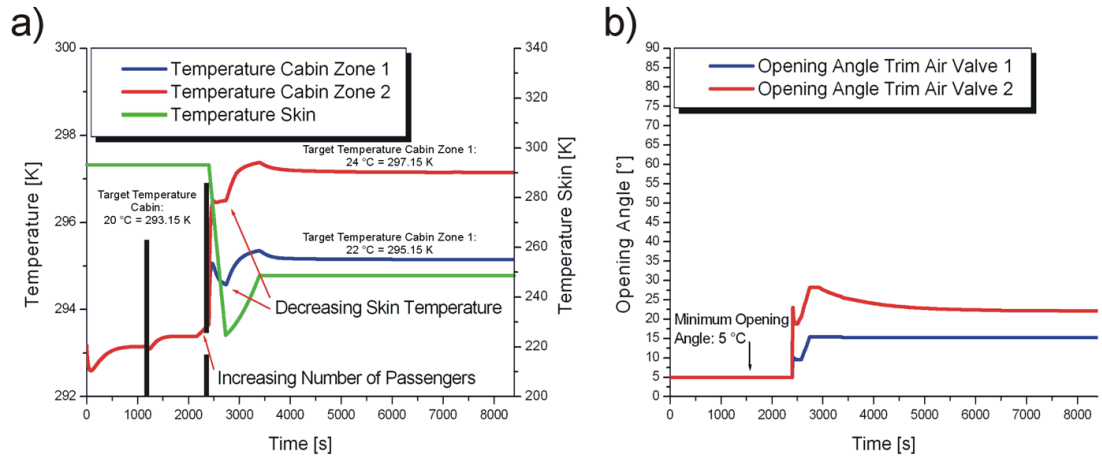

Figure 14: a) Simulated temperature profiles in zone and zone 2 and the used skin temperature profile. b) Opening angle of trim air valves of zone 1 and zone 2

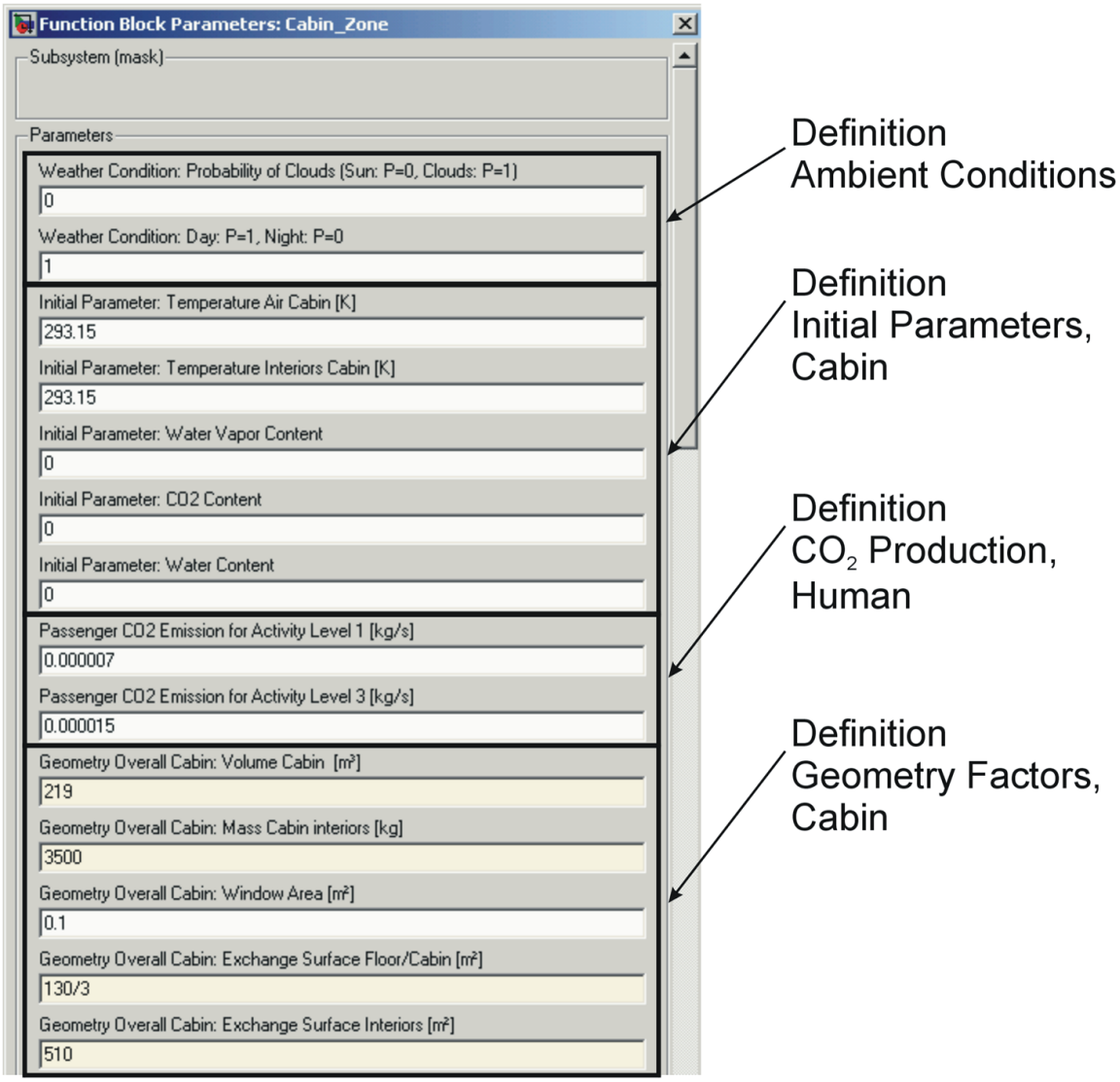

Figure 15a: Input parameter mask of a cabin model. The parameters shown correspond to the A320.

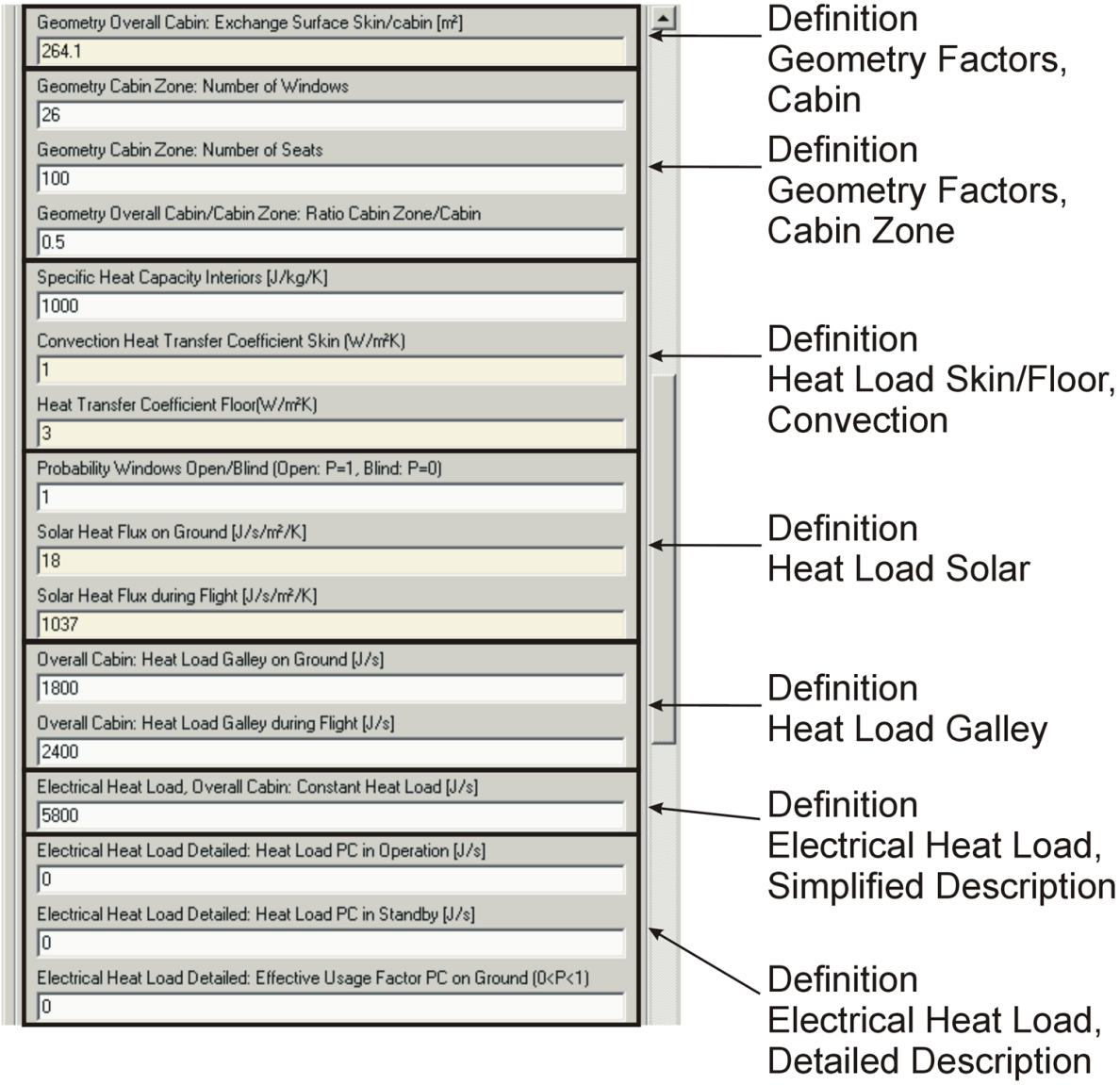

Figure 15b: Input parameter mask of a cabin model. The parameters shown correspond to the A320.

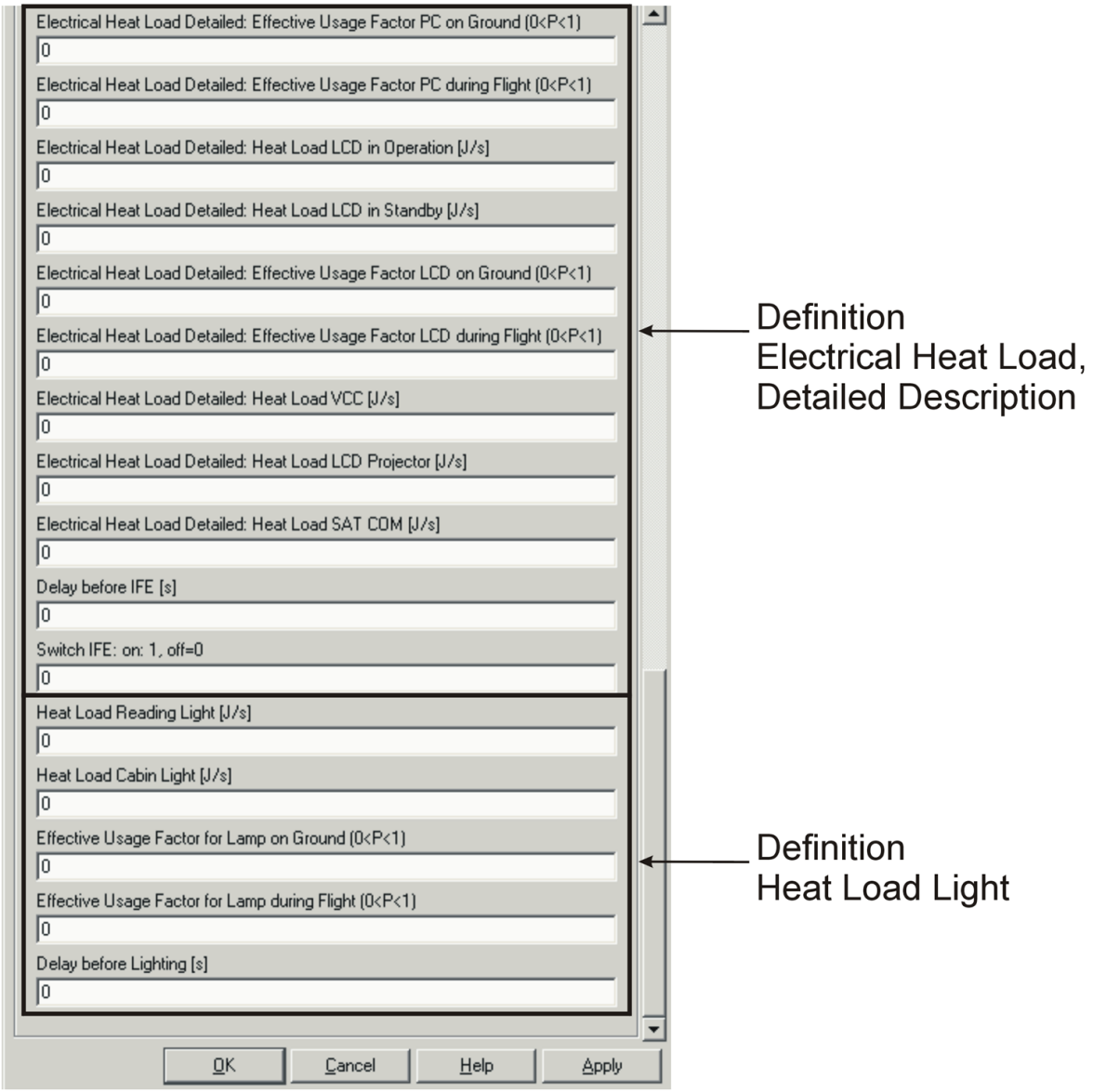

Figure 15c: Input parameter mask of a cabin model. The parameters shown correspond to the A320.

3.3 Dynamical Simulations of Heat Exchangers

The algorithm of a heat exchanger can be divided in static and dynamic description. Within the static description the overall heat transfer at the static equilibrium (see TN_PD, Equation 56 … 61) is calculated. Within the dynamic description the additional response time of the heat exchanger has to be estimated.

The response time is characterized by the thermal capacity of the heat transfer material. In general, a heat exchanger is composed of aluminum. The specific heat capacity has a value of 900 J/kg K.

In Figure 16 different heat exchanger types like plat fin heat exchanger and tubular heat exchanger are shown. In industrial applications also tube shell heat exchangers are used. In the following considerations the different types are specified by a characteristic map (see Figure 29).

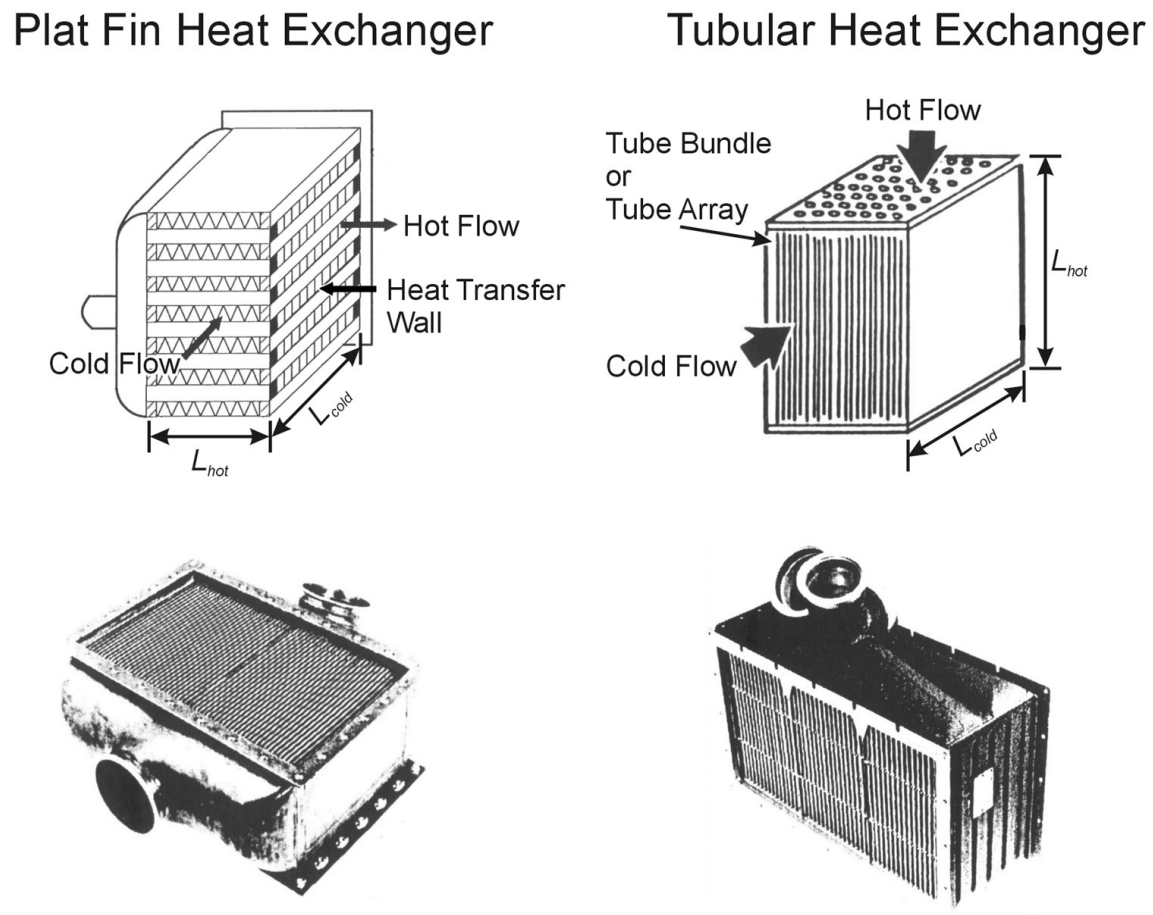

Figure 16: Different heat exchanger types (**Allied-Signal 1990**)

Important for the inner structure of the algorithm is the configuration of the heat exchanger. In the case of an efficiency equal 1 the outgoing temperature of the cold side $T_{cold,out}$ is equal the outgoing temperature of the hot side $T_{hot,out}$ (see Figure 16 and Figure 17). In counter flow or

cross flow configuration the outgoing temperature of the hot side $T_{hot,out}$ is equal the incoming temperature of the cold side $T_{cold,in}$ (see Figure 17).

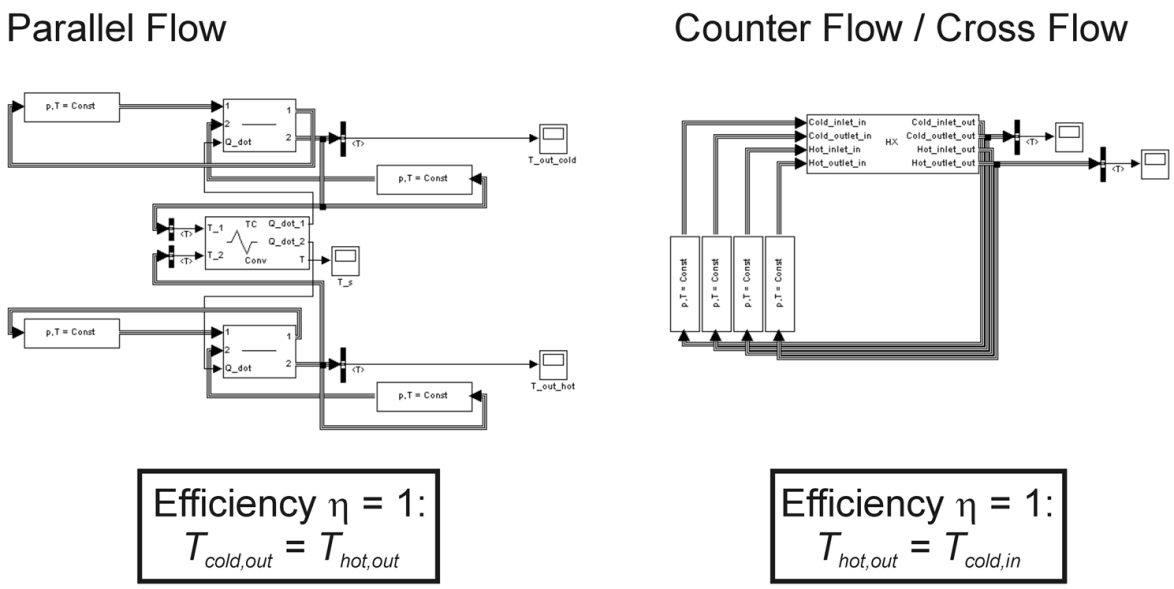

Figure 17: Different heat exchanger configurations

The algorithm of a counter flow or cross flow configuration is described in TN_PD, Equation 62 and 63. In an analogous way the algorithm of a parallel flow configuration can be derived (see Equation 2). Both configurations are compared with help of a parameter set shown in Table 5

$$\dot{Q}_{\max} = \left(T_{hot,in} - T_{cold,in}\right) \frac{\dot{m}_{cold}\ \dot{m}_{hot}\ \bar{c}_{p,cold}\ \bar{c}_{p,hot}}{\dot{m}_{cold}\ \bar{c}_{p,cold} + \dot{m}_{hot}\ \bar{c}_{p,hot}}$$

$$T_{hot}(x) = T_{wall} + \left[T_{hot,in} - T_{wall}\right] \exp(-a_{hot}\ \frac{x}{L_{hot}})$$

$$T_{cold}(x) = T_{wall} + \left[T_{cold,in} - T_{wall}\right] \exp(-a_{cold}\ \frac{x}{L_{cold}})$$

$$\eta_{cold} = \eta_{hot} = \eta = \frac{\dot{m}_{cold}\ \bar{c}_{p,cold}\ (T_{cold}(L_{cold}) - T_{cold,in})}{\dot{Q}_{\max}} = \frac{\dot{m}_{hot}\ \bar{c}_{p,hot}\ (T_{hot,in} - T_{hot}(L_{hot}))}{\dot{Q}_{\max}}$$

$$\Downarrow$$

$$a_{cold} = -\ln\left(1 - \frac{\eta\ \dot{Q}_{\max}}{\dot{m}_{cold}\ \bar{c}_{p,cold}\ (T_{wall} - T_{cold,in})}\right) = \frac{\alpha_{cold}\ A_{cold}}{\dot{m}_{cold}\ \bar{c}_{p,cold}} = \frac{F_{\alpha A,cold}}{\dot{m}_{cold}\ \bar{c}_{p,cold}}$$

$$a_{hot} = -\ln\left(1 - \frac{\eta\ \dot{Q}_{\max}}{\dot{m}_{hot}\ \bar{c}_{p,hot}\ (T_{hot,in} - T_{wall})}\right) = \frac{\alpha_{hot}\ A_{hot}}{\dot{m}_{hot}\ \bar{c}_{p,hot}} = \frac{F_{\alpha A,hot}}{\dot{m}_{hot}\ \bar{c}_{p,hot}} \qquad (2)$$

$$\Downarrow$$

$$\overline{T}_{cold} = T_{wall} + (T_{cold,in} - T_{wall})(1 - e^{-a_{cold}})/a_{cold}$$
$$\overline{T}_{hot} = T_{wall} + (T_{hot,in} - T_{wall})(1 - e^{-a_{hot}})/a_{hot}$$

$$\Downarrow$$

$$\dot{Q}_{wall,cold} = F_{\alpha A,cold}\ (T_{wall} - \overline{T}_{cold})$$
$$\dot{Q}_{wall,hot} = F_{\alpha A,hot}\ (T_{wall} - \overline{T}_{hot}) \qquad (2)$$

Table 5: List of parameters (see Figure 17)

Parameter Cold Side	
Pressure Inlet:	100200 Pa
Pressure Outlet:	99700 Pa
Temperature Inlet:	344.15 K
Parameter Hot Side	
Pressure Inlet:	226300 Pa
Pressure Outlet:	221000 Pa
Temperature Inlet:	448.15 K
Parameter Heat Transfer Wall	
Mass:	15 kg
Specific Heat Capacity:	900 J/kg K
Initial Parameter: Temperature:	311.15 K
Parallel Flow: Parameter Duct, Cold Side	
Diameter:	0.108 m
Length:	1 m
Minor Loss Coefficient:	0
Mode:	1
Parallel Flow: Parameter Duct, Hot Side	
Diameter:	0.0436 m
Length:	1 m
Minor Loss Coefficient:	0

Mode:	1
Counter Flow: Parameter Duct, Cold Side	
K_1:	492.3 Pa
m_1:	1.45
Counter Flow: Parameter Duct, Hot Side	
K_1:	39365.7 Pa
m_1:	1.827

The given parameters are related to the mass flows $\dot{m}_{cold} = 0.888$ kg/s and $\dot{m}_{hot} = 0.407$ kg/s. Assuming that both configurations are working on the same heat transfer superscripts a_{cold} and a_{hot}, the heat transfer efficiency of parallel flow configuration is much smaller than the efficiency of the counter respectively cross flow configuration (see Equation 3). Because of the higher efficiency in industrial applications always counter or cross flow heat exchanger are used.

The result of the comparison is shown in Figure 18a and 18b. Under parallel flow conditions the outlet temperature of the hot side is always higher than the outlet temperature of the cold side.

$$\begin{gathered} a_{cold} = 0.913 \\ a_{hot} = 1.056 \\ \Downarrow \\ \begin{array}{cc} \text{Parallel Flow :} & \text{Counter Flow :} \\ \text{Efficiency } \eta = 0.6264 & \text{Efficiency } \eta = 0.8625 \end{array} \end{gathered} \tag{3}$$

Additionally, the parallel configuration requires only one heat transfer wall temperature. By contrast the algorithm of a counter flow heat exchanger requires two independent wall temperatures (see Figure 18b).

A heat exchanger can be classified by a dimensionless value *NTU* (NTU: *Number of Transfer Units*) (see Equation 4)

$$\begin{gathered} \frac{1}{NTU} = \dot{m}_{min}\ \bar{c}_p \left[\frac{1}{F_{\alpha A,cold}} + \frac{1}{F_{\alpha A,hot}} \right] \\ \dot{m}_{min} = \begin{Bmatrix} \dot{m}_{cold}, \dot{m}_{cold} \geq \dot{m}_{hot} \\ \dot{m}_{hot}, \dot{m}_{hot} > \dot{m}_{cold} \end{Bmatrix} \end{gathered} \tag{4}$$

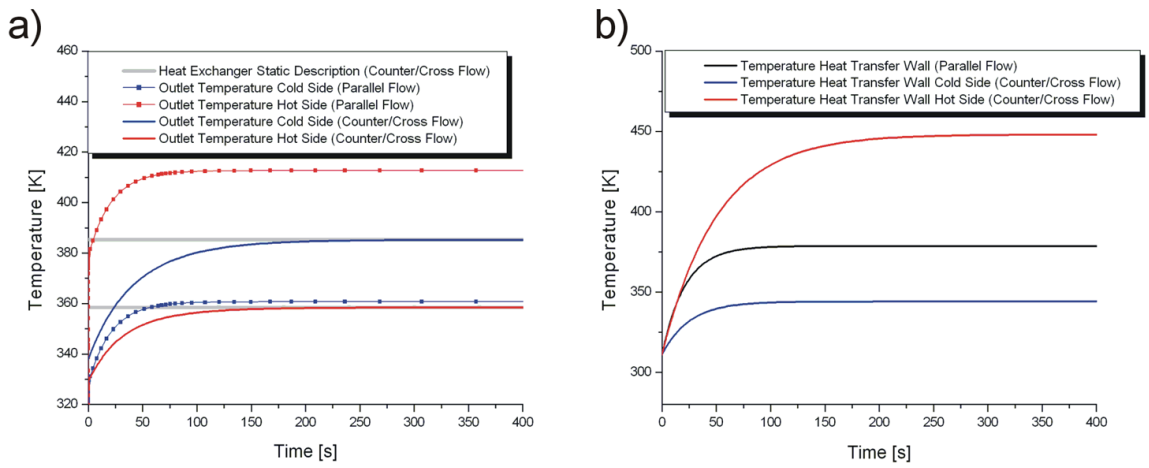

Figure 18: a) Simulated outlet temperature profiles of different heat exchanger types
b) Simulated temperature profiles of the heat transfer walls

4 Validation of the FLECS Database

The FLECS components were checked for stability and real time capability. Simulation results obtained with FLECS components have been compared with results generated by other flow system simulation programs.

The aim is now to validate FLECS components in a larger aircraft context as it is needed for ECS modeling. In a first step, an air distribution network as shown in Figure 1 and Figure 19 is applied. This network is part of the environmental control system of an aircraft.

4.1 Supply Duct System

The network consists of ducts that distribute the air from a mixing point into the respective cabin zone. In the mixing point a cold air flow coming from the mixing unit is mixed with hot trim air (see Figure 1).

The air is pushed into the network via the supply duct (see Figure 19). From the supply duct the air is channeled through 7 riser ducts and into an oval duct. At the outlet of the oval duct the airflow is split into 4 cross ducts. Finally, the air enters the cabin through the cabin inlets. Each duct is characterized by its length, wall thickness, thickness of the isolation and diameter (or major and minor axis in case of the oval duct).

A simulated duct component can be generated by a combination of a flow resistance and a volume (see Figure 5). To model the correct dynamics of a long duct, it can even be built up from a combination of several flow resistances and several volumes. Through the duct wall heat transfer takes place. Two different processes have to be considered: a) heat convection between the airflow in the duct and the wall and b) the conduction through the wall and the isolation.

The convection heat transfer coefficient follows from the flow properties characterized by the Reynolds number. The heat conductivity coefficient is determined from the thickness of the wall and the isolation and the thermal properties of the two materials. Another important parameter for the heat transfer is the ambient temperature of the air surrounding the ducts.

Both the wall and the isolation are considered as thermal capacity. A thermal capacity is defined by the mass and the specific heat capacity. Using the library various duct and isolation geometries can be modeled easily.

During a test flight with an Airbus A340-600 the temperature profiles were recorded for 23735 s. Temperature measurements were taken at the inlet of the supply duct, at the inlet of the cabin and in the cabin (see Figure 19). Different tests were carried out during the flight.

These tests changed the cabin parameters drastically. The change in cabin parameters has to be taken into account when looking at results from the cabin simulation. For the validation in this paper only the data sets from cabin zone 7 were used (see Figure 20).

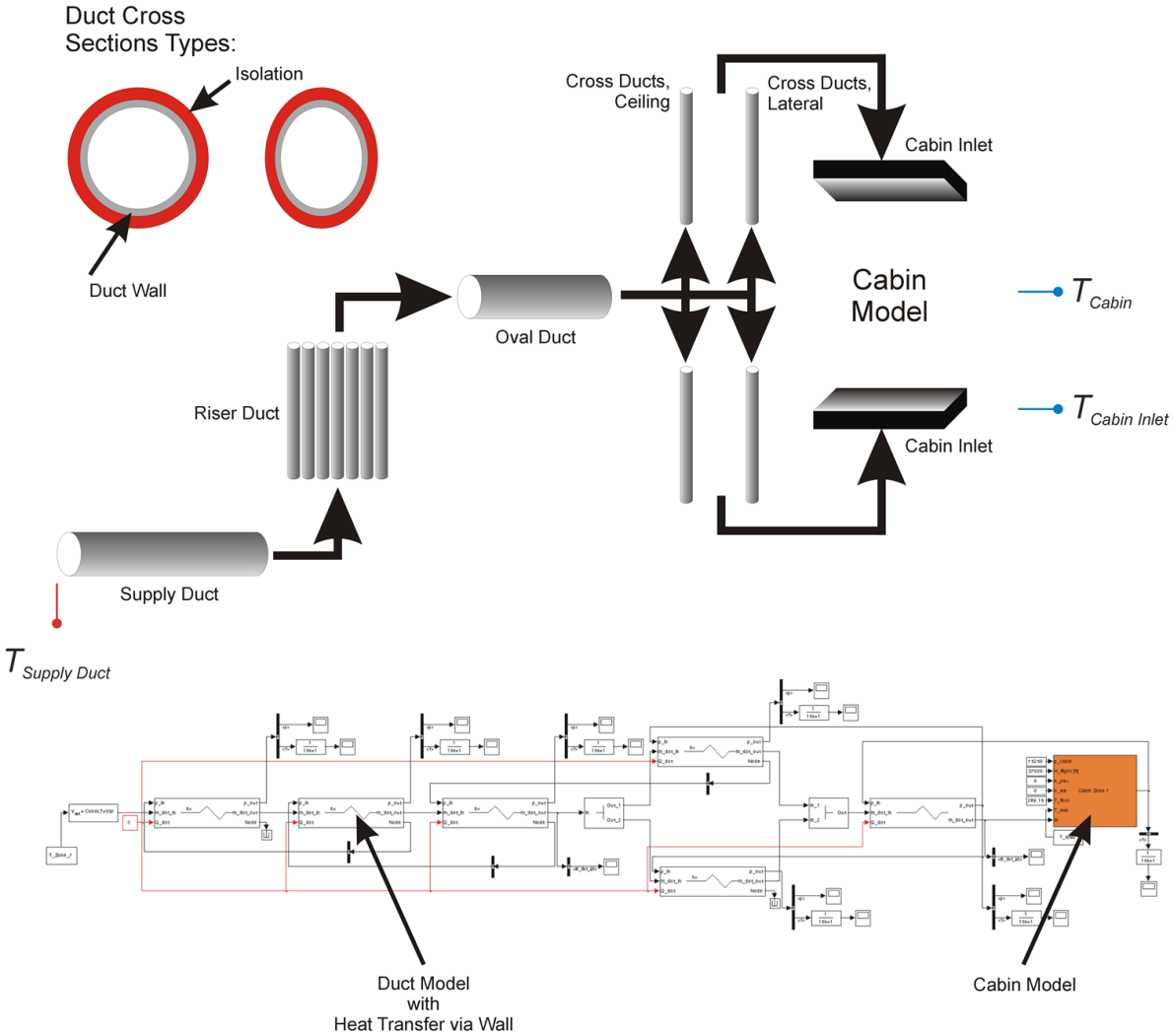

Figure 19: Supply duct system of an A340-600 in combination with a cabin model

The validation of the FLECS components is done by a comparison of simulated and measured temperature profiles (Figure 20). Almost all component parameters were left as initially set. However, a few unknown parameters had to be identified with the simulation:

a) The ambient temperature of the ducts was not recorded during the flight test and was hence unknown.
b) The heat capacity of the cabin inlet was unknown due to its irregular shape.

The air distribution network is characterized by the following duct parameters:

- Length
- Diameter
- Thickness Wall
  - Thickness Isolation
  - Specific Heat Capacity Wall
  - Specific Heat Capacity Isolation
  - Density Wall
  - Density Isolation
  - Heat Conductivity coefficient:
    - Wall
    - Isolation

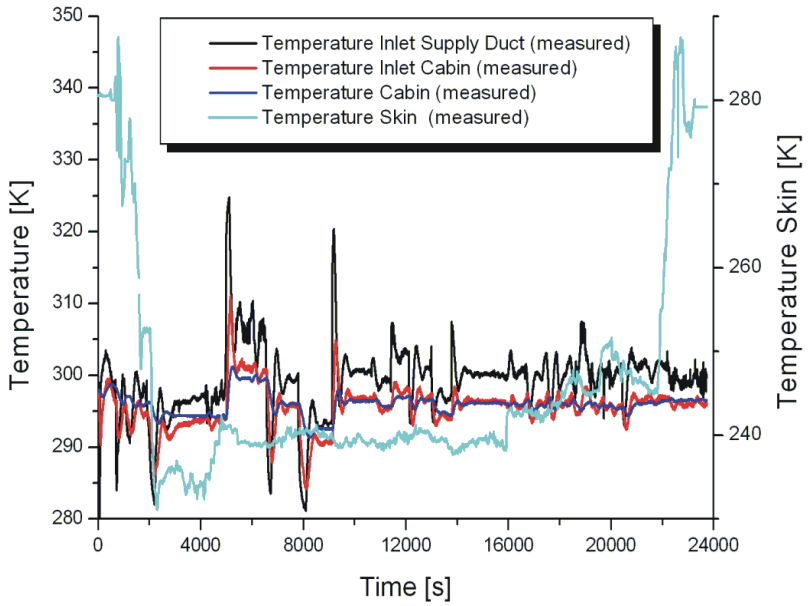

Figure 20: Measured datasets of supply duct inlet temperature, the cabin inlet temperature, the cabin temperature and the skin temperature

The duct parameters can be calculated by known geometry or looked up for the materials used. These parameters are fixed during the simulation.

Boundary conditions for the simulation:

- Constant volume flow
- Temperature profile at the supply duct inlet

Parameter identification was used to find the ambient temperature of the ducts because this parameter was not measured during the test flight. From other test flights the range for the ambient temperature is known to differ within a range of 10 °C … 15 °C (283.15 K … 288.15 K) for the flight conditions of this test. For the simulation an ambient temperature of 12.5 °C = 285.65 K was selected. This value gave the best match between simulated

temperature profiles and measured values and falls within the reasonable range for this parameter.

In addition to the given duct parameters, the cabin inlet had to be defined. Within the air distribution network, the flow velocity differs in the range 10 m/s … 20 m/s. At the cabin inlet the velocity is reduced to around 1 m/s … 2 m/s. Therefore, the heat capacity of the cabin inlet plays an important role. The thermal capacity of an airflow system defines the dynamic. The higher the capacity the more the dynamic response of a system is damped and delayed.

The cabin inlet can be described by the same model as the ducts. The heat capacity of the cabin inlet can be adjusted by changing the length of the inlet. The required flow velocity defines the diameter, and the density is defined by the used materials.

Heat capacities cabin inlet:

- Heat capacity wall: 5702 J/K
- Heat capacity isolation: 143 J/K

The two parameters, duct ambient temperature and air inlet length were identified with the aim of reaching the best fit of the dynamic response of the system. The heat capacity is given above (instead of the length) because this is the end result and important for the simulation.

Another factor, which has an influence on the dynamic, is the discretization of the duct components. For the simulation, each duct was divided up into 5 equal pieces. This led to many different results compared to no discretization of the ducts. However, an even finer discretization, e.g. into 10 equal pieces, led to almost the same result, as obtained with 5 equal pieces (a temperature difference of less than 0.58 K).

The simulated response of the duct system compared to the input temperature profile is shown in Figure 21. The overlap between the measured and the simulated cabin inlet temperature is obvious. In the time range 4000 s … 14000 s the average temperatures of the measured and the simulated dataset have a deviation of 0.07 K. Also, the dynamic response of the real system can be reproduced by the simulation model.

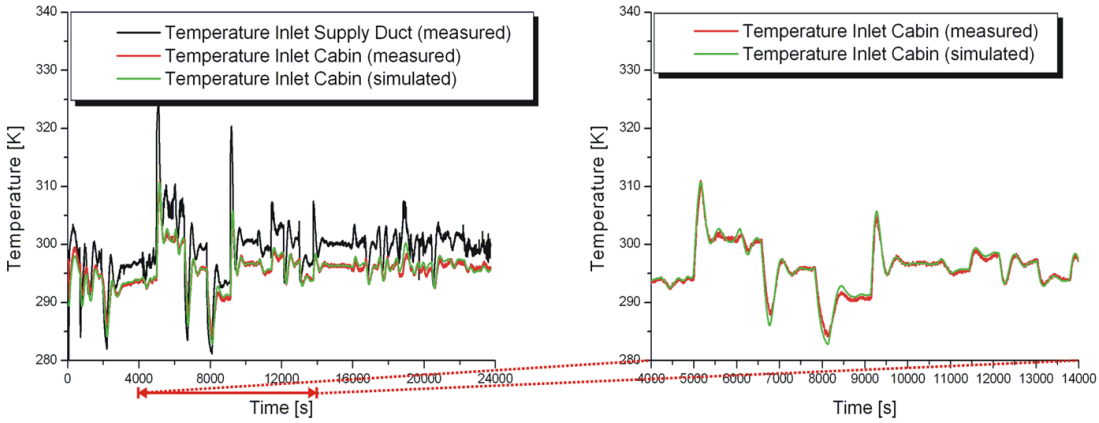

Figure 21: Measured datasets of supply duct inlet temperature, the cabin inlet temperature and the simulated cabin inlet temperature. The time range 4000 s … 14000 s is enlarged

Table 6: List of parameters supply duct system (see Figure 19)

Boundary Limits	
Mass Flow:	0.567 kg/s
Ambient Temperature:	285.65 K
Initial Parameter	
Pressure:	75254 Pa
Temperature Air/Wall:	298.88 K
Water Vapor Content:	0
CO_2 Content:	0
Water Content:	0
Parameter Supply	
Discretization:	5
Number of identical Units:	1
Length Major Axis:	0.195 m
Length Minor Axis:	0.195 m
Length:	21 m
Thickness Wall:	0.0005 m
Thickness Isolation:	0.0120 m

Density Wall:	2000 kg/m³
Density Isolation:	6 kg/m³
Specific Heat Capacity Wall:	1200 J/kg K
Specific Heat Capacity Isolation:	1000 J/kg K
Thermal Conductivity Wall:	0.250 W/m K
Thermal Conductivity Isolation:	0.055 W/m K
Minor Loss Coefficient:	1
Mode:	1
Parameter Riser Duct	
Discretization:	5
Number of identical Units:	7
Length Major Axis:	0.067 m
Length Minor Axis:	0.067 m
Length:	4 m
Thickness Wall:	0.0005 m
Thickness Isolation:	0.0320 m
Density Wall:	2000 kg/m³
Density Isolation:	12 kg/m³
Specific Heat Capacity Wall:	1200 J/kg K
Specific Heat Capacity Isolation:	1000 J/kg K
Thermal Conductivity Wall:	0.250 W/m K
Thermal Conductivity Isolation:	0.040 W/m K
Minor Loss Coefficient:	1
Mode:	1
Parameter Oval Duct	
Discretization:	5
Number of identical Units:	1

Length Major Axis:	0.30 m
Length Minor Axis:	0.19 m
Length:	2.5 m
Thickness Wall:	0.001 m
Thickness Isolation:	0.012 m
Density Wall:	2000 kg/m³
Density Isolation:	6 kg/m³
Specific Heat Capacity Wall:	1200 J/kg K
Specific Heat Capacity Isolation:	1000 J/kg K
Thermal Conductivity Wall:	0.250 W/m K
Thermal Conductivity Isolation:	0.055 W/m K
Minor Loss Coefficient:	1
Mode:	1
Parameter Cross Duct, Ceiling/Lateral	
Discretization:	5
Number of identical Units:	2
Length Major Axis:	0.2964/0.1510 m
Length Minor Axis:	0.0664/0.0590 m
Length:	2.25 m
Thickness Wall:	0.001 m
Thickness Isolation:	0.012/0.008 m
Density Wall:	2000 kg/m³
Density Isolation:	6 kg/m³
Specific Heat Capacity Wall:	1200 J/kg K
Specific Heat Capacity Isolation:	1000 J/kg K
Thermal Conductivity Wall:	0.250 W/m K
Thermal Conductivity Isolation:	0.055 W/m K

Minor Loss Coefficient:	1
Mode:	1
Parameter Cabin Inlet	
Discretization:	1
Number of identical Units:	1
Length Major Axis:	0.7562 m
Length Minor Axis:	0.7562 m
Length:	1 m
Thickness Wall:	0.001 m
Thickness Isolation:	0.010 m
Density Wall:	2000 kg/m³
Density Isolation:	6 kg/m³
Specific Heat Capacity Wall:	1200 J/kg K
Specific Heat Capacity Isolation:	1000 J/kg K
Thermal Conductivity Wall:	0.250 W/m K
Thermal Conductivity Isolation:	0.055 W/ m K
Minor Loss Coefficient:	1
Mode:	1

4.2 Cabin Model

The cabin of the Airbus A340-600 consists of 8 zones. Only the measured data of cabin zone 7 is considered in the simulation. The simulation model of the cabin is described by the following parameters:

Ambient conditions (A340-600 test flight):

- Flight altitude
- Skin temperature
- Mach number

Cabin zone 7 parameters (A340-600):

- Air volume

- Mass interior
- Specific heat capacity interior
- Exchange surface cabin/floor
- Exchange surface interior
- Exchange surface cabin/skin
- Number windows
- Area windows
- No passengers
- No galley
- Convection heat transfer coefficient:
- Skin
- Floor

The skin temperature was measured during the flight (see Figure 20). The skin temperature changes between -41.98 °C = 231.17 K and 14.38 °C = 287.53 K. The flight altitude varies between 0 ft … 41000 ft. The cabin pressure has been assumed to a fixed value of 752 hPa. This value corresponds to a cabin altitude of 8000 ft. No passengers or dummies were present in zone 7 during the test flight.

Cabin zone 7 overall electrical heat loads were:

- Heat load skin
- Heat load floor
- Heat load electrical (IFE + lights)
- Heat load solar

Heat capacities of cabin zone 7:

- Heat capacity air
- Heat capacity interior

Compared to the air distribution network, the cabin interior can only be described in a simplified way by means of a representative mass, a specific heat capacity and an assumed exchange surface. The thermal capacities of the aircraft skin and the cabin floor are neglected.
These crude assumptions have a detrimental effect on the accuracy of the simulation results. The advantage of a simplified cabin interior model is however given by the fact that the few parameters of the model as described above can be easily identified from measured cabin temperatures.

Due to the simplifications of the cabin interior, the simulated cabin temperature cannot map the measured cabin temperature with the same accuracy (see Figure 22) as it was the case with the simulation of cabin inlet temperature (see Figure 21).

Additional deviation between measured and simulated data is due to the fact that during the flight different test were carried out. For example, the recirculation was switched off.

Note: In the time range 4000 s… 14000 s the airflow and recirculation was kept constant. This guarantees a useful comparison between measurements and simulation for this case.

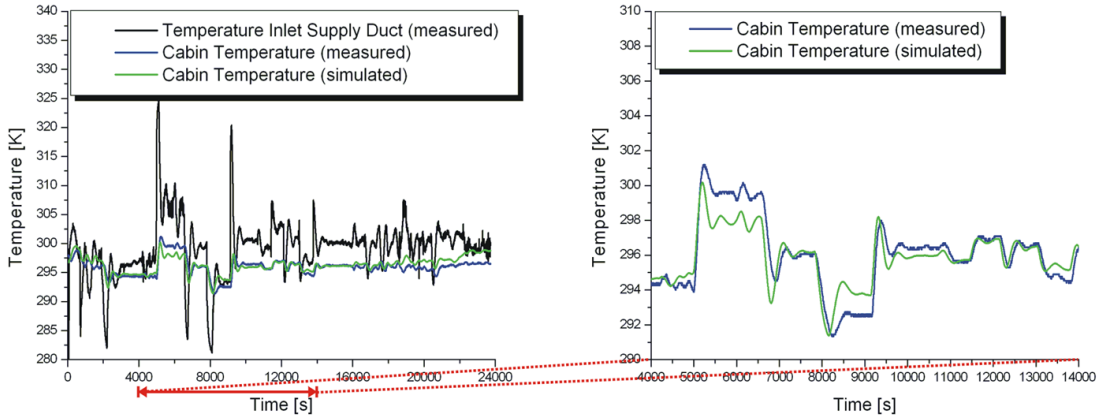

Figure 22: Measured datasets of supply duct inlet temperature, the cabin temperature and the simulated cabin inlet temperature. The time range 4000 s … 14000 s is enlarged

Table 7: List of parameters cabin model (see Figure 19)

Boundary Limits	
Pressure:	75250 Pa
Altitude:	37000 ft
Temperature Floor:	289.15 K
Initial Parameter	
Temperature Air/Interiors:	297.85 K
Water Vapor Content:	0
CO_2 Content:	0
Water Content:	0
Cabin Parameter	
Air Volume:	60 m³
Mass Interiors:	1280 kg
Window Area:	0.0877 m²
Number Windows:	11
Number Seats:	64
Exchange Surface Floor:	37 m²
Exchange Surface Interiors:	128 m²
Specific Heat Capacity Interiors:	840 J/kg K
Convection Heat Transfer Coefficient Interiors:	3 W/m² K
Exchange Surface Skin:	67 m²
Convection Heat Transfer Coefficient Skin:	1 W/m² K
Solar Flux:	1182 W/m²
Overall Heat Load:	3362 W

4.3 Air Conditioning Pack

An air conditioning pack (see Figure 23 and Figure 25) is an air cycle refrigeration system that uses the air passing through and into the airplane as the refrigerant. This is accomplished by a combined turbine and compressor machine (commonly called an air cycle machine, ACM, see Figure 24), valves for temperature and flow control, and heat exchangers using outside air to dispense waste heat.

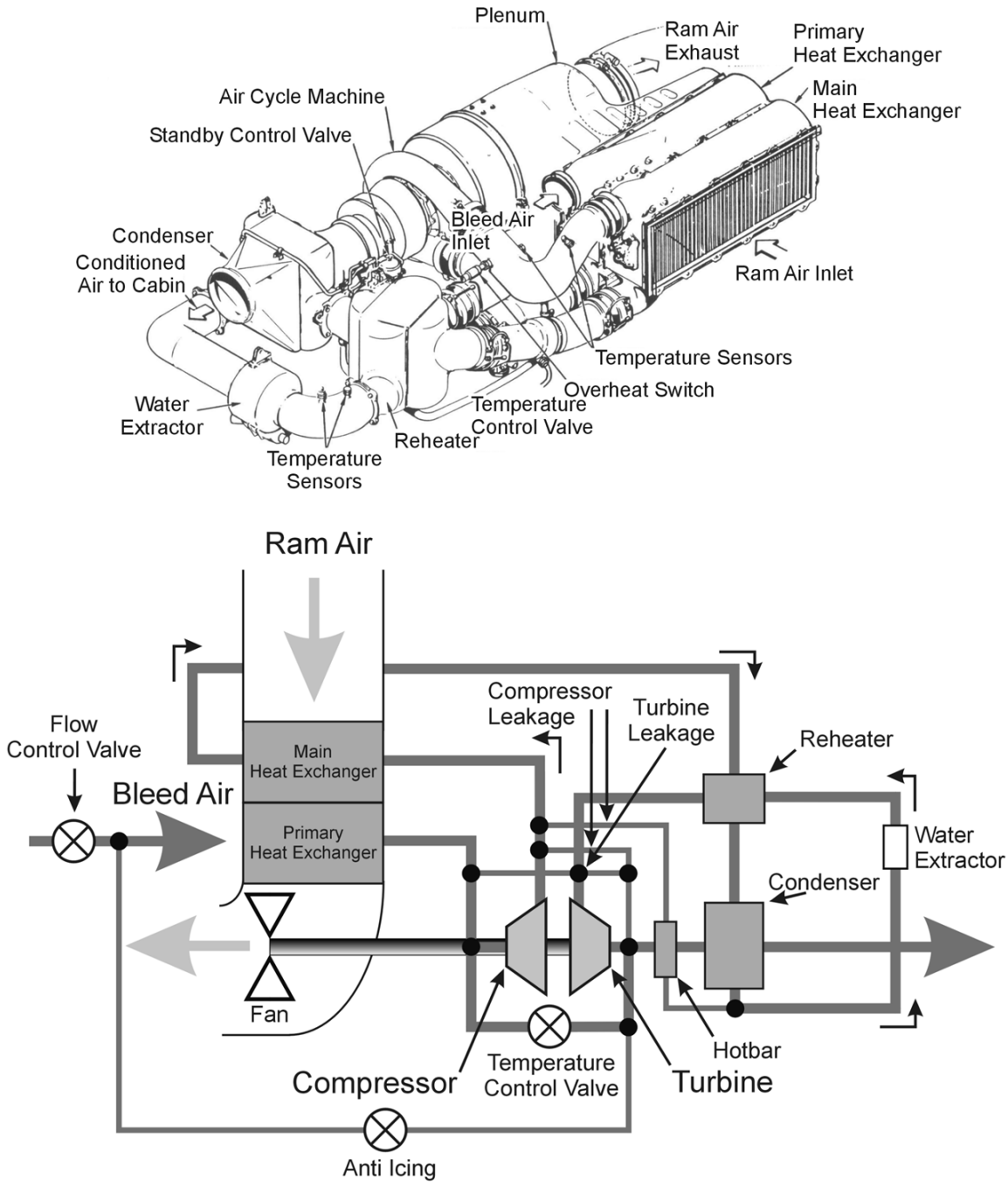

Figure 23: Schematic diagram of an aircraft pack (**Allied-Signal 1990**)

The air conditioning pack provides essentially dry, sterile, and dust free conditioned air to the airplane cabin at the proper temperature, flow rate, and pressure to satisfy pressurization and temperature control requirements. For the most modern aircraft, this is approximately between 3.38 g/s … 5.66 g/s per passenger. To ensure redundancy, two air conditioning packs are placed at the disposal. An equal quantity of filtered recirculated air is mixed with the air per passenger. An equal quantity of filtered recirculated air is mixed with the air from the air conditioning packs (see Figure 25).

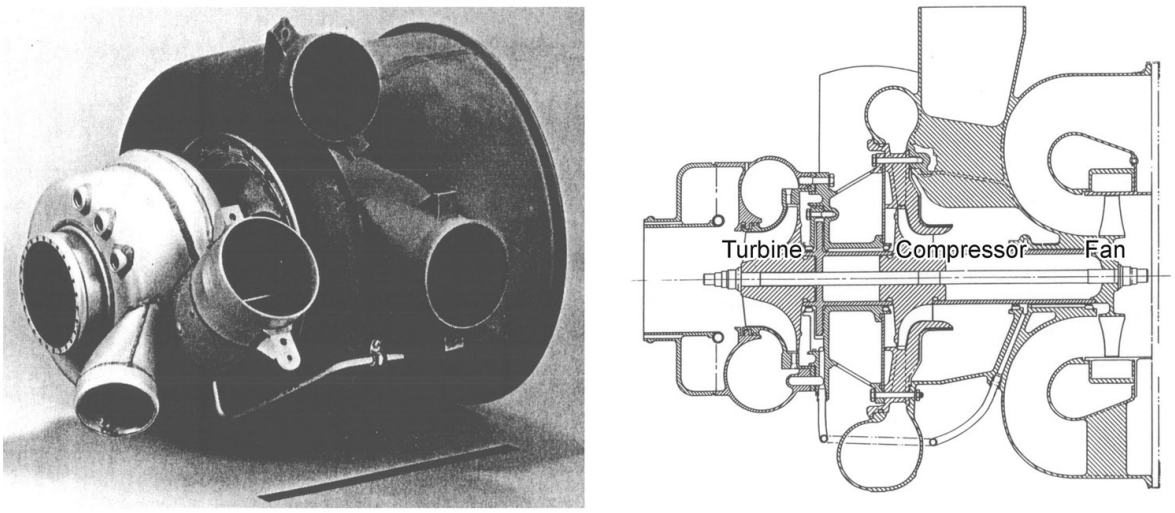

Figure 24: Schematic diagram of an air cycle machine (**Allied-Signal 1990**)

The quantity of supply air results in a complete cabin air exchange in about every two and one-half minutes, or about 25 air changes per hour. Temperature control is the predominant driver of outside airflow requirements.

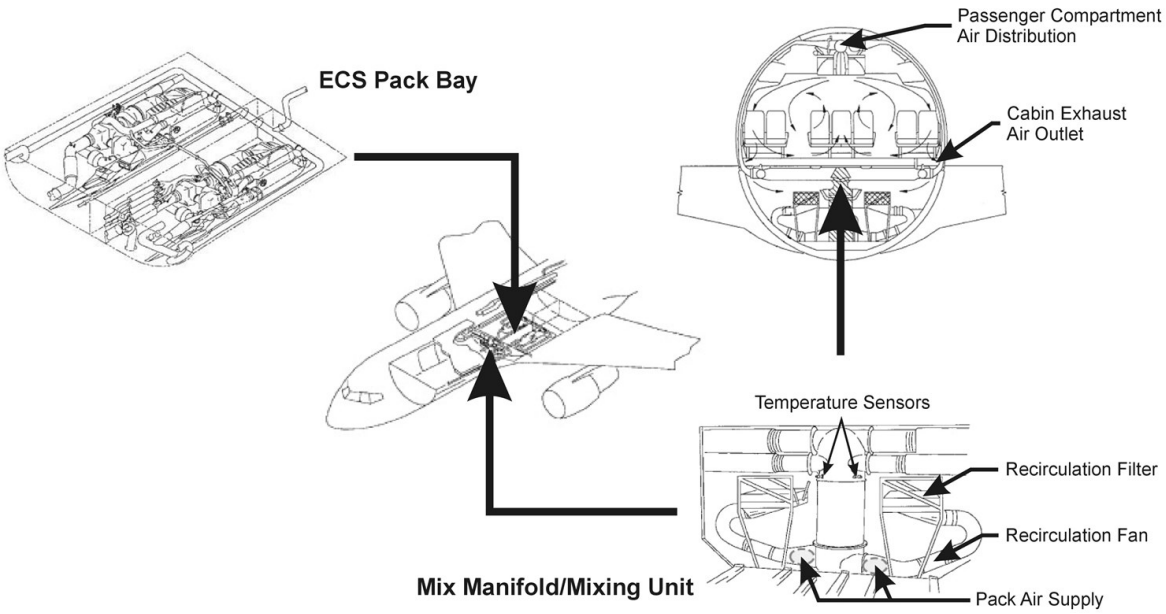

Figure 25: Schematic diagram of an aircraft environmental control system

The recirculated air from the cabin entering the mix manifold is essentially sterile. 99.9 % of the bacteria and viruses produced by the passengers have been removed by high-efficiency particulate air type filters (HEPA-type). These filters are used on the most modern aircraft. Gases are not removed by the filters.

The bleed system is a important part of the ECS. As outside air enters the compressor stages of the engine core, it is compressed to 220000 Pa … 240000 Pa and a temperature of 175 K … 200 K. Some of this air is then extracted from the engine core through one of two bleed port openings in the side of the engine. Which bleed port extracts the air depends on the positioning of valves that control the bleed ports (see Figure 26). One bleed port is at the engine's fifteenth compressor stage, commonly called "high stage." The second is at the eighth compressor stage, commonly called "low" or "intermediate stage." The exact stage can vary depending on engine type. The high stage is the highest air pressure available from the engine compressor. At low engine power, the high stage is the only source of air at sufficient pressure to meet the needs of the bleed system.

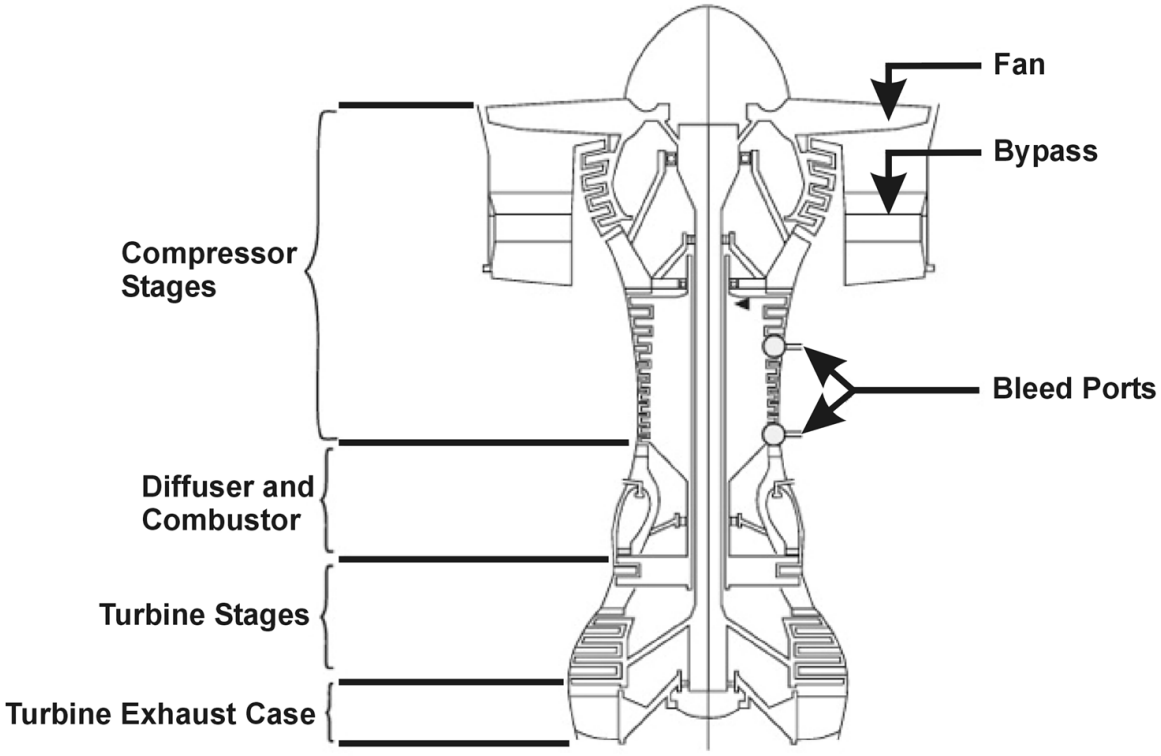

Figure 26: Schematic diagram of an engine core

The bleed system consists of several valves and a heat exchanger (the precooler). It automatically provides air at the proper temperature and pressure required to meet the needs of all pneumatic services on the airplane. These services include air conditioning packs, cabin ventilation system, potable water pressurization, wing and engine anti-ice protection, air-driven hydraulic pump, hydraulic reservoir pressurization, cargo heat, and cabin pressurization.

Because the engine must cope with widely varying conditions from ground level to flight at an altitude of up to 43,100 feet, the air at the high or low stage of the engine compressor will seldom exactly match the needs of the pneumatic systems. Excess energy must be discarded as waste heat. The bleed system constantly monitors engine conditions and always selects the least wasteful port. Even so, bleed temperatures often exceed safe levels for delivery to downstream systems. Safe temperature levels are temperatures at which fuel will not “auto” ignite. The function of the precooler is to automatically discharge excess energy back into the atmosphere as waste heat. This ensures that the temperature of the pneumatic manifold is always well below that which could ignite fuel.

4.3.1 Simulation Model of an Air Conditioning Pack

The Simulink simulation model shown in Figure 27 is based on a configuration of an A320 Pack. The pack is a combination of an ACM, valves for temperature and flow control, and heat exchangers. The inner algorithm structure of these different components are defined as specialized flow resistance. In contrast to generalized flow resistance discussed in the technical note TN_PD, a specialized flow resistance is defined by a characteristic map.

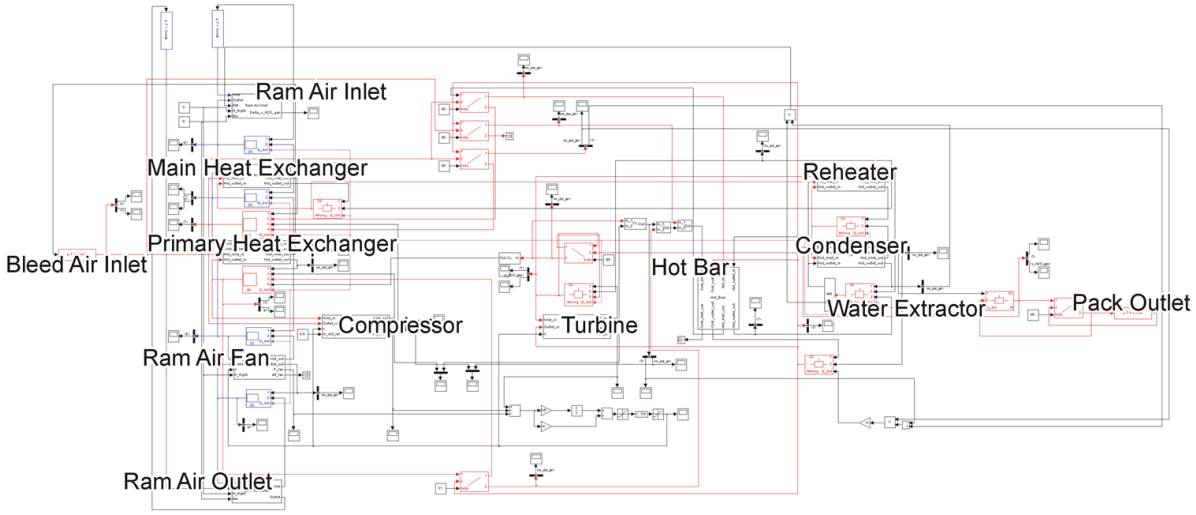

Figure 27a: Simulink simulation model of a pack

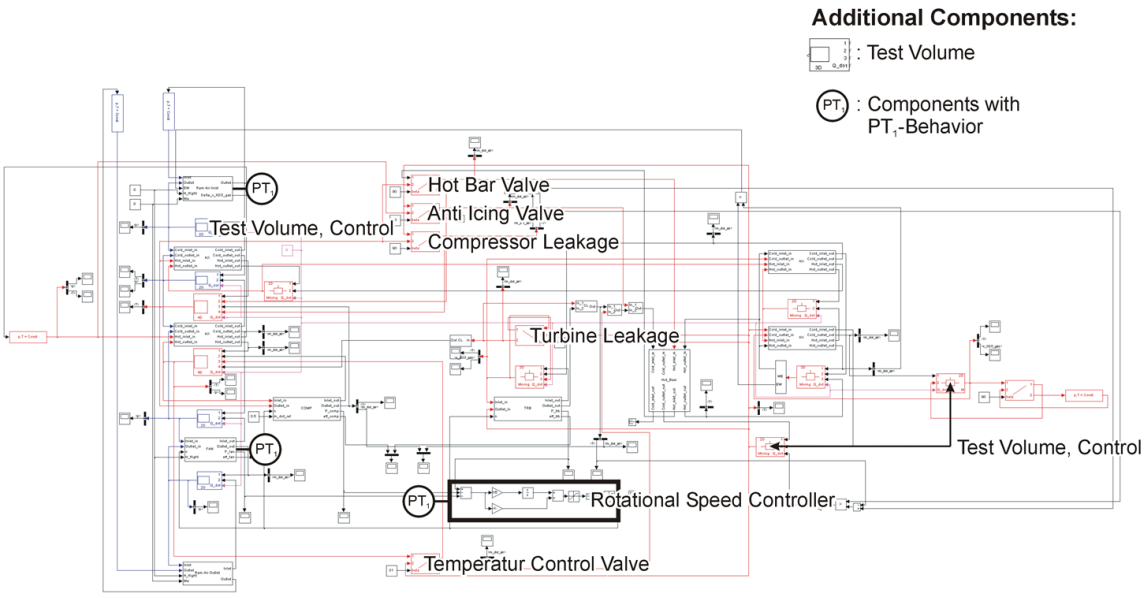

Figure 27b: Simulink simulation model of a pack

Stability

In general, a specialized flow resistance isn't related to an internal heat capacity, and therefore shows a steady state behavior. The different specialized flow resistances are linked together with help of generalized volumes, in following called test volumes V_{test} (see Figure 27). Sources of fluctuations are the condensation and evaporation processes, which occur inside the pack. To ensure a stable dynamical behavior of the overall system under assumption of time dependent boundary limits, like flight altitude and ambient temperature, the size of the different test volumes has to be adjusted. In addition to the test volumes the inertia of the pack can be enhanced using PT_1 elements (see Figure 27). By default, the pack bay ventilation, the ram air fan and the rotational speed controller can be delayed by a PT_1 element.

Heat Exchanger

The heat exchangers of the pack model are defined in counter/cross flow configuration (see Figure 17, Figure 27 and Figure 28).

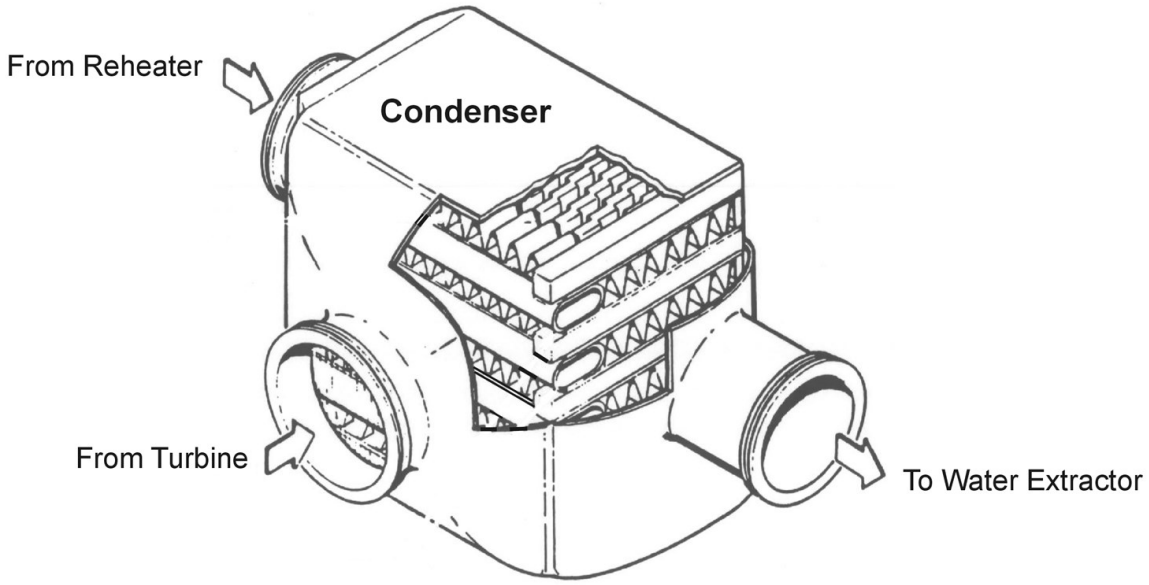

Figure 28: Schematic diagram of a condenser

Table 8: List of parameters of the heat exchangers inside the pack

Primary Heat Exchanger:	
Mass:	15 kg
Specific Heat Capacity:	900 J/kg K
Cold Side	
K_1:	492.3 Pa
m_1:	1.45
Hot Side	
K_1:	39365.7 Pa
m_1:	1.827
Main Heat Exchanger:	
Mass:	15 kg
Specific Heat Capacity:	900 J/kg K
Cold Side	
K_1:	886.14 Pa
m_1:	1.45
Hot Side	
K_1:	54180.2 Pa
m_1:	1.812
Reheater:	
Mass:	5 kg
Specific Heat Capacity:	900 J/kg K
Cold Side	
K_1:	21641.9 Pa
m_1:	1.784
Hot Side	
K_1:	33939.2 Pa

m_1:	1.756
Condenser:	
Mass:	5 kg
Specific Heat Capacity:	900 J/kg K
Cold Side	
K_1:	8111.9 Pa
m_1:	1.942
Hot Side	
K_1:	42447.7 Pa
m_1:	1.678

The characteristic efficiency maps of the different heat exchangers are shown in Figure 29.

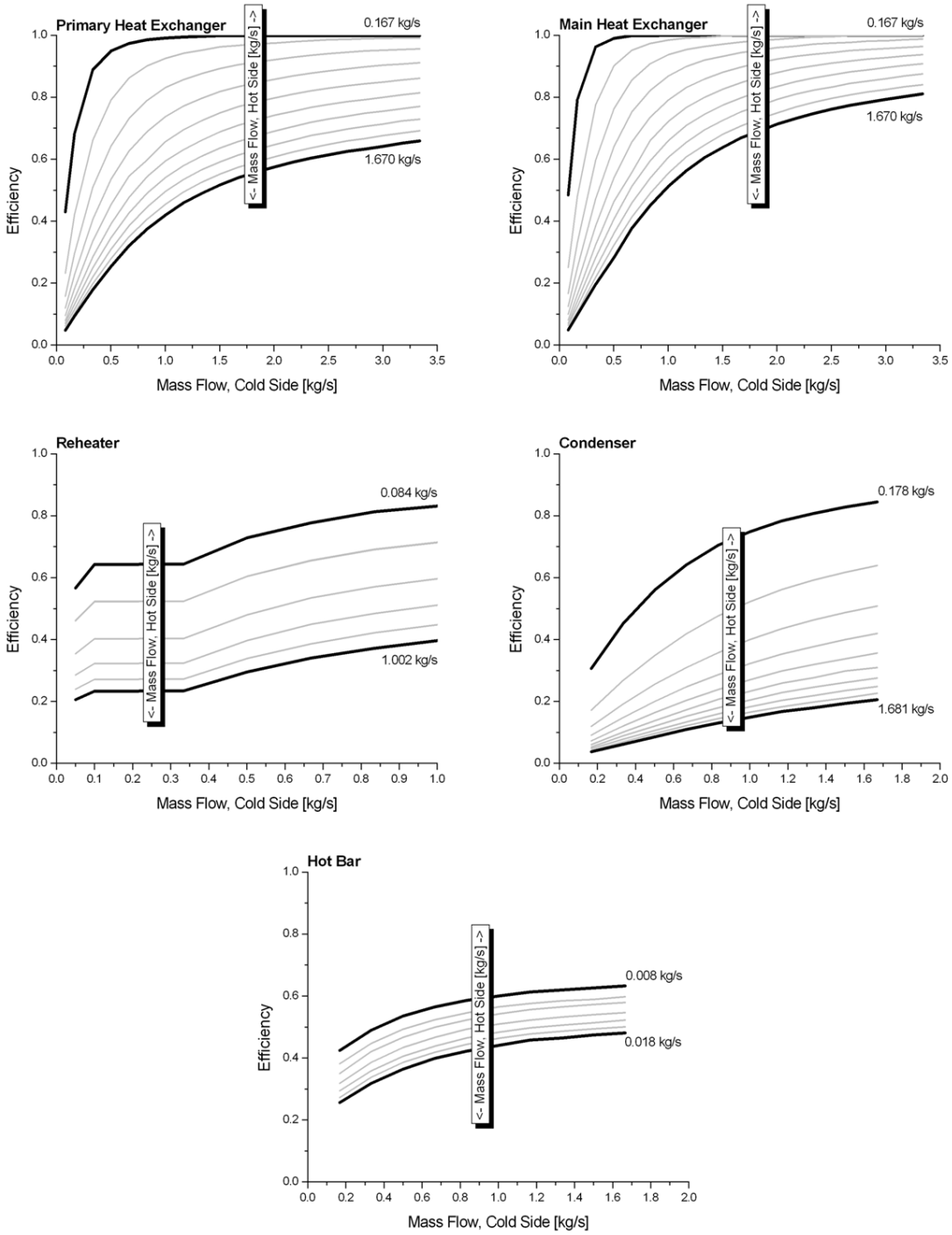

Figure 29: Characteristic maps of the different heat exchanger inside the pack model

The hot bar heat exchanger is defined by a particular inner structure. The flow properties inside the cold and hot side aren't known. Therefore, the hot bar model block has to be connected with a volume element and a flow resistance (see Figure 30).

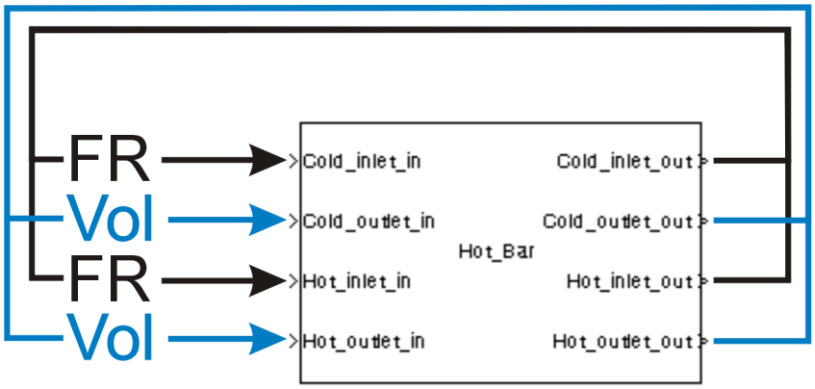

Figure 30: Inner structure of a hot bar element

Ram Air Channel

Various air inlet systems and particularly ram air inlets are known in the field of aircraft construction. These air inlet systems include recessed air channel inlets that are arranged on various aerodynamic surface areas of the aircraft. These inlets serve to deflect a portion of the boundary layer airflow from the exterior of the aircraft, so that the boundary layer air can flow into the interior of the aircraft in a suitable airflow channel, to be used by any one of a number of different systems of the aircraft.

The **NACA sink inlets** (see Figure 31, NACA: *National Advisory Committee for Aeronautics*) is a common form of low-drag intake design. It allows air to be drawn into an internal duct, often for cooling purposes, with a minimal disturbance to the flow. The design was originally called a "submerged inlet," since it consists of a shallow ramp with curved walls recessed into the exposed surface of a streamlined body, such as an aircraft, for example in the form of ram air inlets for providing cool air to the air conditioning packs. The purpose of a NACA duct is to increase the flow rate of air through it while not disturbing the boundary layer. NACA ducts are useful when air needs to be drawn into an area which isn't exposed to the direct air flow the scoop has access to. A NACA sink inlet is conventionally arranged in the belly fairing of the aircraft for providing external air for cooling the bleed air extracted from the jet engines in corresponding heat exchangers of the air conditioning systems.

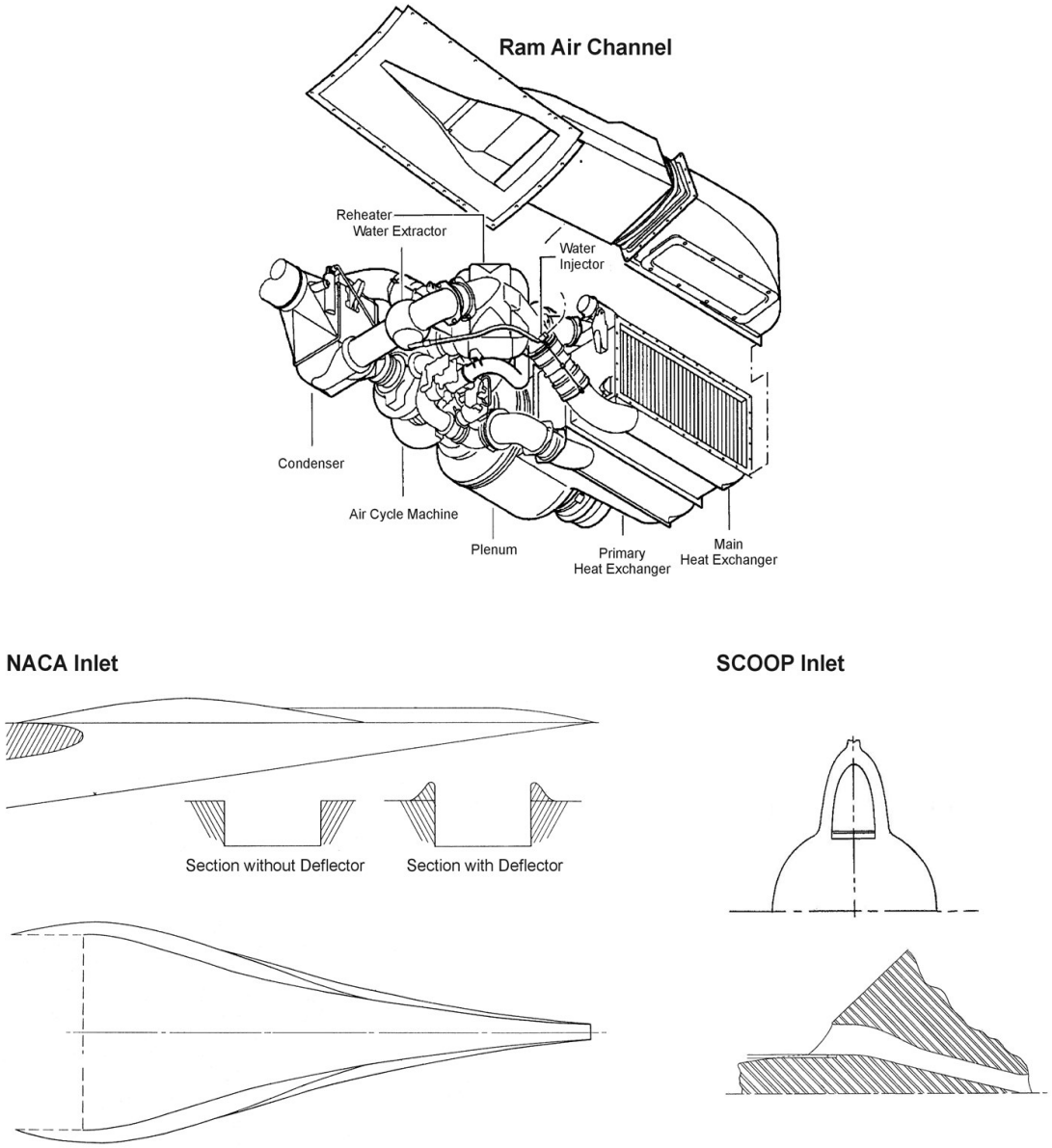

Figure 31: Schematic diagram of a ram air channel and of NACA respectively Scoop configuration of a ram air inlet

Additionally, a so-called pack bay ventilation inlet is provided to ventilate the air conditioning pack bay and also for tempering the aircraft structure. This pack bay ventilation inlet is typically arranged in the forward portion of the belly fairing. Moreover, two sink inlets are typically provided on the cowling of an engine, whereby one of the inlets serves to provide cooling air for carrying out the first stage cooling of the bleed air extracted from the engine, and the second inlet provides air for ventilating the intermediate space between the engine and the cowling.

During cruise flight of the aircraft the aerodynamic energy of the air supply is provided by the aerodynamic flow of the surrounding air relative to the air inlet edges or lips of the NACA sink inlets (see Figure 31). During ground operations the required volume flow of external air is sucked through the air inlet.

The structure and configuration of the overall air intake is largely determined by the inlet geometry of the ram air channel inlet itself. The generalized ram air channel is embodied as an air inlet flap that includes a substantially planar flap body. The inflowing ram air mass flow is controlled by the effective area of inlet flap. With the help of ram air flaps the outlet temperature of compressor respectively the pack discharge temperature can be regulated. Protecting the compressor of material damage the outlet temperature should not exceeds 180 °C.

Scoops, or positive pressure intakes, are useful when high volume air flow is desirable. They work on the principle that the air flow compresses inside an "air box", when subjected to a constant flow of air. The air box has an opening that permits an adequate volume of air to enter, and the expanding air box itself slows the air flow to increase the pressure inside the box. The fundamental equations describing the ram air channel are shown in Equation 5.

Ram Air Inlet, Ground Case $h_{flight} = 0$:

Ram Air Outlet :

$$p = p_{ambient}$$

$$\rho = \rho_{ambient}$$

$$T = T_{ambient}$$

$$x_{H2O,gas} = x_{H2O,gas,ambient}$$

$$x_{CO2} = x_{CO2,ambient}$$

$$x_{H2O,liq} = x_{H2O,liq,ambient}$$

$$\dot{m}_{air} = \sqrt{\frac{2\,\Delta p\,A^2\,\rho_{air}}{\zeta}}\,,\ \rho_{air} = \frac{\rho}{1 + x_{H2O,gas} + x_{CO2}}$$

Ram Air Inlet, Flight Case $h_{flight} > 0$:

$$p_{total} = p = p_{ambient}\,(1 + r_p\,\frac{\gamma - 1}{2}\mathrm{Ma}^2)^{\frac{\gamma}{\gamma - 1}}$$

$$T_{total} = T = T_{ambient}\,(1 + r_T\,\frac{\gamma - 1}{2}\mathrm{Ma}^2)$$

$$\text{Pressure Recovery Factor}: r_p = \sqrt{\frac{A}{A_{\max}}}\,(0.497 + 0.751\,\mathrm{Ma}^2)$$

$$\text{Temperature Recovery Factor}: r_T = 0.9$$

$$\rho_{total} = \rho = \frac{p_{total}}{R\,T_{total}}$$

$$x_{H2O,gas} = x_{H2O,gas,ambient}$$

$$x_{CO2} = x_{CO2,ambient}$$

$$x_{H2O,liq} = x_{H2O,liq,ambient}$$

$$\dot{m} = \sqrt{\frac{1}{\zeta}}\,\frac{A\,p_{total}}{\sqrt{T_{total}}}\,\sqrt{\frac{\gamma}{R}}\,\mathrm{Ma}\,(1 + \frac{\gamma - 1}{2}\,\mathrm{Ma}^2)^{-\frac{\gamma+1}{2(\gamma-1)}}$$

$$\dot{m}_{air} = \frac{\dot{m}}{1 + x_{H2O,gas} + x_{CO2}}$$

Mass Flow Ram Air Channel (Plenum) :

$$h_{flight} = 0 : \dot{m}_{plenum} = \dot{m}$$

$$h_{flight} > 0 : \dot{m}_{plenum} = \frac{\dot{m}}{0.79\text{-}0.8\,10^{-5}\ h_{flight}} \qquad (5)$$

Water Injection :

$$x_{H2O,liq} = x_{H2O,liq,ambient} + \frac{\dot{m}_{H2O,liq,injection}}{\dot{m}_{air}}$$

$$\Downarrow$$

Evaporation (see TN_PD)

Pack Bay Ventilation (PBV) **:**

$$T = \frac{\dot{m}_{air}\ T + \dot{m}_{air,PBV}\ T_{PBV}}{\dot{m}_{air} + \dot{m}_{air,PBV}}$$

$$x_{H2O,gas} = \frac{\dot{m}_{air}\ x_{H2O,gas} + \dot{m}_{air,PBV}\ x_{H2O,gas,PBV}}{\dot{m}_{air} + \dot{m}_{air,PBV}}$$

$$x_{CO2} = \frac{\dot{m}_{air}\ x_{CO2} + \dot{m}_{air,PBV}\ x_{CO2,PBV}}{\dot{m}_{air} + \dot{m}_{air,PBV}}$$

$$x_{H2O,liq} = \frac{\dot{m}_{air}\ x_{H2O,liq} + \dot{m}_{air,PBV}\ x_{H2O,liq,PBV}}{\dot{m}_{air} + \dot{m}_{air,PBV}}$$

$$x_{H2O,gas} = x_{H2O,gas,ambient}$$

$$x_{CO2} = x_{CO2,ambient}$$

$$x_{H2O,liq} = x_{H2O,liq,ambient}$$

$$\dot{m}_{air} = \begin{Bmatrix} \dot{m}_{air} + \dot{m}_{air,PBV} & \dot{m}_{air} > \dot{m}_{air,PBV} \\ 0 & \dot{m}_{air} < \dot{m}_{air,PBV} \end{Bmatrix} \quad (5)$$

A is the area of the ram air inlet respectively outlet by a given opening angle. $A_{\max}$ is the maximum feasible area of the ram air inlet. Assuring a stable algorithm, the pack bay ventilation is delayed by a PT_1 element. Additionally, the pack bay ventilation is defined by a time offset t_0. Starting at t_0 the ram air flow and the pack bay flow are mixed. Also, the response of ram air fan is delayed with help of a PT_1 element. According to Equation 5 The mass flow through the ram air channel is a function of the minor loss coefficient ζ. In the case of a NACA scoop configuration ζ can be estimated using Equation 6.

Ground Case $h_{flight} = 0$ **:**

$$\zeta = \exp(1 - \frac{A}{A_{\max}})$$

Flight Case $h_{flight} > 0$ **:** (normal case)

$$\zeta = 1.4 \ldots 1.6$$

Ram Air Outlet :

$$\zeta = 1 \tag{6}$$

In the ground case the ambient air is sucked into the ram air channel with help of the ram air fan (see TN_PD). In the flight case the ram air fan is described as flow resistance (see Figure 32). The description as flow resistance requires a certain form of the characteristic maps. The measured characteristic maps have the form shown in Figure 32a. The Simulink model block requires the transposed characteristic maps (see Figure 32b).

Based on the compression inside the fan, the air temperature is raised up. The relative temperature derivation is shown in Figure 32c.

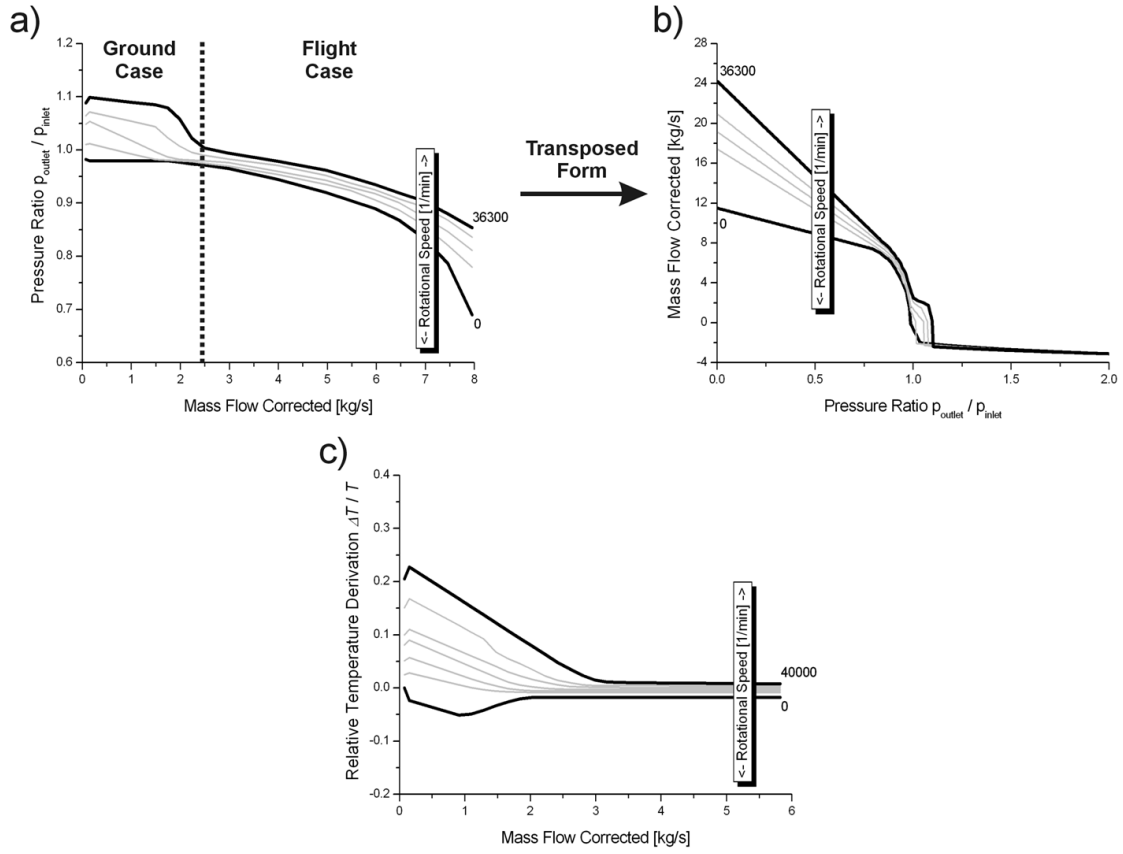

Figure 32: Characteristic maps of the ram air fan

Air Cycle Machine

The air cycle machine is a combination of a turbine and a compressor (see Figure 24 and Figure 33). The bleed air, which is pushed through the pack system, drives the turbine. The driven turbine transfers the decreased power P_{trb} to the shaft.

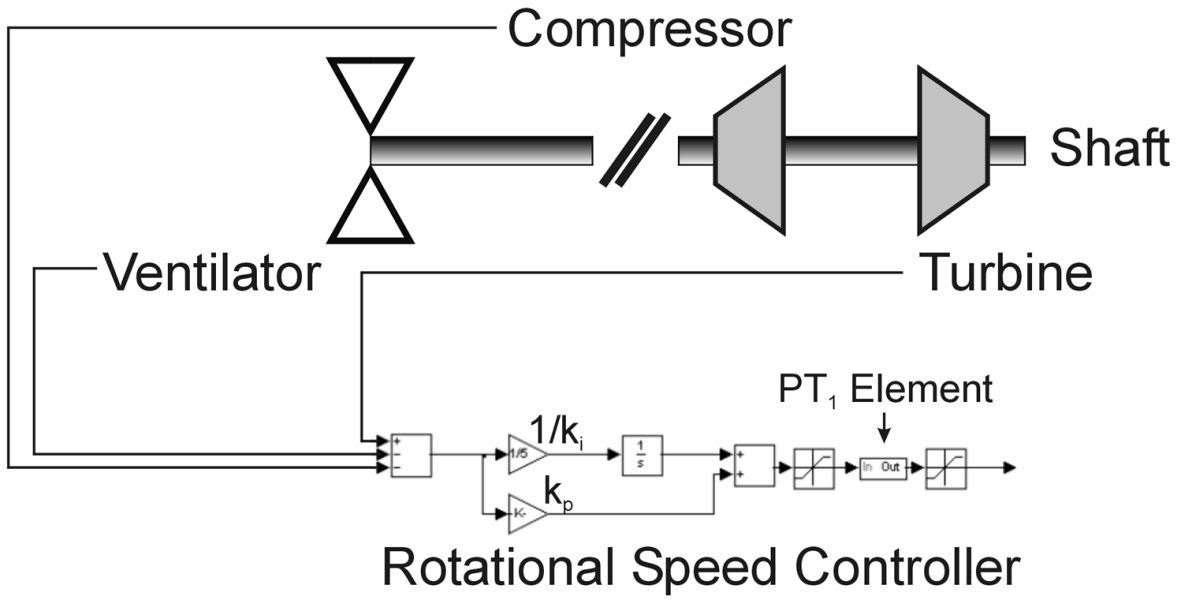

Figure 33: Schematic diagram of a combination of a ram air fan, a compressor and a turbine affixed to a single shaft

In the case that the compressor and the ram air fan are affixed to the same turbine shaft, the turbine power supplies the compressor (P_{comp}) and the ram air (P_{fan}). At the static equilibrium the condition Equation 7 is fulfilled.

$$\textbf{Static Equilibrium :}\ P_{trb} = P_{comp} + P_{fan} \tag{7}$$

The turbine power is a function or the rotational speed. During a dynamical simulation the rotational speed is controlled by a so-called rotational speed controller shown in Figure 33. Adjusting the controller to the inertia of the shaft a PT_1 element can be used.

Both components of the ACM are defined as specialized flow resistance. The inner structure is discussed in TN_PD. Analogous to the description of the ram air fan, the components are defined by characteristic maps shown in Figure 34 and Figure 35. The inner structure of a specialized flow resistance requires a certain form of the characteristic map. This transposed form is shown in Figure 34b and Figure 35b. Assuring a stable algorithm and therefore a usable transposed map, the measured characteristic maps (see Figure 34a and Figure 35a) need to be linear expanded (see Figure 34a).

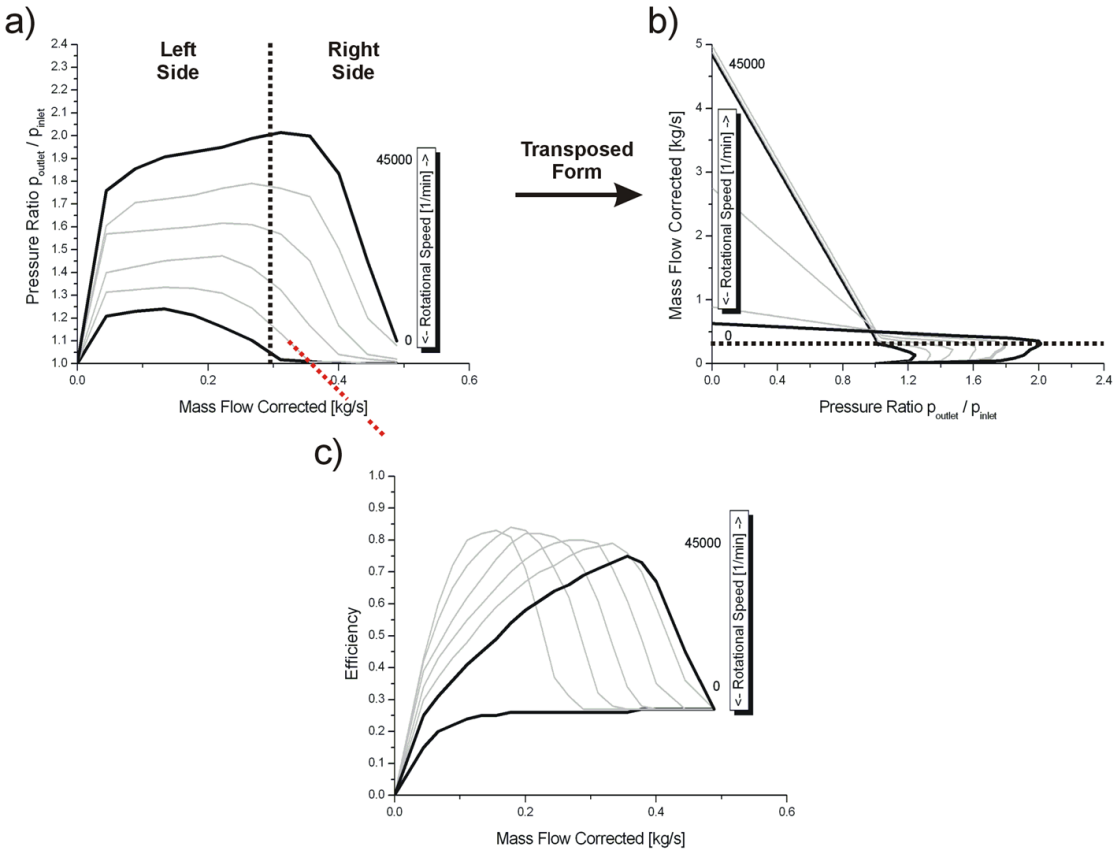

Figure 34: Characteristic maps of a compressor

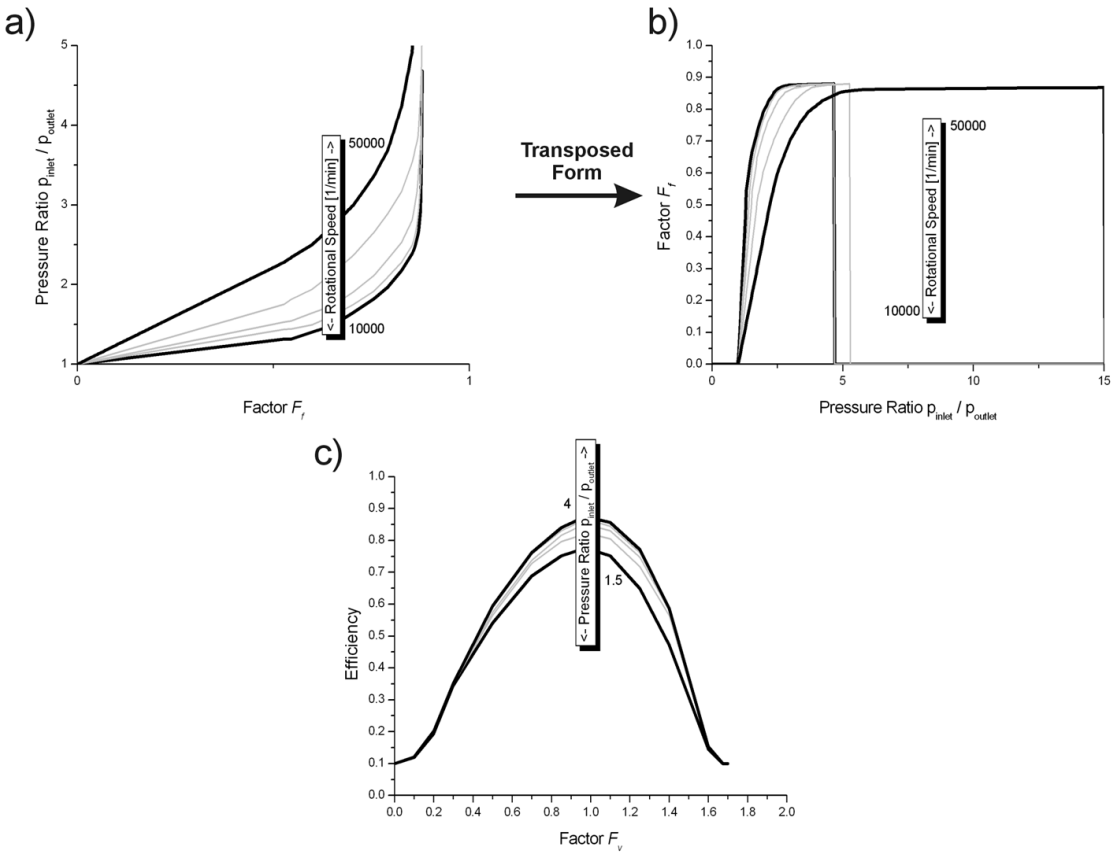

Figure 35: Characteristic maps of the turbine

Bypass Mass Flows

The outlet temperature of the pack is controlled by the temperature control valve (see Figure 23). In general, the opening angle of the temperature valve can be varied in a range from 0° … 45°. The pack system is protected against icing by the anti-icing mass flow in the order of 0.0005 kg/s. The anti-icing mass flow is bled off in front of the primary heat exchanger and is injected into the air flow after the compressor. At the outlet of the compressor a certain mass flow is bled off. This compressor leakage is split in mass flow supplying the hot bars (0.007 kg/s), which are located at the outlet of the turbine protecting the turbine against icing. The hot bar mass flow is injected into the airflow in front of the water extractor. The other part of the compressor leakages is used to heat up the turbine material, without being injected again.

The turbine leakages are used to supply the different bearings inside the air cycle machine. By passing the bearings the air is heated up in a range from 10 °C … 70 °C (see Figure 36).

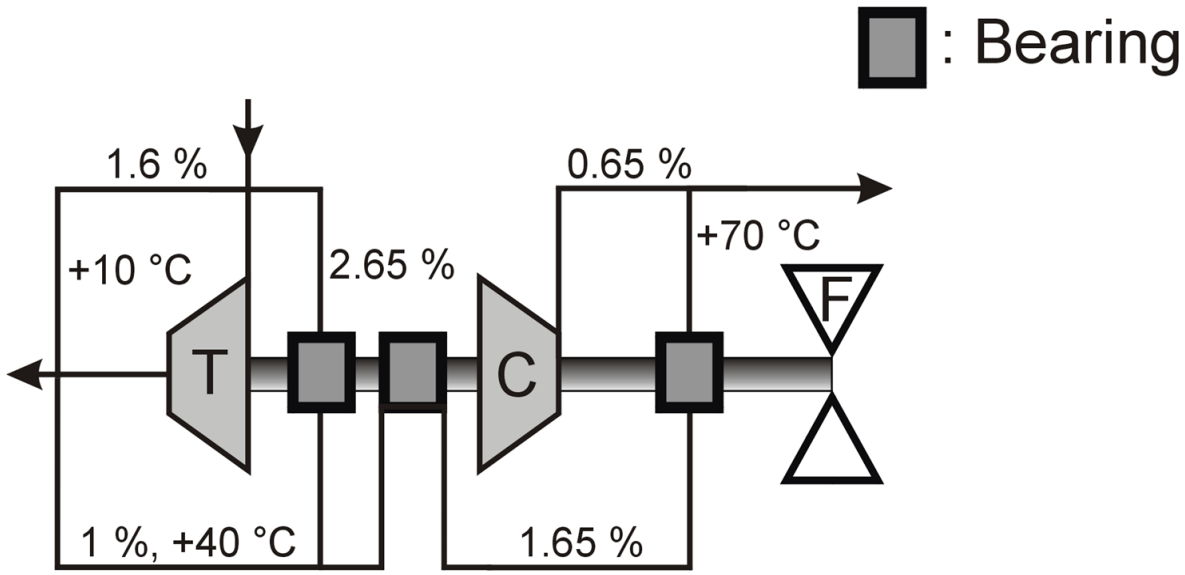

Figure 36: Bearing configuration inside a pack (A320)

As discussed, bypass mass flow configuration is related to the pack system used on an A320.

The bypass valves can be described with help of incompressible valve components discussed in the TN_PD. The different effective nozzle areas are given in Table 9.

Table 9: List of parameters of the bypass valves inside the pack

Temperature Control Valve:	
Area:	0.0005 m²
Anti-Icing Valve:	
Area:	0.000001 m²
Hot Bar Valve:	
Area:	0.00004 m²
Compressor Leakage:	
Area:	0.0001 m²
Turbine Leakage:	
Area:	0.0000165 m²

Validation

In the following paragraphs the A320 pack will be validated using standard test cases and reference data from the manufacturer. The A320 pack can be described with the components respectively characteristic maps discussed above.

In comparison the results of a pack simulation consisting of static heat exchangers respectively dynamic heat exchangers will be compared. The stability of the overall pack simulation is defined by the size of the test volumes (see Figure 27). Two test volume types can be distinguished. A reasonable size of the test volume V_{test} differs in a range between 0.1 m² … 0.5 m². The size of the test volume $V_{test,control}$ differs in a range between 1 m² … 5 m². Suppressing fluctuations the $V_{test,control}$ blocks have to be placed at the ram air inlet and in front of the condenser respectively at the pack outlet.

In the case of static heat exchangers basically the thermal capacity and therefore the response of the pack simulation model (see Figure 27) is defined by the overall size of all test volumes (see Figure 37). In the following the response time τ_{pack} of the pack system is the point the derivation between the simulated pack outlet temperature T_{pack} and the reference value T_{ref} given by the manufacturer is less than 1 °C ($|T_{pack} - T_{ref}| < 1$ °C, see dotted blue line in Figure 37).

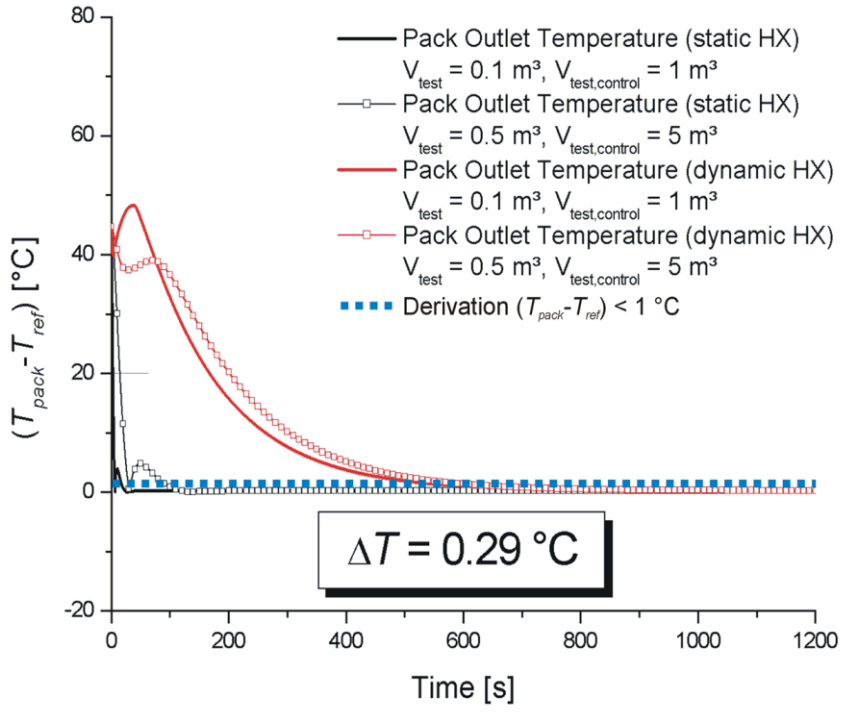

Figure 37: Comparison of a pack simulation with static and dynamic heat exchangers and different test volume sizes (A00C2, see Table 12)

Static Heat Exchangers (see Figure 37):
V_{test} = 0.1 m³, $V_{test,control}$ = 1 m³: τ_{pack} = 19 s
V_{test} = 0.5 m³, $V_{test,control}$ = 5 m³: τ_{pack} = 98 s

In the case of dynamic heat exchangers, the thermal capacity of the test volumes can be neglected. The response time τ_{pack} of the pack system is basically defined by the thermal capacity of the heat exchangers.

Dynamic Heat Exchangers (see Figure 37):
V_{test} = 0.1 m³, $V_{test,control}$ = 1 m³: τ_{pack} = 608 s
V_{test} = 0.5 m³, $V_{test,control}$ = 5 m³: τ_{pack} = 658 s

For dynamic heat exchangers the heat capacity is fixed by the mass (see Table 8). Additionally, the inertia of the overall system can be delayed by PT_1 elements. Components with PT1 behavior are the pack bay ventilation (τ_{PBV}), the ram air fan (τ_{fan}) and the rotational speed controller (τ_n).

The global parameters for the manufacturer given test cases (see Table 11) are shown in Table 10.

Table 10: List of global parameters of the validation of the A320 pack

Turbine:	
Nozzle Area:	0.00069 m²
Pack Bay Ventilation:	
Response Time τ_{PBV}:	10 s
Ram Air Fan:	
Response Time τ_{fan}:	5 s
Rotational Speed Controller (see Figure 33):	
k_i:	5 s
k_p:	500
Response Time τ_n:	5 s
Test Volumes:	
V_{test}:	0.5 m³
$V_{test,control}$:	5 m³

Table 11: Test cases pack validation

A00C2 (see Figure 37):	Ground APU (ISA Cold)
G00H2 (see Figure 38):	Ground Idle (ISA Hot)
M10H2 (see Figure 39):	Climb (ISA Hot)
M20H2 (see Figure 40):	Climb (ISA Hot)
M30H2 (see Figure 41):	Climb (ISA Hot)
C35H2 (see Figure 42):	Cruise (ISA Hot)

Table 12: List of global parameters test case A00C2

Ambient Conditions:	
Pressure:	101300 Pa
Temperature:	250.15 K
Water Vapor Content:	0.0005
Boundary Limits:	
Pressure Bleed Air:	220100 Pa
Temperature Bleed Air:	393.15 K
Outlet Pressure Pack:	103900 Pa
Altitude:	0
Mach Number:	0
Ram Air Inlet:	
Maximum Area:	0.04050 m²
Effective Area:	0.00445 m²
Minor Loss Coefficient:	2.4
Mass Flow Pack Bay Ventilation:	0.00017 kg/s
Temperature Pack Bay Ventilation:	393.15 K
Ram Air Outlet:	
Maximum Area:	0.07000 m²
Effective Area:	0.00770 m²

Minor Loss Coefficient:	1
Turbine:	
Corrected Isentropic Efficiency:	0.86
$\Rightarrow \Delta\eta_{trb}$	0.0547
Water Extractor:	
Efficiency Water Separation:	0
Initial Parameter Test Volumes:	
Pressure:	103900 Pa
Temperature:	250.15 K
Water Vapor Content:	0.0005
Initial Parameter Test Volumes, Ram Air Channel:	
Pressure:	101300 Pa
Temperature:	250.15 K
Water Vapor Content:	0.0005

Test Case 1 (G00H2):

Ambient Conditions:	
Pressure:	101300 Pa
Temperature:	311.15 K
Water Vapor Content:	0.019
Boundary Limits:	
Pressure Bleed Air:	233210 Pa
Temperature Bleed Air:	448.15 K
Outlet Pressure Pack:	103400 Pa
Altitude:	0
Mach Number:	0

Ram Air Inlet:	
Maximum Area:	0.04050 m²
Effective Area:	0.04050 m²
Minor Loss Coefficient:	1
Mass Flow Pack Bay Ventilation:	0.035 kg/s
Temperature Pack Bay Ventilation:	379.65 K
Ram Air Outlet:	
Maximum Area:	0.07000 m²
Effective Area:	0.07000 m²
Minor Loss Coefficient:	1
Turbine:	
Corrected Isentropic Efficiency:	0.88
$\Rightarrow \Delta\eta_{trb}$	0.0636
Water Extractor:	
Efficiency Water Separation:	0.825
Initial Parameter Test Volumes:	
Pressure:	103400 Pa
Temperature:	311.15 K
Water Vapor Content:	0.019
Initial Parameter Test Volumes, Ram Air Channel:	
Pressure:	101300 Pa
Temperature:	311.15 K
Water Vapor Content:	0.019

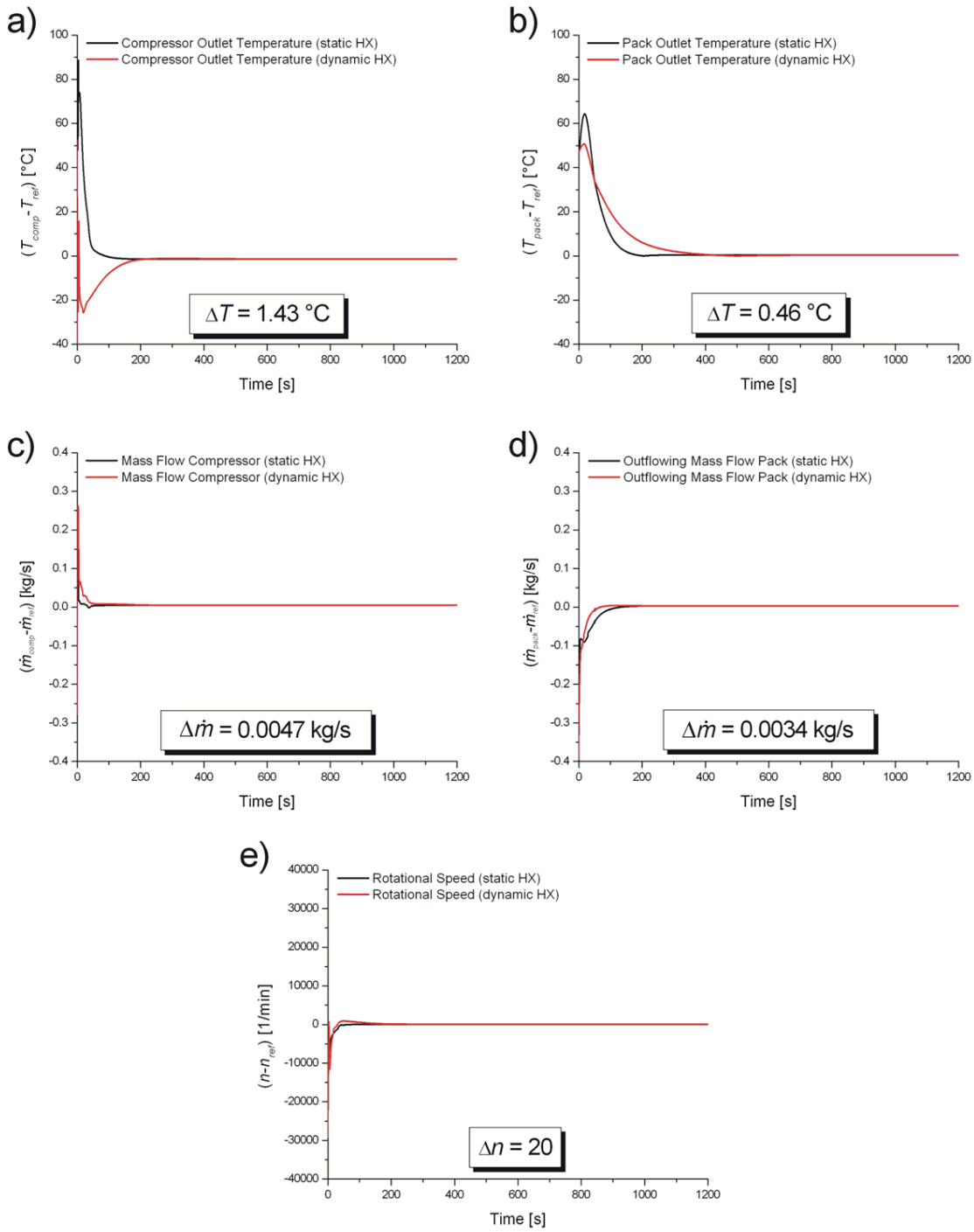

Figure 38: Test case G00H2, a) Compressor outlet temperature, b) Pack outlet temperature, c) Mass flow compressor, d) Out flowing mass flow pack, e) Rotational Speed

Test Case 2 (M10H2):

Ambient Conditions:	
Pressure:	69700 Pa
Temperature:	291.25 K
Water Vapor Content:	0.0186
Boundary Limits:	
Pressure Bleed Air:	250580 Pa
Temperature Bleed Air:	473.15 K
Outlet Pressure Pack:	100900 Pa
Altitude:	10000
Mach Number:	0.45
Ram Air Inlet:	
Maximum Area:	0.04050 m²
Effective Area:	0.01347 m²
Minor Loss Coefficient:	1.38
Mass Flow Pack Bay Ventilation:	---
Temperature Pack Bay Ventilation:	---
Ram Air Outlet:	
Maximum Area:	0.07000 m²
Effective Area:	0.02329 m²
Minor Loss Coefficient:	1
Turbine:	
Corrected Isentropic Efficiency:	0.87
$\Rightarrow \Delta\eta_{trb}$	0.0131
Water Extractor:	
Efficiency Water Separation:	0.864
Initial Parameter Test Volumes:	

Pressure:	100900 Pa
Temperature:	291.25 K
Water Vapor Content:	0.0186
Initial Parameter Test Volumes, Ram Air Channel:	
Pressure:	69700 Pa
Temperature:	291.25 K
Water Vapor Content:	0.0186

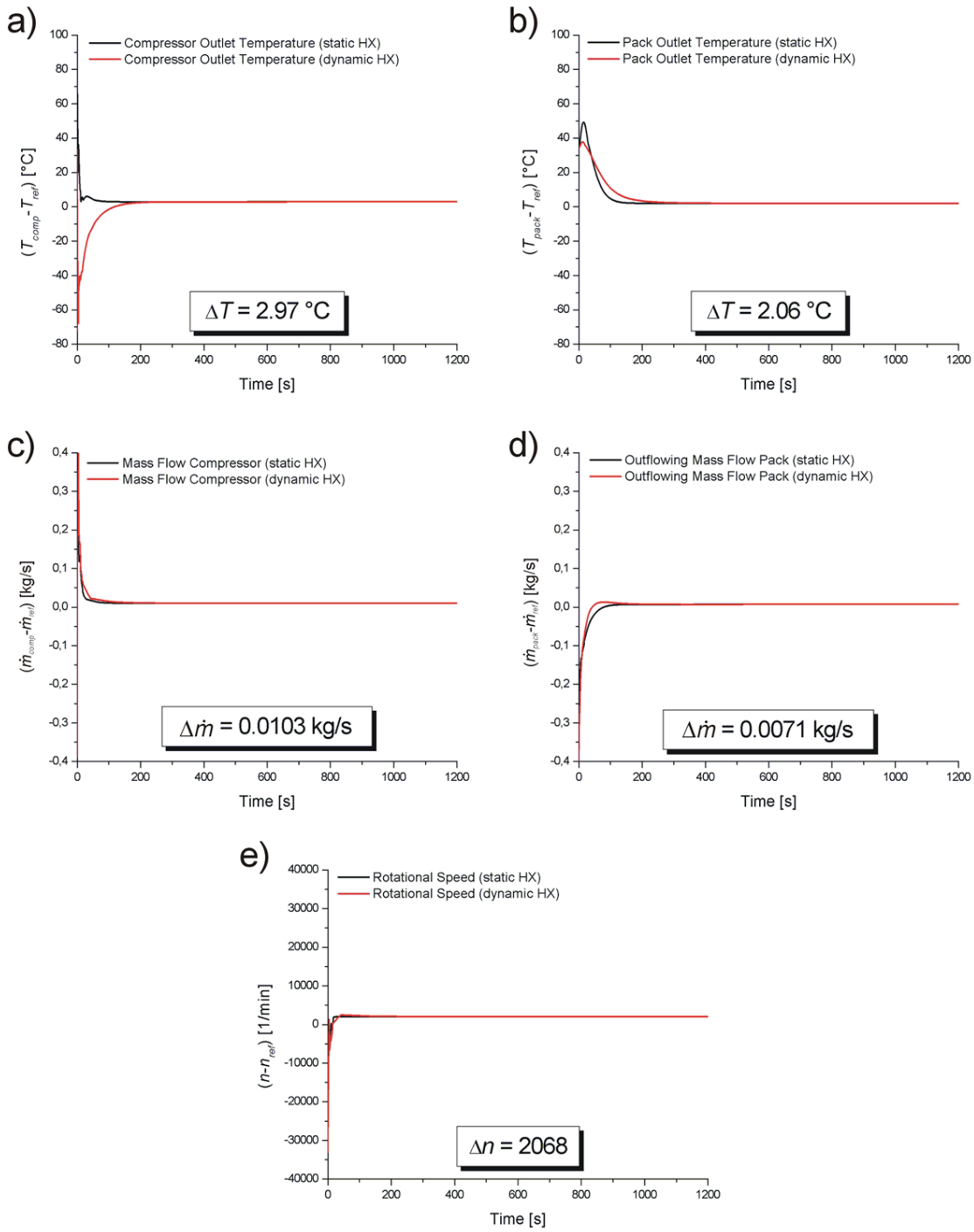

Figure 39: Test case M10H2, a) Compressor outlet temperature, b) Pack outlet temperature, c) Mass flow compressor, d) Out flowing mass flow pack, e) Rotational Speed

Test Case 3 (M20H2):

Ambient Conditions:	
Pressure:	46600 Pa
Temperature:	271.45 K
Water Vapor Content:	0.007
Boundary Limits:	
Pressure Bleed Air:	235720 Pa
Temperature Bleed Air:	473.15 K
Outlet Pressure Pack:	93600 Pa
Altitude:	20000
Mach Number:	0.6
Ram Air Inlet:	
Maximum Area:	0.04050 m²
Effective Area:	0.00911 m²
Minor Loss Coefficient:	1.39
Mass Flow Pack Bay Ventilation:	---
Temperature Pack Bay Ventilation:	---
Ram Air Outlet:	
Maximum Area:	0.07000 m²
Effective Area:	0.01575 m²
Minor Loss Coefficient:	1
Turbine:	
Corrected Isentropic Efficiency:	0.86
$\Rightarrow \Delta\eta_{trb}$	0.0040
Water Extractor:	
Efficiency Water Separation:	0.754
Initial Parameter Test Volumes:	

Pressure:	93600 Pa
Temperature:	271.45 K
Water Vapor Content:	0.007
Initial Parameter Test Volumes, Ram Air Channel:	
Pressure:	46600 Pa
Temperature:	271.45 K
Water Vapor Content:	0.007

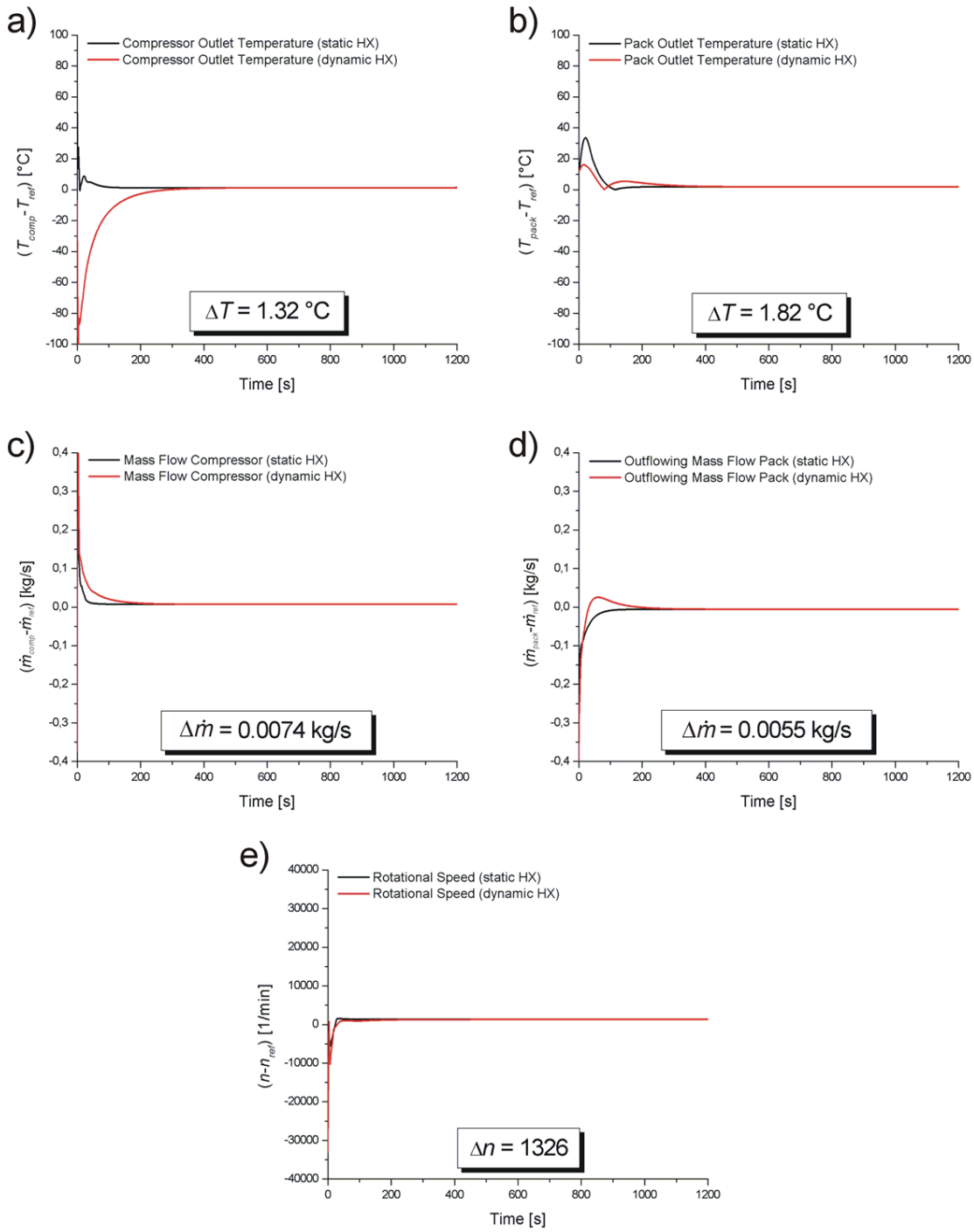

Figure 40: Test case M20H2, a) Compressor outlet temperature, b) Pack outlet temperature, c) Mass flow compressor, d) Out flowing mass flow pack, e) Rotational Speed

Test Case 4 (M30H2):

Ambient Conditions:	
Pressure:	30100 Pa
Temperature:	251.55 K
Water Vapor Content:	0.0017
Boundary Limits:	
Pressure Bleed Air:	219200 Pa
Temperature Bleed Air:	473.15 K
Outlet Pressure Pack:	86600 Pa
Altitude:	30000
Mach Number:	0.76
Ram Air Inlet:	
Maximum Area:	0.04050 m²
Effective Area:	0.00883 m²
Minor Loss Coefficient:	1.48
Mass Flow Pack Bay Ventilation:	---
Temperature Pack Bay Ventilation:	---
Ram Air Outlet:	
Maximum Area:	0.07000 m²
Effective Area:	0.01526 m²
Minor Loss Coefficient:	1
Turbine:	
Corrected Isentropic Efficiency:	0.84
$\Rightarrow \Delta\eta_{trb}$	-0.0188
Water Extractor:	
Efficiency Water Separation:	0
Initial Parameter Test Volumes:	

Pressure:	86600 Pa
Temperature:	251.55 K
Water Vapor Content:	0.0017
Initial Parameter Test Volumes, Ram Air Channel:	
Pressure:	30100 Pa
Temperature:	251.55 K
Water Vapor Content:	0.0017

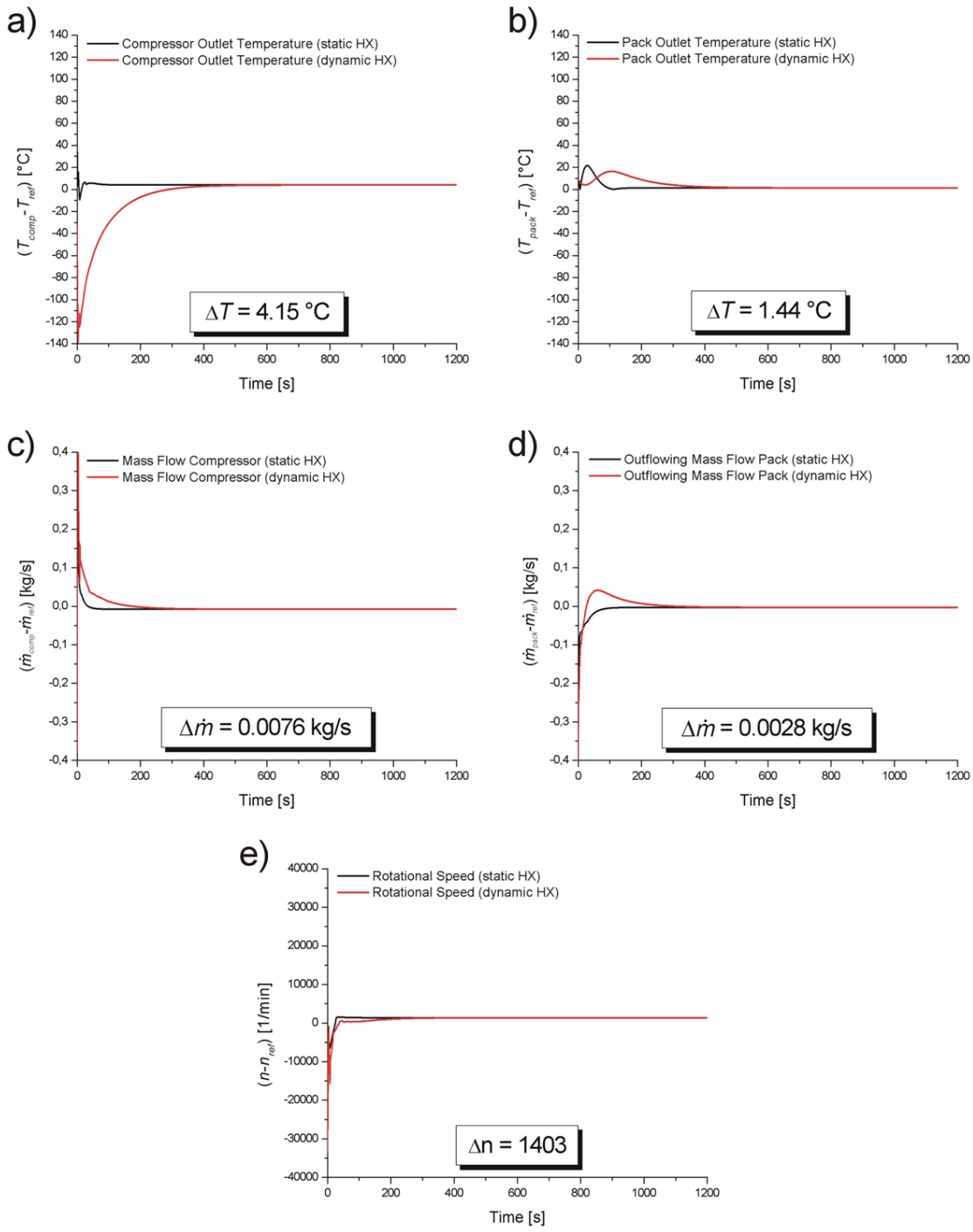

Figure 41: Test case M30H2, a) Compressor outlet temperature, b) Pack outlet temperature, c) Mass flow compressor, d) Out flowing mass flow pack, e) Rotational Speed

Test Case 5 (C35H2):

Ambient Conditions:	
Pressure:	23800 Pa
Temperature:	241.65 K
Water Vapor Content:	0.0008
Boundary Limits:	
Pressure Bleed Air:	202600 Pa
Temperature Bleed Air:	468.15 K
Outlet Pressure Pack:	81900 Pa
Altitude:	35000
Mach Number:	0.78
Ram Air Inlet:	
Maximum Area:	0.04050 m²
Effective Area:	0.00937 m²
Minor Loss Coefficient:	1.56
Mass Flow Pack Bay Ventilation:	---
Temperature Pack Bay Ventilation:	---
Ram Air Outlet:	
Maximum Area:	0.07000 m²
Effective Area:	0.01619 m²
Minor Loss Coefficient:	1
Turbine:	
Corrected Isentropic Efficiency:	0.83
$\Rightarrow \Delta\eta_{trb}$	-0.0308
Water Extractor:	
Efficiency Water Separation:	0
Initial Parameter Test Volumes:	

Pressure:	81900 Pa
Temperature:	241.65 K
Water Vapor Content:	0.0008
Initial Parameter Test Volumes, Ram Air Channel:	
Pressure:	23800 Pa
Temperature:	241.65 K
Water Vapor Content:	0.0008

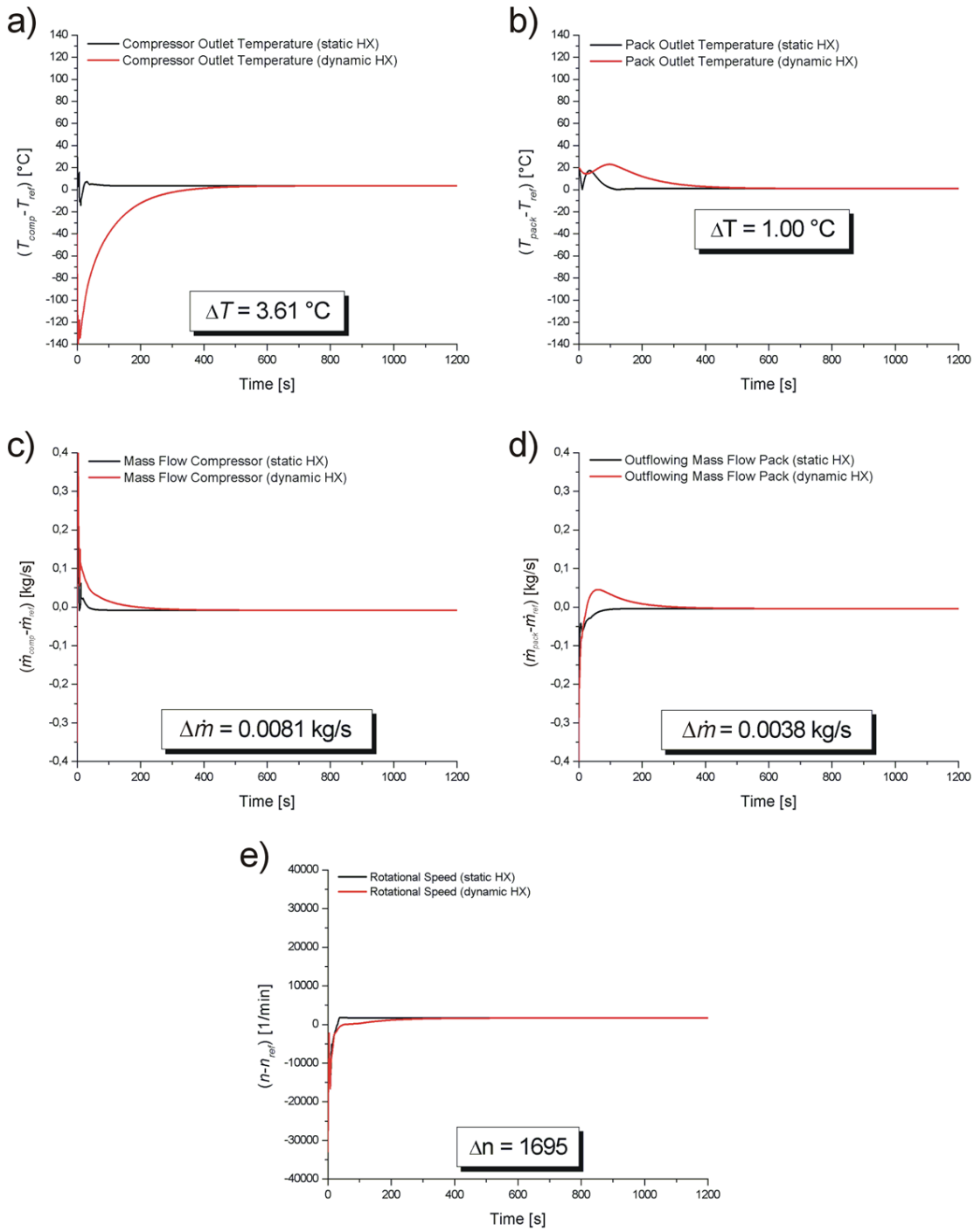

Figure 42: Test case C35H2, a) Compressor outlet temperature, b) Pack outlet temperature, c) Mass flow compressor, d) Out flowing mass flow pack, e) Rotational Speed

4.3.2 Simulation of an Aircraft Cabin Temperature Control in Combination with a Dynamic Pack Model

The dynamic pack model is embedded in a simulation of an aircraft cabin temperature control discussed in Section 3.2. Additionally to the time dependent profiles of the boundary limits shown in Figure 13, time dependent profiles of the minor loss coefficient (ram air inlet), the effective surface of the ram air inlet and outlet are defined (see Figure 43).

In contrast to the simulation shown in Section 3.2, the response time τ_{sensor} of the different temperatures sensors must be considered. The time τ_{sensor} is fixed to a value of 15 s. The results of the simulation are shown in Figure 43.

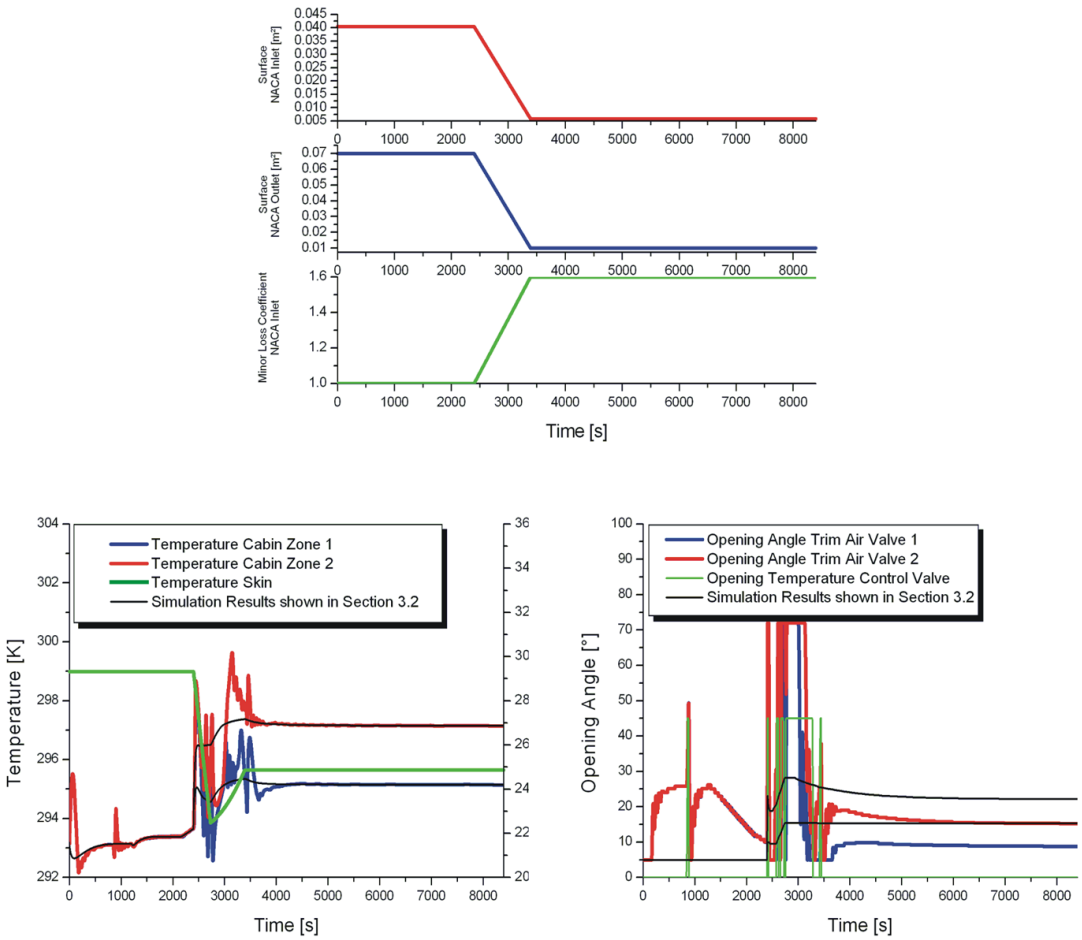

Figure 43: Results of a simulation of an aircraft cabin temperature control

4.4 Vapor Compression Cycle

The vapor compression cycle is the principle upon which conventional air conditioning systems, heat pumps, and refrigeration systems are able to cool (or heat, for heat pumps) and dehumidify air in a defined volume (e.g., a living space, an interior of a vehicle, a freezer, etc.).

The vapor-compression cycle is made possible because the refrigerant is a fluid that exhibits specific properties when it is placed under varying pressures and temperatures. A typical vapor compression cycle system is a closed loop system and includes a compressor, a condenser, an expansion device and an evaporator. The various components are connected via a conduit (usually copper tubing). A refrigerant continuously circulates through the four components via the conduit and will change state, as defined by its properties such as temperature and pressure, while flowing through each of the four components.

The main operations of a vapor compression cycle are compression of the refrigerant by the compressor, heat rejection by the refrigerant in the condenser, throttling of the refrigerant in the expansion device, and heat absorption by the refrigerant in the evaporator. Refrigerant in the majority of heat exchangers is a two-phase vapor-liquid mixture at the required condensing and evaporating temperatures and pressures. Some common types of refrigerants include R22, R134a, and R410a. In the following, R134a is considered as refrigerant.

In the vapor compression cycle, the refrigerant nominally enters the compressor as a slightly superheated vapor (its temperature is greater than the saturated temperature at the local pressure) and is compressed to a higher pressure. The compressor includes a motor (usually an electric motor) and provides the energy to create a pressure difference between the suction line and the discharge line and to force the refrigerant to flow from the lower to the higher pressure. The pressure and temperature of the refrigerant increases during the compression step. The pressure of the refrigerant as it enters the compressor is referred to as the suction pressure and the pressure of the refrigerant as it leaves the compressor is referred to as the head or discharge pressure. The refrigerant leaves the compressor as highly superheated vapor and enters the condenser. A “typical” air-cooled condenser comprises single or parallel conduits formed into a serpentine-like shape so that a plurality of rows of conduit is formed parallel to each other. Although the present document refers to air-cooled condensers, the invention also applies to other types of condensers (for example, water-cooled).

Metal fins or other aids are usually attached to the outer surface of the serpentine-shaped conduit to increase the transfer of heat between the refrigerant passing through the condenser and the ambient air. A fan mounted close to the condenser for pumping outdoor ambient air through the rows of conduit also increases the transfer of heat.

As refrigerant enters a condenser, the superheated vapor first becomes saturated vapor in the first section of the condenser, and the saturated vapor undergoes a phase change in the

remainder of the condenser at approximately constant pressure. Heat is rejected from the refrigerant as it passes through the condenser and the refrigerant nominally exits the condenser as slightly subcooled liquid (its temperature is lower than the saturated temperature at the local pressure).

The expansion (or metering) device reduces the pressure of the liquid refrigerant thereby turning it into a saturated liquid-vapor mixture at a lower temperature, before the refrigerant enters the evaporator. This expansion is also referred to as the throttling process. The expansion device is typically a capillary tube or fixed orifice in small capacity or low-cost air conditioning systems, and a thermal expansion valve (TXV or TEV) or electronic expansion valve (EXV) in larger units. The TXV has a temperature-sensing bulb on the suction line. It uses the temperature information along with the pressure of the refrigerant in the evaporator to modulate (open and close) the valve to try to maintain proper compressor inlet conditions. The temperature of the refrigerant drops below the temperature of the indoor ambient air as the refrigerant passes through the expansion device. The refrigerant enters the evaporator as a low quality saturated mixture ("quality" is defined as the mass fraction of vapor *x* in the liquid-vapor mixture).

A direct expansion evaporator physically resembles the serpentine-shaped conduit of the condenser. Ideally, the refrigerant completely boils by absorbing energy from the defined volume to be cooled (e.g., the interior of a refrigerator). To absorb heat from this volume of air, the temperature of the refrigerant must be lower than that of the volume to be cooled. Nominally, the refrigerant leaves the evaporator as slightly superheated gas at the suction pressure of the compressor and reenters the compressor thereby completing the vapor compression cycle. (It should be noted that the condenser and the evaporator are types of heat exchangers).

An air compressor driven by an electric motor is usually positioned in front of the evaporator, a separate fan/motor combination is also usually positioned next to the condenser. Inside the evaporator the heat transfer is from the compressed ambient air to the refrigerant flowing through the evaporator. For the condenser, the heat transfer is from the refrigerant flowing through the condenser to the ambient air.

4.4.1 Inner Structure of a Vapor Compression Cycle (VCM)

The algorithm of vapor compression cycle (VCM) is based on the characteristic maps shown in Figure 44. Using characteristic maps has the advantage that the VCM model can be used easily for other refrigerants. The condenser R134a flow is cooled by a cold airflow ($\dot{m}_{cold,air}$, $T_{cold.air,inlet}$). Inside the Evaporator a hot airflow ($\dot{m}_{hot,air}$, $T_{hot,air,inlet}$) is cooled down to a target temperature $T_{hot,target}$.

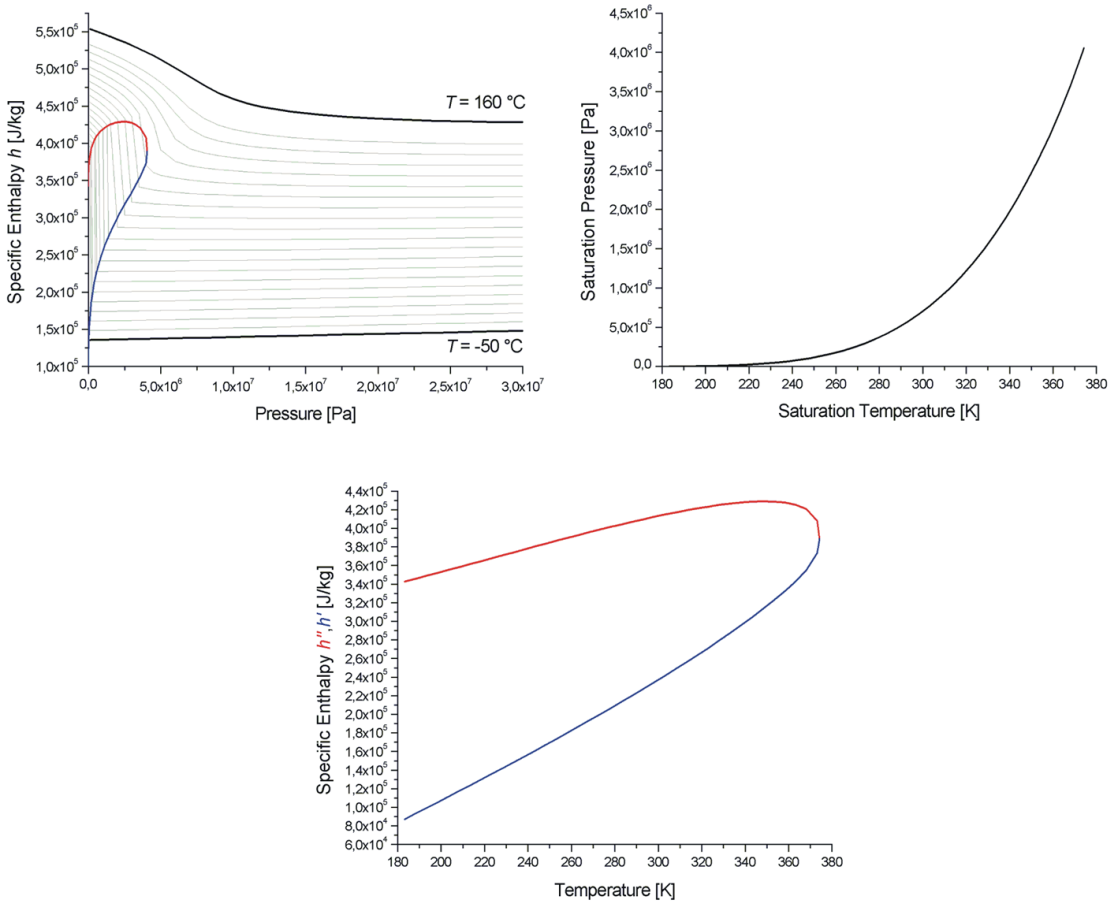

Figure 44: Characteristic maps of vapor compression cycle model

1. Evaporator (see Figure 45):

Cooling:

$$\dot{Q}_{evap} = \dot{m}_{hot,air}\ c_{p,air}\ (T_{hot,air,inlet} - T_{hot,air,target})$$

Mass flow of the refrigerant:

$$\dot{m}_{R134a} = \frac{\dot{Q}_{evap}}{h_1 - h_4}$$

Saturation Temperature:

$$T_{evap,sat}(p_{evap}) = T_{hot,air,inlet} + (\frac{1}{\eta_{evap}})\ (T_{hot,air,target} - T_{hot,air,inlet})$$

Outlet Parameter:

$$h_{evap,outlet} = h_1 = h''(p_{evap}) + \Delta h_{superheating}\ ,\ \Delta h_{superheating} = \frac{(T_{cold,air,inlet} - T_{hot,air,target})}{T_{hot,air,target}}\ \dot{Q}_{evap}$$

$$h_{evap,inlet} = h_4 = h'(p_{evap}) + x\ (h''(p_{evap}) - h'(p_{evap}))$$

$$T_{evap,outlet} = \frac{h_{evap,outlet}}{c_{p,R134a}}, c_{p,R134a} = \frac{h''(p_{evap})}{T_{evap,sat}}$$

2. Compressor (see Figure 45):

Isentropic Compression:

$$T_{comp,isentropic} = T_{evap}\left(\frac{p_{comp}}{p_{evap}}\right)^{\frac{\gamma_{R134a}-1}{\gamma_{R134a}}}, \gamma_{R1134a} = 1.13$$

$$h_{comp,isentropic} = h(p_{comp}, T_{comp,isentropic})$$

Outlet Parameter:

$$h_{comp,outlet} = h_2 = h_{evap,outlet} + \frac{1}{\eta_{comp}}(h_{comp,isentropic} - h_{evap,outlet})$$

$$T_{comp,outlet} = \frac{h_{comp,outlet}}{c_{p,R134a}}, c_{p,R134a} = \frac{h_{comp,isentropic}}{T_{comp,isentropic}}$$

$$P_{comp} = \dot{m}_{R134a}\,(h_{comp,outlet} - h_{evap,outlet})$$

3. Condenser (see Figure 45):

Subcooling:

$$T_{cond,outlet} = T_{comp,outlet} + \eta_{cond}\,(T_{cold,air,inlet} - T_{comp,outlet})$$

$$\Delta T_{cond} = T_{cold,air,inlet} - T_{cond,outlet}$$

Outlet Parameter:

$$T_{cold,air,cond} = T_{cond,sat}(p_{comp}) - \Delta T_{cond}$$

$$h_{cond,outlet} = h_3 = h_4 = h''(p_{comp}) - \frac{\dot{m}_{cold,air}}{\dot{m}_{R134a}} c_{p,air}\,(T_{cold,air,cond} - T_{cold,air,inlet})$$

$$\dot{Q}_{cond} = \dot{m}_{R134a}\,(h_{comp,outlet} - h_{cond,outlet})$$

$$T_{cold,air,outlet} = T_{cold,air,inlet} + \frac{\dot{Q}_{cond}}{\dot{m}_{cold,air}\; c_{p,air}}$$

Derivation Enthalpy:

$$\frac{\Delta h}{h} = \Delta hh = \frac{h_{cond,outlet} - h_{evap,inlet}}{h_{evap,inlet}}$$

Derivation Cold Air Mass Flow:

$$\dot{m}_{cold,air,target} = \frac{\dot{m}_{R134a}\,(h''(p_{comp}) - h_{evap,inlet})}{c_{p,air}\,(T_{cold,air,cond} - T_{cold,air,inlet})}$$

$$\frac{\Delta\dot{m}}{\dot{m}} = \Delta\dot{m}\dot{m} = \frac{\dot{m}_{cold,air,target} - \dot{m}_{cold,air}}{\dot{m}_{cold,air}}$$

The specific outlet enthalpy $h_{cond,outlet}$ is calculated without knowledge of the calculated specific inlet enthalpy $h_{evap,inlet}$. In general, both enthalpies aren't equal. Therefore the derivation Δhh can be used to adjust the cold airflow.

The discussed algorithm is a non-closed cycle and can be used as dynamic vapor cycle model with help of a set of different controllers (see Section 4.4.3).

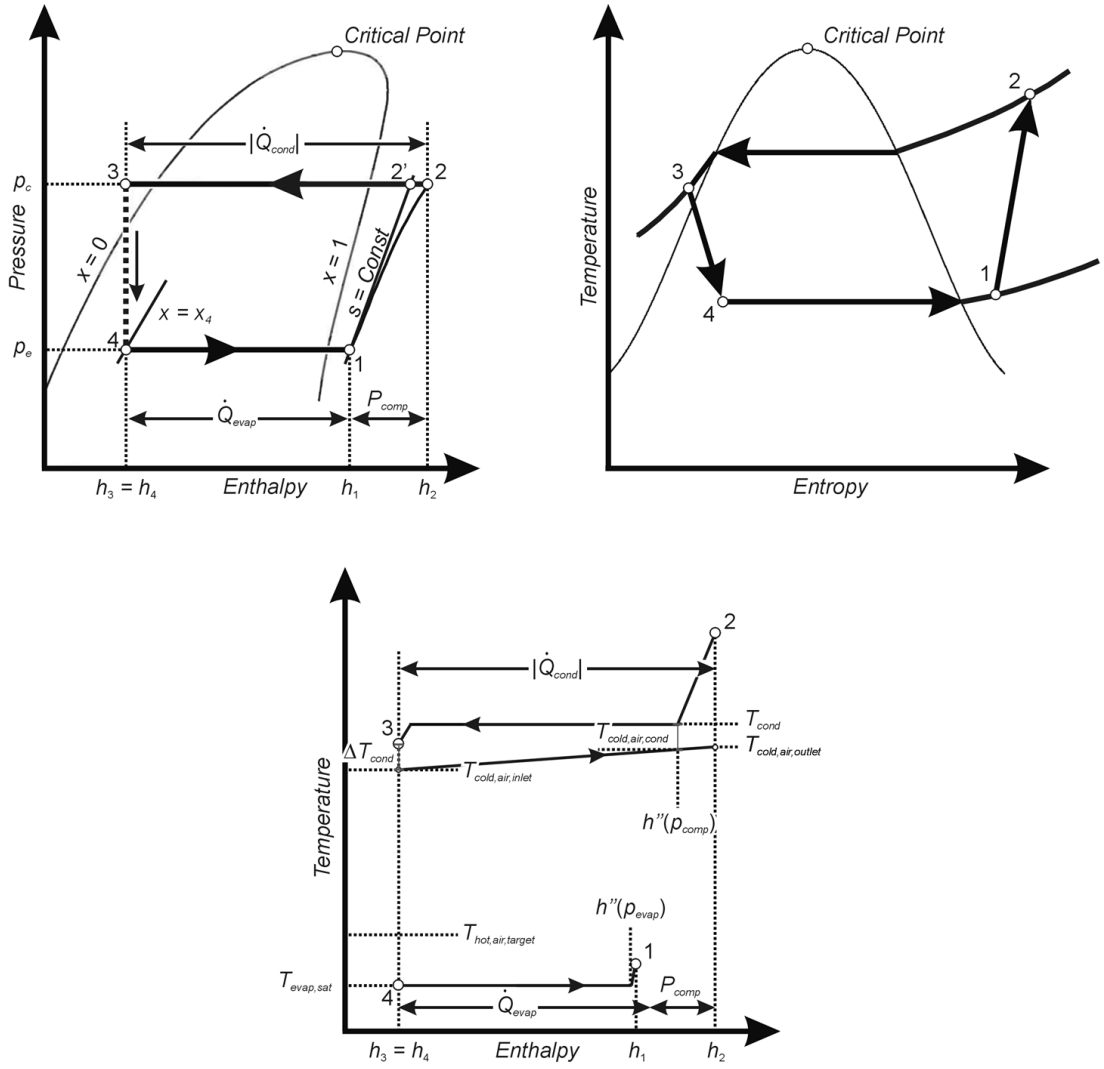

Figure 45: *p-h*, *T-s* respectively *T-h* diagrams of R134a refrigerant

4.4.2 Validation of the Vapor Compression Cycle (VCM)

The VCM algorithm discussed above can be validated with help of an example given in [**Baehr 2006**] (see Table 13).

Table 13: Validation Example [**Baehr 2006**]

	p kPa	t °C	h kJ/kg
1	**115**	**−20,00**	387,15
2′	**750**	*40,99*	*426,68*
2	**750**	*52,06*	*437,82*
3	**750**	**24,00**	233,13
4	**115**	−23,37	233,13

Cooling Capacity, Evaporator: 35000 W

Cooling Capacity R134a Flow, Condenser: 46510 W

Mass Flow R134a: 0.227 kg/s

Power Consumption Compressor: 11514 W

Mass Fraction of Vapor *x*: 0.3

The example shown in Table 13 is related with water cooling of the R134a Flow inside the evaporator and an ambient temperature $T_{ambient} = T_{cold,air,inlet}$ of 18 °C. Ensuring a sufficient cooling in the case of air cooling an airflow of $\dot{m}_{cold,air} = 8$ kg/s has to be assumed. The mass flow of the hot air is fixed to $\dot{m}_{hot,air} = 0.5$ kg/s

Table 14: Set of efficiencies

Efficiencies:	
Heat Transfer Efficiency Evaporator η_{evap}:	0.90
Isentropic Efficiency Compressor η_{comp}:	0.78
Heat Transfer Efficiency Condenser η_{cond}:	0.80

The algorithm can be validated using the set of efficiencies shown in Table 14. The results of the simulation are shown in Figure 46.

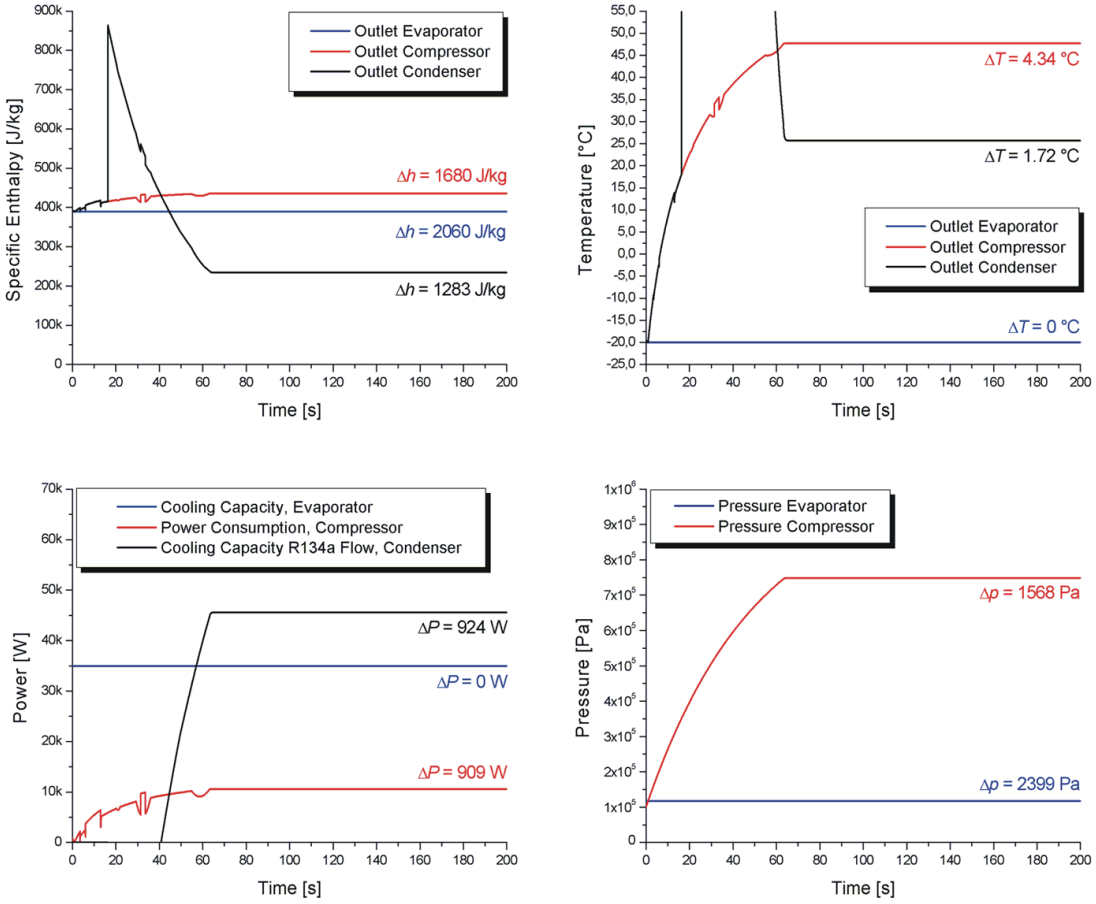

Figure 46: Validation of the VCM algorithm with help of an example given in [**Baehr 2006**]

4.4.3 Control Aspects of the Vapor Compression Cycle

VCM Compressor Controller

This controller controls the compressor pressure p_{comp} ensuring a closed refrigerant loop $\dot{Q}_{cond} = \dot{Q}_{evap} + P_{comp}$. The controller is characterized by a response time $\tau_{vcm,comp}$. The VCM compressor controller is a part of the inner structure of the VCM model.

Using the VCM model as an aircraft air conditioning pack additionally three other controllers must be defined.

Ram Air Fan Rotational Speed Controller

This controller controls the rotational speed of the ram air fan. In general, as higher the rotational speed as higher the ram air mass flow. The ram air mass flow and the ram air inlet temperature define the cooling capacity of the R134a flow inside the condenser. As actuating variable, the value Δhh is used. The controller is characterized by a response time $\tau_{n,fan}$.

Flow Controller

This controller controls the volume flow of the hot bleed air to a target value $\dot{V}_{target}$. The control variable is the opening angle β_{FCV} of flow control valve (FCV). as higher the rotational speed as higher the ram air mass flow. The ram air mass flow and the ram air inlet temperature define the cooling capacity of the R134a flow inside the condenser. As actuating variable, the value Δhh is used. The controller is characterized by a response time τ_{FCV}. Knowing the volume flow $\dot{V}_{target}$ the mass flow $\dot{m}_{FCV}$ through the flow control valve can be calculated using Equation 8.

$$\dot{m}_{FCV} = V_{target} \frac{p_{cabin}}{287.057\ T_0} \tag{8}$$

Air Compressor Rotational Speed Controller

This controller controls the rotational speed of the air compressor assuring a outlet pressure $p_{air,comp,outlet} \geq p_{cabin}$ + 27500 Pa and a outlet temperature $T_{air,comp,outlet} \geq$ 50 °C = 323.15 K. The controller is characterized by a response time $\tau_{air,comp}$.

4.4.4 Dynamic Simulation of a VCM Air Conditioning System

With the help of the discussed algorithm and control aspects a VCM air conditioning system can be built up (see Figure 47). Additionally, to the VCM model a VCM air conditioning system requires a ram air channel and an air compressor.

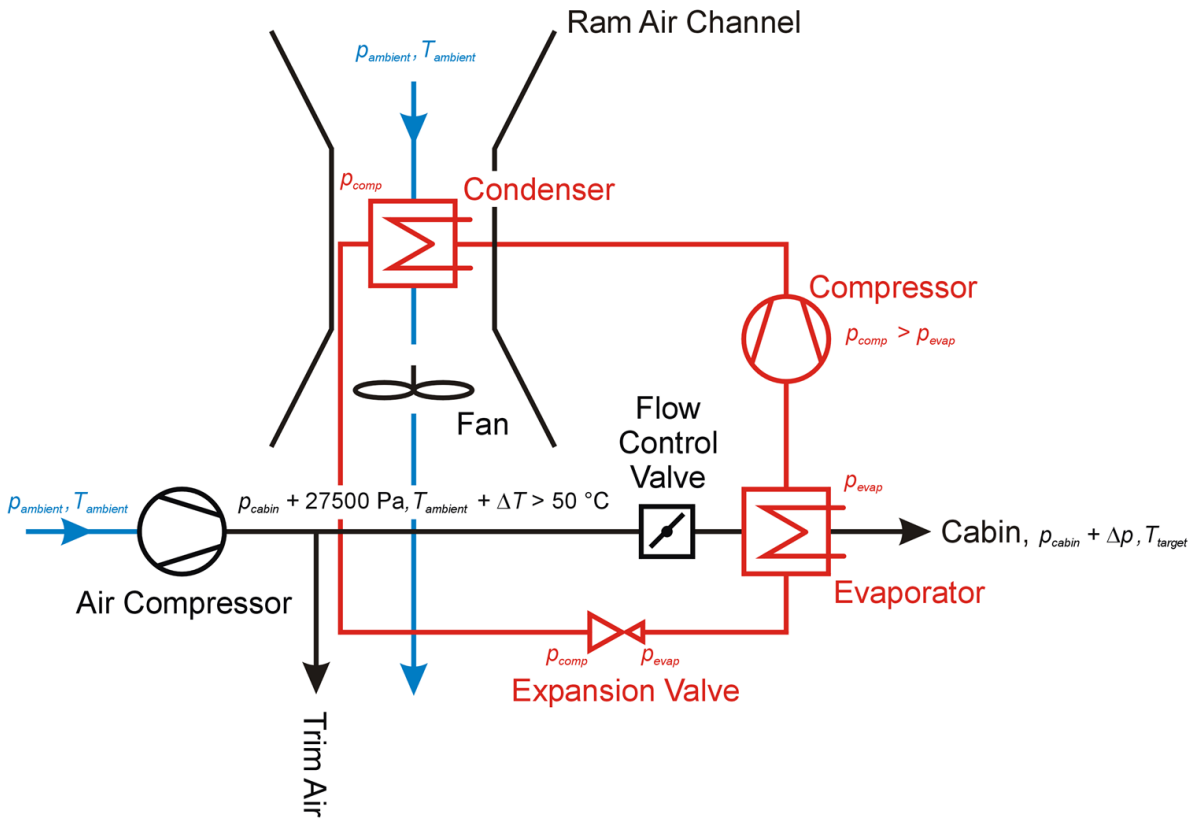

Figure 47: Arrangement for the vapor compression system inside air conditioning system

The dynamic behavior of the VCM air conditioning system is characterized by a set of efficiencies (see Table 15) and a characteristic map of the air compressor (see Figure 48).

Table 15: Set of efficiencies

Efficiencies:	
Heat Transfer Efficiency Evaporator η_{evap}:	0.80
Isentropic Efficiency Compressor η_{comp}:	0.80
Heat Transfer Efficiency Condenser η_{cond}:	0.80

The target value $\dot{V}_{target}$ of the flow controller is fixed to 0.31 m³/s. The target temperature of the bleed air is given as input variable of the simulation (see Figure 49). The response times of the different controllers are $\tau_{vcm,comp} = \tau_{n,fan} = 20$ s and $\tau_{FCV} = \tau_{air,comp} = 5$ s. Three different test cases (1: ISA Cold Day, 2: ISA Standard Day, 3: ISA Hot Day) are discussed.

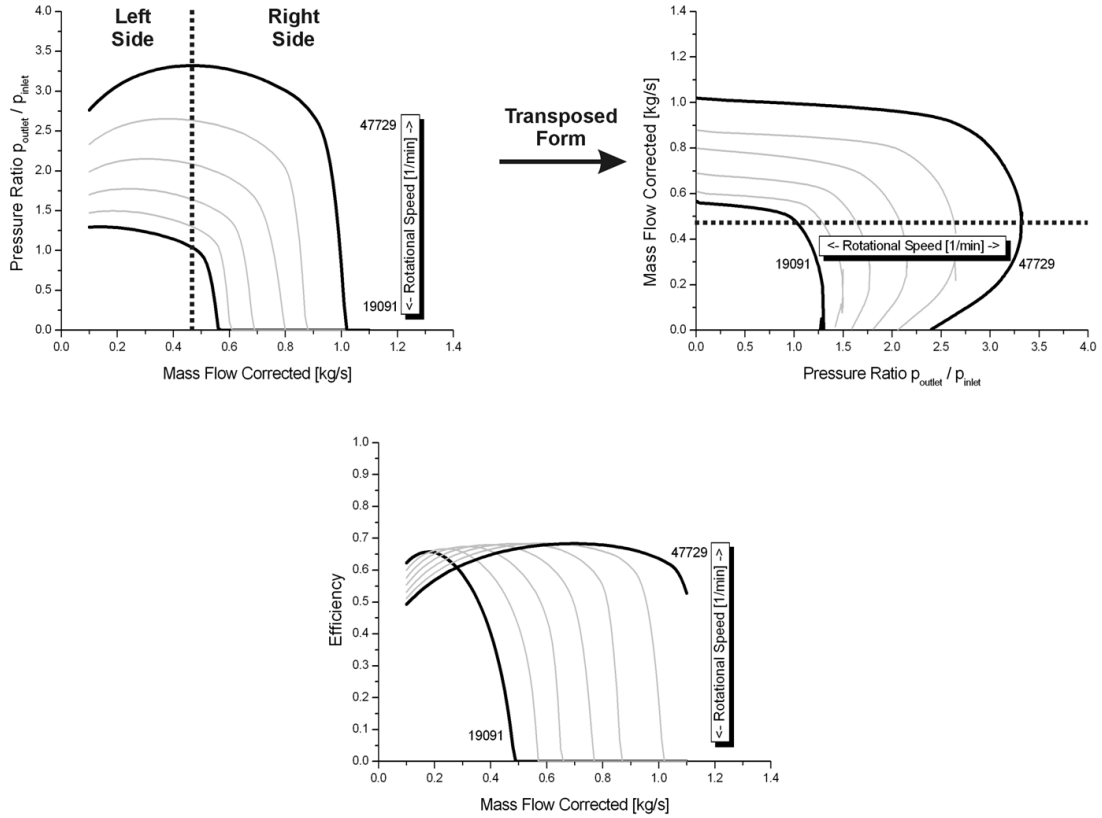

Figure 48: Characteristic maps of the air compressor

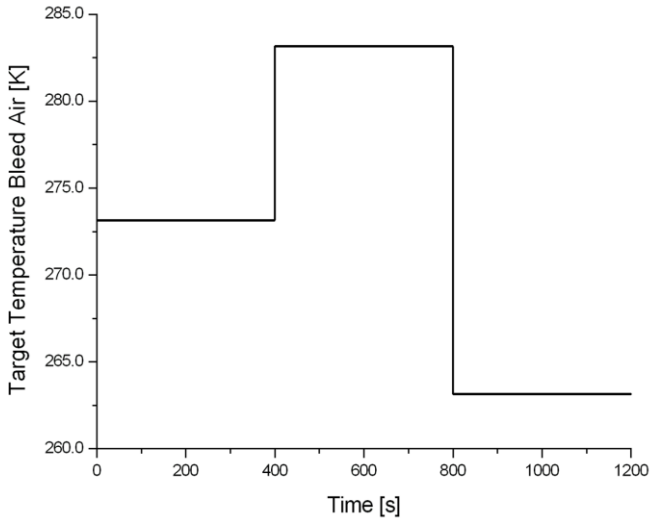

Figure 49: The target temperature of the bleed air

1. ISA Cold Day:

Ambient Pressure:	101300 Pa
Ambient Temperature:	250.15 K = -23 °C

2. ISA Standard Day:

Ambient Pressure:	101300 Pa
Ambient Temperature:	288.15 K = 15 °C

3. ISA Hot Day:

Ambient Pressure:	101300 Pa
Ambient Temperature:	311.15 K = 38 °C

Results and Comments

In the case that the system is controlled to a pressure $p_{comp} < p_{evap}$, the VCM compressor power consumption P_{comp} is set to zero (see Figure 50g and Figure 50i, ISA Cold Day). The variable Δhh can be used to check if the refrigerant loop is closed. In the case ISA Cold Day and ISA Standard Day the relative derivation Δhh is smaller than 5 % (see Figure 51), and therefore the loop is fully or almost closed. In the case ISA Hot Day Δhh is significantly higher than 5 %. Therefore, the loop is only partially closed. Under these ambient conditions a cascade refrigeration cycle should be used (see Figure 52).

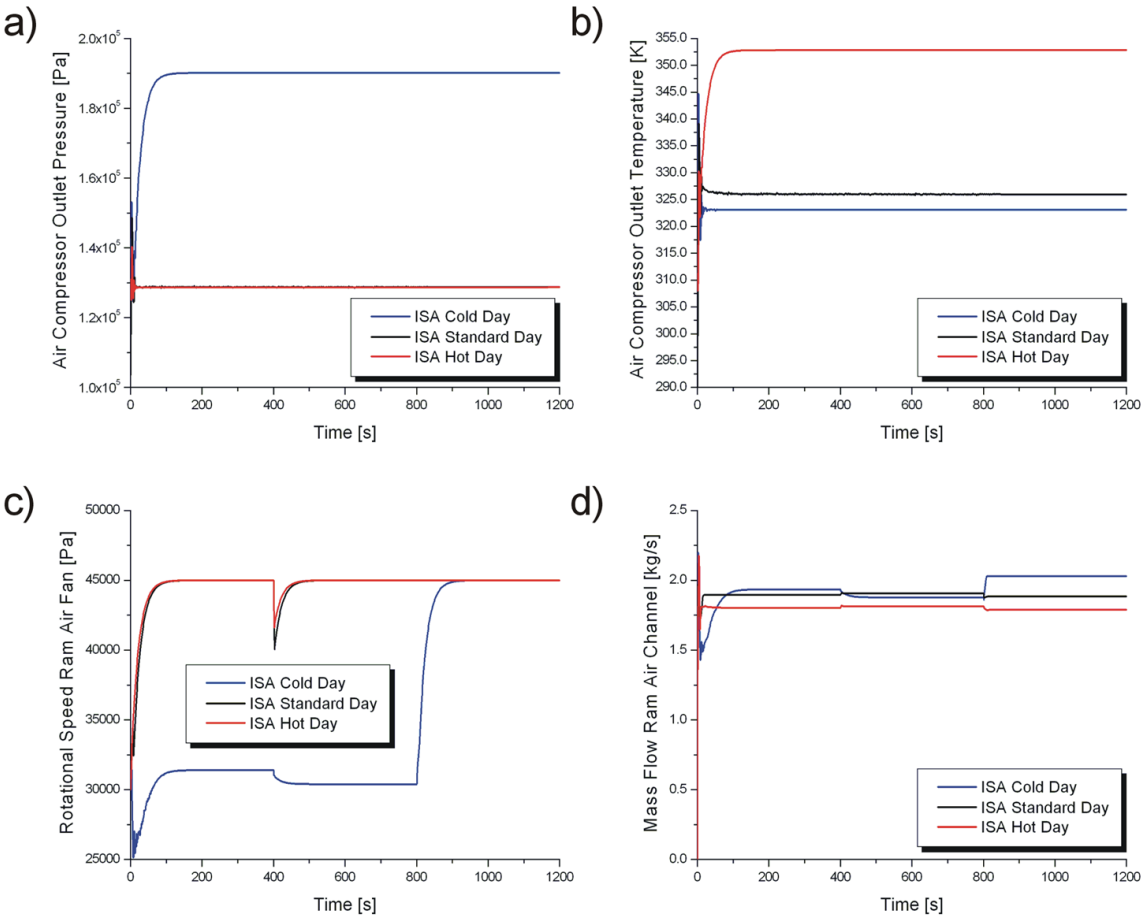

Figure 50: The dynamic behavior of the VCM air conditioning system under different ambient conditions

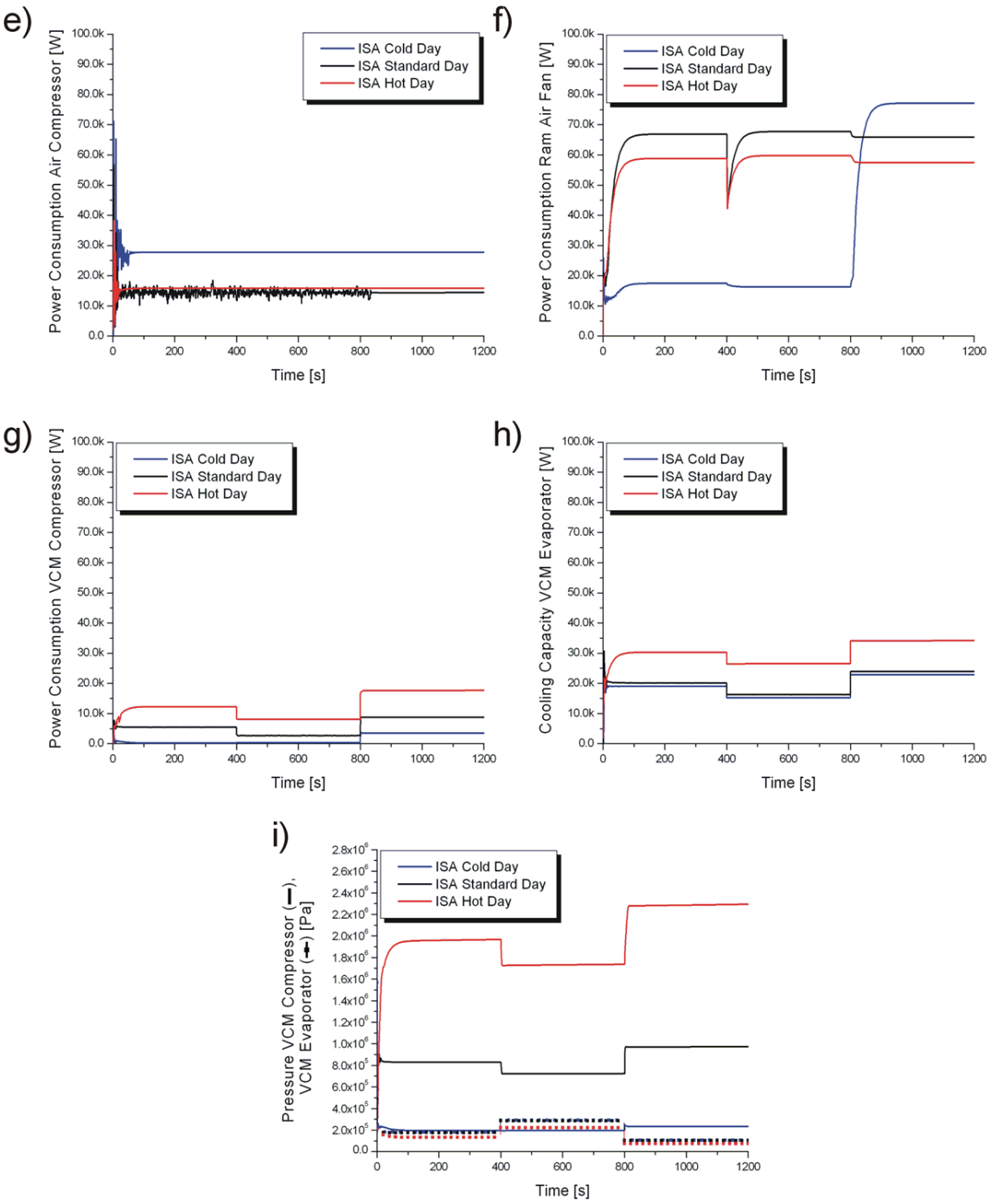

Figure 50: The dynamic behavior of the VCM air conditioning system under different ambient conditions

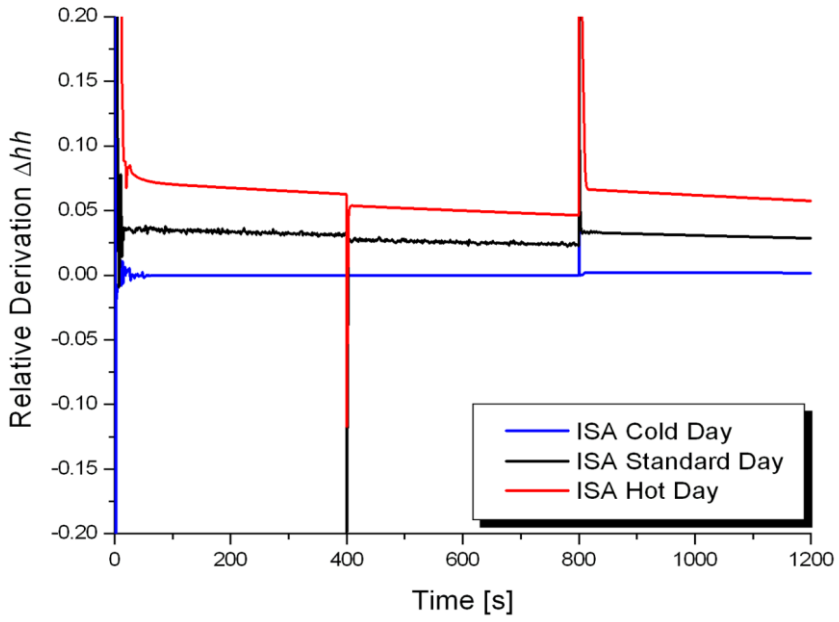

Figure 51: The relative derivation *Δhh* under different ambient conditions

This cycle will lead to a decrease in the temperature at point 3, meaning increasing cooling capacity. Additionally, this configuration will minimize the power consumption of the compressor. With this cycle, it is not an obligation to use the same refrigerant. If the refrigerants are different, the appropriate *T-s* diagram has to be used.

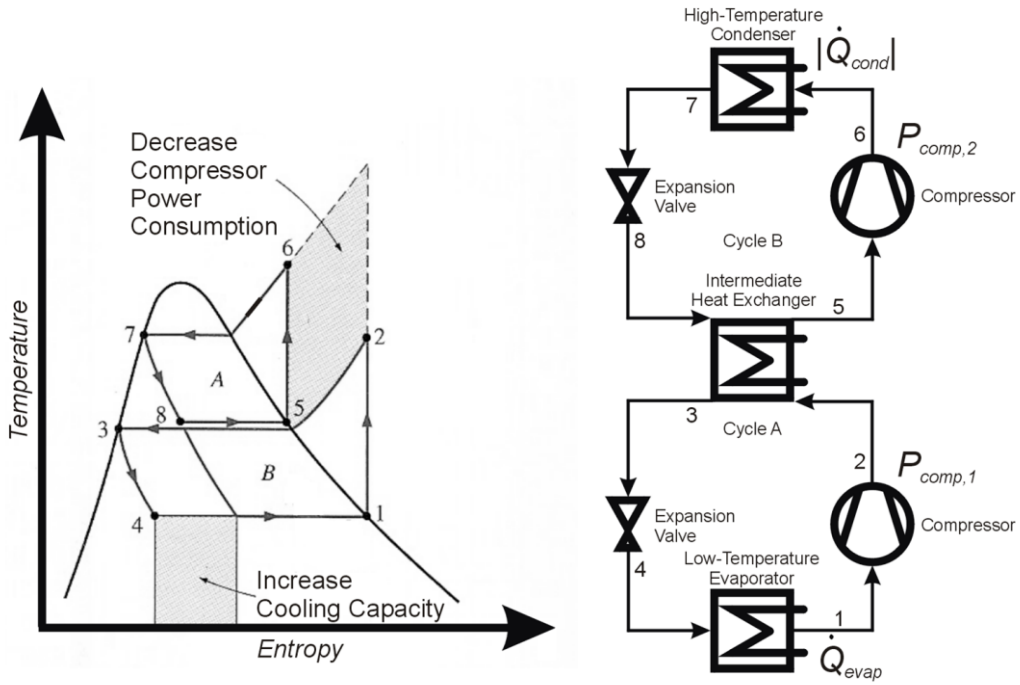

Figure 52: A cascade refrigeration cycle

4.4.5 Comparison of an Air Conditioning System Consisting of an ACM and a VCM Pack Model

In this section the performance of air conditioning consisting of an ACM pack is compared with a system consisting of a VCM pack. The parameterization of the overall system e.g. the trim air system or the cabin model is already mentioned in Section 3.2.

The dimension of the ram air inlet is given in Table 12. Inside the VCM systems the area of the ram air inlet is fixed to the maximum value ($\zeta = 1$). The outlet temperature of the VCM model shows a steady state behavior (see Figure 49). The outlet temperature is a input value of the simulation and is fixed by the pack controller (see Figure 11). To compare both systems also the ACM pack model has to be defined in a steady state configuration. A steady state model can be described by mass flow source. The temperature is fixed by the pack controller. The mass flow can be calculated with help of Equation 8 ($\dot{V}_{target} = 0.34$ m³/s).

Inside the ECS system the rotational speed of the recirculation fan is fixed to 7500 1/min assuring a ratio $\dot{m}_{recirculation} / m_{pack} = 1$. The floor temperature inside the cabin model is always 10 °C smaller than the average temperature of the cabin ($T_{floor} = 0.5\ (T_{zone,1} + T_{zone,2}) - 10$ °C).

Response time controller

VCM System:	
VCM Compressor Controller:	20 s
Ram Air Fan Rotational Speed Controller:	20 s
Flow Controller:	5 s
Air Compressor Rotational Speed Controller:	5 s

Global Parameter

On ground:	ISA standard day ($T_{ambient} = 15$ °C, $p_{ambient} = 101300$ Pa)
In flight:	ISA conditions
Bleed air temperature:	200 °C = 473.15 K
Trim air pressure:	p_{cabin} + 27500 Pa
Trim air temperature (ACM):	200 °C = 473.15 K
Trim air temperature (VCM):	$T_{air,comp,outlet}$

Aircraft Mission

Time: 0 s … 1200 s
The aircraft is on ground. The boarding starts. The target temperature of the cabin is 21 °C. In 20 minutes, 200 passengers enter the cabin (see Figure 53), assuming a constant flow of passengers. The heat load, which flows into the cabin, increases significantly.

Time: 1200 s … 2250 s
1200 s: The boarding is completed. The aircraft starts. In 1050 s the aircraft climbs to a flight altitude of 35000 ft (climb rate 2000 ft/min) (see Figure 53). The ambient conditions are described by an ISA condition. Knowing the ambient temperature $T_{ambient}$ the skin temperature T_{skin} can be calculated ($T_{skin} = T_{ambient}(1 + 0.18\ Ma^2)$, Ma: Mach number). The target temperature of the cabin zone 1 is 22 °C = 295.15 K, the target temperature of the cabin zone 2 is 24 °C = 297.15 K. The cabin pressure is fixed to 81224 Pa.

Time: 2250 s … 5850 s
Cruise: The target temperature of cabin zone 1 is 22 °C = 295.15 K, the target temperature of the cabin zone 2 is 24 °C = 297.15 K. The cabin pressure is fixed to 81224 Pa.

Time: 2250 s … 6900 s
Descent: In 1050 s the aircraft with a rate of 2000 ft/min. The target temperature of the cabin zone 1 is 22 °C = 295.15 K, the target temperature of the cabin zone 2 is 24 °C = 297.15 K.

The profiles of the aircraft altitude, cabin pressure, Mach number and Skin temperature are shown in Figure 53. In flight the minor loss coefficient of the ram air inlet is fixed to 1.5 (see Equation 6). The simulated temperature profiles in zone 1 and zone 2 are shown in Figure 54a*. the trim air opening angle is shown in Figure 54b*. The power consumption of the ACM system can be calculated using a enthalpy equation (see Equation 9 and Figure 54c*).

$$P_{ACM} = \dot{m}_{pack}\ c_p (T_{bleed,air} - T_{pack,outlet}) \tag{9}$$

The overall power consumption of the VCM system is the sum of the power consumption of the ram air fan P_{fan}, the air compressor $P_{air,comp}$ and the VCM Compressor P_{comp} (see Equation 10 and Figure 54c).

$$P_{VCM} = P_{fan} + P_{air,comp} + P_{comp} \tag{10}$$

* Figure 54 is missing.

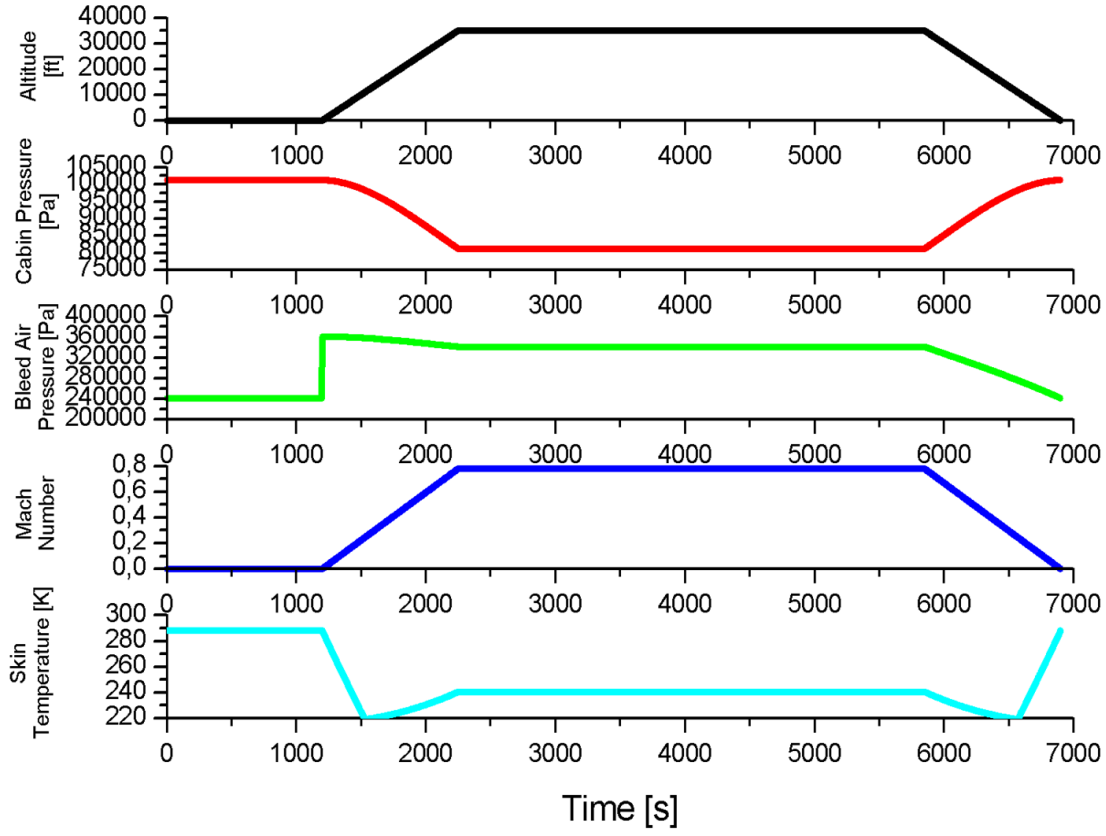

Figure 53: Results of a simulation of an aircraft cabin temperature control process

Bibliography

Allied-Signal 1990 Allied-Signal Aerospace Company, Inc.: Airesearch Enviromental Control System: An Overview. Los Angeles : 1990. – Presentation

Baehr 1995 BAEHR, Hans Dieter; TILLNER-ROTH, Reiner: *Thermodynamische Eigenschaften umweltverträglicher Kältemittel*. Berlin : Springer. 1995

Baehr 2006 BAEHR, Hans Dieter: *Thermodynamik*. Berlin : Springer. 2006

Böswirth 2000 BÖSWIRTH, Leopold: *Technische Strömungslehre*. Wiesbaden : Vieweg, 2000

Bohl 1998 BOHL, Willi: *Technische Strömungslehre* : *Stoffeigenschaften von Flüssigkeiten und Gasen, Hydrostatik, Aerostatik, Inkompressible Strömungen, Kompressible Strömungen, Strömungsmeßtechnik*. Würzburg : Vogel, 1998

Chawla 1990 CHAWLA, J. M.; WISKOT, G.: *Wärmeübertragung* : *Berechnung mit dem PC*. Düsseldorf : VDI, 1992

Eichholz 2005 EICHHOLZ, J.; Airbus Deutschland GmbH, EYVCG : Standardization of Simulation Models in EYV. Hamburg : Airbus, 2005 (EYVC048/05). – Firmenschrift

Gupta 1998 GUPTA, J. Y.: *Fundamentals of Heat Exchanger and Pressure Vessel Technology*. New York : Hemisphere Publishing Corporation, 1985

Herwig 2004 HERWIG, Heinz: *Strömungsmechanik* : *Eine Systematische Einordnungvon Begriffen und Konzepten der Strömungsmechanik*. Wiesbaden : Vieweg, 2004

Incropera 2003 INCROPERA, FRANK P.; DEWITT, DAVID P.: *Fundamentals of Heat and Mass Transfer*. New York : John Wiley & Sons, 2002

Idel'chik 1994 IDEL'CHIK, L. E.: *Handbook of Hydraulik Resistance*. Boca Raton : CRC Press, 1994

Mishra 2004 MISHRA, Manish; DAS, P.K.; SARANG, Sunil: Transient behaviour of crossflow heat exchangers with longitudinal conduction and axial dispersion. In: *International Journal of Heat Transfer*, Vol. 126 (2004), No. 3, pp. 425-433

Mishra 2006 MISHRA, Manish; DAS, P.K.; SARANG, Sunil: Transient behaviour of crossflow heat exchangers due to perturbations in temperature and flow. In: *International Journal of Heat and Mass Transfer*, Vol. 49 (2006), Issues 5-6, pp. 1083-1089

Patankar 1980 PATANKAR, Suhas V.: *Numerical heat transfer and fluid flow*. Pristol, PA : Taylor & Francis, 1980

Podhorsky 1990 PODHORSKY, M.; KRIPS, H.: *Wärmetauscher* : *Allgemeine Probleme der Konstruktion und Berechnung*. Essen : Vulkan, 1990 (FDBR-Fachbuchreihe, Band 5)

Roetzel 1998 ROETZEL, Wilfried; XUAN, Yimin: *Dynamic Behaviour of Heat Exchanger*. Southhampton : WitPress, 1999 (Developments in Heat Transfer, Vol. 3)

Scholz 1999 SCHOLZ, Dieter: *Entwicklung eines CAE- Werkzeuges zum Entwurf von Flugsteuerungs- und Hydrauliksystemen*. Düsseldorf : VDI, 1997 (Fortschritt-Berichte VDI, Reihe 20, Nr. 262)

Shah 2003 SHAH, Ramesh K.; SEKULIĆ, Dušan P.: *Fundamentals of Heat Exchanger Design*. New York : John Wiley & Sons, 2003

Thoma 2000 THOMA, J.; OULD BOUAMANA, B.: *Modelling and Simulation in Thermal and Chemical Engineering* : *A Bond Graph Approach*. Berlin : Springer, 2000

VDI 2002 VEREIN DEUTSCHER INGENIEURE (Hrsg.): *VDI-Wärmeatlas* : *Berechnungsblätter für den Wärmeübergang*. Berlin : Springer, 2002

Wagner 1998 WAGNER, Walter: *Wärmetauscher* : *Grundlagen, Aufbau und Funktion Thermischer Apparate*. Würzburg : Vogel, 1993

Wesseling 2000 WESSELING, Pieter: *Principles of Computational Fluid Dynamics*. Springer : Berlin, 2000

Wylie 1993 WYLIE, E. B.; STREETER, V. L.: *Fluid Transients in Systems*. Englewood : Printice-Hall, 1993